Achievable Power Uprates in Pressurized Water Reactors Using Uranium Nitride Fuel

by

Guillaume Giudicelli

Ingénieur diplômé de l'Ecole Polytechnique, 2016

SUBMITTED TO THE DEPARTMENT OF NUCLEAR SCIENCE AND ENGINEERING IN PARTIAL FULFILLMENT OF THE REQUIREMENTS FOR THE DEGREE OF

MASTER OF SCIENCE IN NUCLEAR SCIENCE AND ENGINEERING AT THE MASSACHUSETTS INSTITUTE OF TECHNOLOGY

FEBRUARY 2017

Signature of Author: _____

Department of Nuclear Science and Engineering

Certified by: _____

Koroush Shirvan

Principal Research Scientist

Thesis Supervisor

Read by: _____

Ronald G. Ballinger

Professor of Nuclear Science and Engineering, and

Materials Science and Engineering

Thesis Reader

Accepted by: _____

Ju Li

Battelle Energy Alliance Professor of Nuclear Science and Engineering

Professor of Materials Science and Engineering

Chair, Committee on Graduate Students

Abstract

Achievable Power Uprates in Pressurized Water Reactors Using Uranium Nitride Fuel

This work aims at investigating the potential benefits of nitride fuel use in pressurized water reactors. The AP1000 is chosen as the reference power plant. Both oxide and nitride fuel are considered and compared using a steady state thermal hydraulics and mechanics parametric optimization study to achieve a maximal core power. A subsequent neutronics study determined the achievable energy extracted per fuel mass (burnup) and sets the core power that allows for an 18-months fuel cycle length. The impact of the change in the core operating temperature on the steam cycle efficiency is considered in order to provide a final evaluation of the electric power uprate.

The steady state limits considered are pressure drop, minimum departure from nucleate boiling ratio, fretting and sliding wear and fuel average and centerline temperatures. These limits were set by the reference design's performance. Two strategies were used to raise the core power while remaining within specified limits: increasing the core mass flow rate and decreasing the core inlet temperature. These two strategies were implemented in a simplified MATLAB tool using correlations and a MATLAB-VIPRE (subchannel simulation tool) interface to better model cross-flows. Designs with smaller pins but with similar pitch-to-diameter ratios compared to the reference design were found to be optimal with regards to these performances for both strategies. Fretting wear was found to be the limiting constraint for these designs for the first strategy, and additional spacer grids can be introduced to reduce fretting wear and to allow a further power increase. MDNBR was found to be the limiting constraint for these designs in the second strategy. The fuel temperature was not limiting for these designs and both oxide and nitride fuel can be utilized with the same uprates.

Both tools provided similar results: smaller fuel pins with similar pitch over diameter ratios allow for better performances than the nominal design in the aforementioned criteria. The most promising strategy proved to be decreasing the core inlet temperature. With this strategy, the possible uprate is 16%, or 550 MWth, in both tools. Such an uprate requires an additional steam generator, and when lowering the core inlet temperature the efficiency of the steam cycle is lowered by 1% as we also need to lower the steam generator saturation pressure. This will require a larger high-pressure turbine. The optimized nitride-fueled design was compared with the oxide-fueled nominal core in terms of neutronics performances. I showed that the new design can reach an 18 month cycle length, at an uprated power, with a 4.3% enrichment and a 60 assembly feed using uranium nitride, compared with a 4.6% enrichment and a 68 assembly feed for the nominal design at the nominal power. With a higher enrichment and a higher feed, a two-year cycle length can be reached even with the uprate. The moderator temperature coefficient, the shutdown margin and the power coefficient of both designs satisfied licensing requirements. A 5% increase in fuel cycle costs was noted with the nitride optimized core, minor compared to the revenue of a 150 MWe uprate. Transient performances, and more extensive fuel performance studies are left for future studies.

Thesis Supervisor: Koroush Shirvan
Title: Principal Research Scientist

Acknowledgments

I am extremely grateful to Koroush Shirvan for his guidance throughout this project. I learned a lot from his expertise in PWR design. His dedication to his students and availability as a supervisor are unparalleled in this institution.

I would like to express my sincere gratitude to Professor Ballinger, first for his contribution throughout the year, bringing his industry and NRC experience to the project, then for his help in redacting this thesis as my thesis reader, and finally as my academic advisor.

I would like to thank Robert Nielsen for his permanent interest in my research. I am thankful for the opportunity to present my work at the ExxonMobil MIT Energy initiative conference.

This work wouldn't have been possible without my roommates Stephen, Shikhar and Pawla. From fruitful discussions to class teamwork, we really nailed this first year at MIT.

I would like to thank Yanin Sukjai for implementing uranium nitride in FRAPCON and checking if my designs weren't causing catastrophic fuel failures.

The author would like to thank ExxonMobil for their generous support of this project and providing funding for the first author through the MIT Energy Initiative Energy Fellows program.

Finally, I'd like to thank those closest to me: my parents, and of course Briana. Your support and understanding has been invaluable, and I look forward to being closer to you in the future.

Table of contents

List of Figures

List of Tables

Chapter 1

Overview

As fossil energy resources are being depleted and as awareness of climate change is growing, nuclear energy could be a viable replacement for fossil fuels with its carbon-free electricity and its plentiful resources [8]. However, at the moment, cheap natural gas is driving the electricity cost down, threatening the economic viability of nuclear power plants. Without radical changes in the nuclear industry, this could mean a phase-out for nuclear energy.

Higher powers or uprates have an immediate effect on improving the economic performance of a nuclear power plant. Uprates of nuclear reactors historically kept the share of nuclear in the US electricity market roughly constant (20%), while no new plants have been built in the US since 1996. The recent EPA-proposed clean power act provides incentives for upgrading current plants' carbon-free capacity. The economic performance of a nuclear power plant is also affected by its capacity factor. Increasing the span between refueling outages, is a straightforward approach in improving NPP's capacity factor, which is already at about $\sim$90% [9].

However, further uprates or longer cycle lengths cannot be performed with the current oxide fuel and the current U^{235} enrichment limit of 5%. By the end of a regular cycle, the core fissile inventory is so low that more than a third of the fuel needs to be replaced. Uranium nitride, a fuel 30% denser than its oxide counterpart, allows loading much more fissile material in the core and sustain the uprate or the longer cycle length.

In order to investigate uprates in pressurized water reactors (PWR), we will first perform a thermal-hydraulics and mechanics parametric study of the core geometry, operating temperature and flow rate. In case of a change in core operating temperature range, we will consider its impact on the steam cycle efficiency. In this study, we will set achieving or exceeding the nominal design's performances in safety features, such as the minimum departure from nucleate boiling ratio, as constraints in our optimization process. We will derive an optimized assembly design from this study, create an AP1000-like optimized core as well as a nominal AP1000 core and compare their neutronics performance. In particular, we will examine the cycle length achievable with the maximum power uprate allowed by the design constraints.

In chapter two, we will present the motivations for and describe uprates in PWRs. In chapter three

we will present the AP1000, the reference plant for this study, and its advanced safety features. Chapter four presents uranium nitride, its potential as a fuel but also the challenges that need to be overcome, such as the reaction between this fuel and water. Chapter five is dedicated to explaining the methodology of the thermal-hydraulics and mechanics study, while chapter six presents its results. A model of the AP600 steam-cycle is used to estimate the potential for an electric power uprate. Chapter 7 regroups the assembly design work on the optimized and nominal geometry, such as managing the burnable poison loading and keeping pin power peaking low. In chapter 8, a core loading pattern is designed and tested with regards to licensing requirements. This allows us to conclude on how much more power a uranium nitride fueled PWR can achieve to produce.

Chapter 2

Motivation

There has not been a new nuclear power plant construction project from 1979 with the Three Mile Island accident to the current AP1000 construction projects at Vogtle and VC Summer power plants and completion of Watts Bar II PWR plant. And yet, the share of nuclear in the US electricity market has remained constant in that period of time. This is because of power uprates in light water reactors. Nuclear power plants were built with significant safety margin. Better knowledge of the core mass flow can help reduce the uncertainty part of the safety margins, and allow uprates known as measurement uncertainty recapture. More sizeable uprates known as stretch uprates can be achieved by optimizing the reactor without major modifications, and finally extended power uprates up to 20% were performed with major modifications of the plant.

Between 1977 and 2014, the NRC approved 154 uprates in light water reactors [10]. Among these, 28 were extended power uprates, 66 were stretch uprates and the rest was measurement uncertainty recapture. This amounted to 21 GW thermal, or the equivalent of approximately 7 additional nuclear reactors. Nowadays, the clean power plan, proposed by the Environmental Protection Agency (EPA) gives emission rate credits to nuclear power plants [11]. These are commodities that can be sold and provide additional revenue to the utility.

In parallel with performing uprates, utilities are also interested in having longer cycle lengths for their reactors. Nowadays, nuclear reactors operate for 18 months, before refueling for 20-30 days. They refuel during spring and autumn, at which time the electricity demand is the lowest. This routine has gotten so efficient, that the load factor for these plants has reached the cap of 0.94, only limited by refueling outages. To go beyond that cap means refueling less often, and depending on market conditions, some utilities are interested in 2 year cycles.

To perform power uprates or have longer cycle lengths, there needs to be more fissile fuel in the reactor. For light water reactors, the fuel is uranium dioxide (UO_2). Natural uranium is made of 99.3% uranium 238 and 0.7% uranium 235. Only ^{235}U is fissile in light water reactors. To bypass this natural constraint, the fuel is enriched in ^{235}U, up to 5% which is a regulatory limit. Fuel enrichment, production and transport facilities are only typically licensed up to this percentage for criticality reasons. To have more fuel in the reactor, either this 5% limit should be increased, or the fuel can be denser. Uranium nitride (UN) shows promise in this regard.

The AP1000, is a promising Gen III+ reactor design, see section 3, which relies on passive safety systems. Currently, 8 units are being built around the world. The AP1000 design will likely dominate US nuclear reactor development in the upcoming decades. Changing the fuel to nitride for nuclear reactors is a process of that same timescale. It is also a reactor that will be exported outside the United States in significant quantities. Countries outside the United States do not have UO_2 fuel fabrication facilities, and have the opportunity to choose a better performing fuel. This is why the AP1000 was chosen as the reference plant for our study.

Chapter 3

Reference Plant: AP1000

The AP-1000 (Advanced Passive 1000 MW-electric), is the latest pressurized water reactor from Westinghouse. It is a 3400 MW thermal reactor and has a Rankine cycle for power conversion. It features passive safety. In case of a loss of onsite power or a breach in the primary coolant circuit, the core is cooled by natural circulation, with no operator intervention, for at least 72 hours before active intervention is required.

It received an NRC license in December 2011, and 4 units are being built in the United States, 2 at the Vogtle and 2 at the V.C. Summer power plant. Another 4 units are being built in China, and the first unit should be operational by 2017 3.3. The Chinese State Nuclear Power Technology Corporation is working with Westinghouse on developing an uprated version, the CAP1400 at 1400 MWe and a 1700 MWe version.

Westinghouse is looking to build 3 AP1000 near Sellafield in the United Kingdom, and in June 2016, the US and India agreed to build 6 units in India.

3.1 Reactor core

The fuel in a PWR is in the form of uranium dioxide pellets, which are stacked and enclosed in a zirconium-alloy cladding to form a fuel pin. These fuel pins are grouped in a square array to form assemblies, as shown in Figure 3.1, and are held together by spacers. In the AP1000, fuel pins have a 9.5 mm diameter, and are 14 feet (4.26m) long. 157 of these assemblies make up the core, and a third to a half of these are replaced at every refueling outage.

The core is placed inside a 15cm thick steel pressure vessel in a pressurized water loop called the primary loop. The coolant is heated in the core and transfers this heat to the secondary loop in the steam generators, starting point of a Rankine cycle. The primary loop and the steam generators are placed inside a concrete containment designed to shield the core from exterior events, or prevent radioactive release in case of a core melt. Figure 3.2 shows the primary and secondary loops, as well as the containment and passive safety features detailed below.

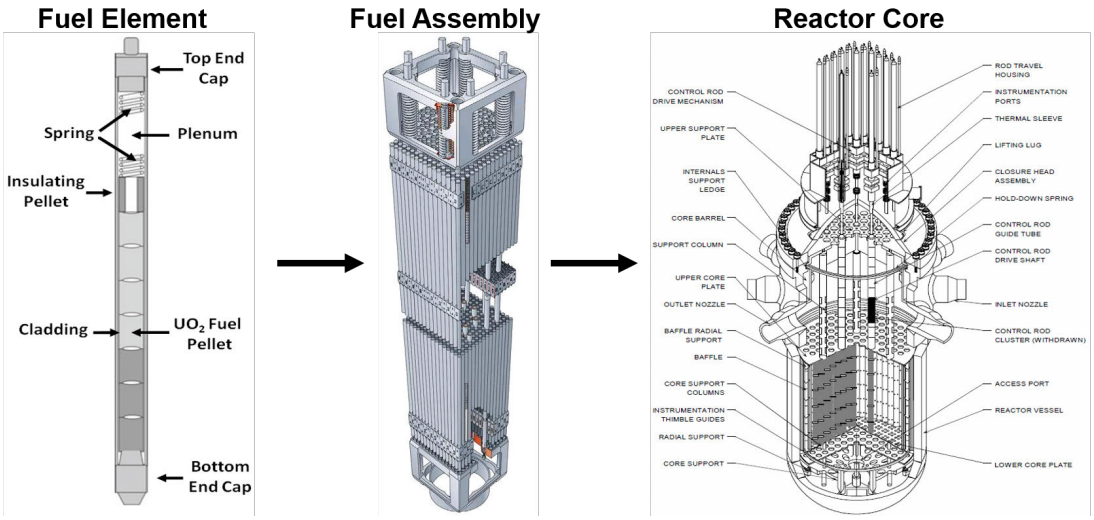

Figure 3.1: Schematic representation of nuclear fuel [1]

3.2 Innovative safety features of the AP1000

Passive safety

The AP 1000 can maintain core cooling and containment integrity during all design basis accidents, including a large-break loss of coolant accident without human intervention, and without external power sources for a period of 72 hours. It relies on natural circulation of the coolant within the primary circuit and through the safety tanks. The safety tanks can provide cooling for 72 hours, which would then need to be topped up through operator action. The passive containment cooling tanks can be seen at the top of the containment in Figure 3.2.

The AP1000 plant's passive safety systems include [12]:

- Passive Core Cooling System (PXS)
- Containment Isolation
- Passive Containment Cooling System (PCS)
- Main Control Room Emergency Habitability System
- High Pressure Safety Injection with Core Makeup Tanks (CMTs)
- Medium Pressure Safety Injection with Accumulators
- Low Pressure Reactor Coolant Make from the IRWST
- Passive Residual Heat Removal
- Automatic Depressurization System

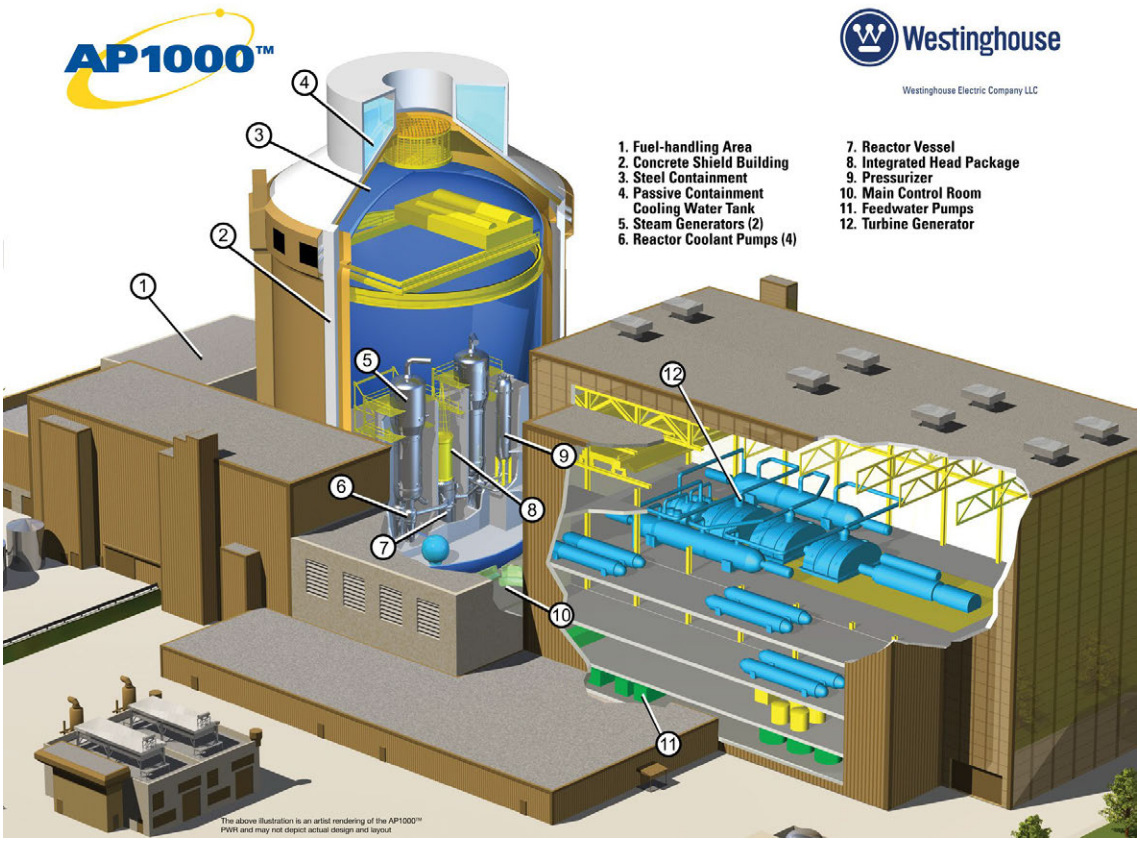

Figure 3.2: Schematic representation of the AP1000

In-vessel retention of core damage

In the event of an unmitigated core melting in conventional PWRs, the core will deposit at the bottom of the pressure vessel, and eventually melt through the 15cm of steel. In the AP1000, an in-containment refueling water storage tank will be drained into the reactor cavity, providing cooling to the outside of the pressure vessel and preventing its failure.

In-vessel safety injection

Different from previous Westinghouse PWR designs, the AP1000 safety injection directly injects water into the pressure vessel, rather than inside the primary loops. This approach avoids losing safety injection if primary loops are compromised.

3.3 Innovative design features of the AP1000

A simpler design [12]

Nuclear reactor economics are degraded by their construction cost and construction time. Westinghouse has attempted to address both issues in the AP1000 design. It has worked on making the plant simpler, and

uses less components. Passive safety components are typically simple well-placed pressurized water tanks, but they allow a reduction in the number of active safety components such as safety-grade pumps. The seismic requirements on these components are very strict and impose significant additional concrete volumes to house them. The following are among the simplifications relative to a typical PWR:

- 50% fewer safety-related valves
- 35% fewer pumps
- 80% less safety-related piping
- 85% less control cable
- 45% less seismic building volume

Modular construction [12]

The AP1000 is using modern modular-based construction techniques. This allows for a reduced construction schedule, with more factory-based manufacturing and assembly of modules, which also allows for pre-testing and inspection of the modules, improving quality and reducing the potential for unexpected delays.

Figure 3.3: Installation of final module, containment water tank, at Sanmen 2 in China (01/2016) [2]

Number of steam generators [12]

The AP1000 primary loop only has 2 steam generators, when previous PWR designs include 3 to 4 steam generators. Limiting the number of steam generators limits the number of components, and structural

supports, without hurting the redundancy of steam generators. Indeed, in each steam generator are thousands of tubes, and the reactor is shut down whenever one of them leaks at a significant rate. The tubes are what matters for redundancy, not the steam generators. Having two or three steam generators doesn't change the degree of redundancy, but it impacts greatly the construction cost of the plant.

Chapter 4

Uranium Nitride

4.1 Physical properties of uranium nitride

Uranium mononitride (UN) or uranium nitride is a ceramic material which has a face-centered cubic crystal lattice of NaCl type. It has a density of 14.3 g/cc, 30% higher than UO_2, the most commonly used fuel in nuclear reactors. Table 4.1 summarizes UN and UO_2 properties. UN has a lower heat capacity, meaning it is easier to cool down but also to heat up. It has a much higher thermal conductivity, which increases with temperature, unlike UO_2. This means that UN is significantly cooler in the reactor, while both fuels have similar melting points. However, UN undergoes dissociation at 1700°C, which increases pin pressure.

Table 4.1: Physical properties of uranium nitride [7]

	UO_2	UN
Theoretical density (g/cm^3)	10.96	14.32
HM density (g/cm^3)	9.67	13.52
Specific heat (J/kg K)	330 (1000 °C)	230 (1000 °C)
Melting point (°C)	~2800	~2700
Dissociation temperature (°C)	N/A	~1700
Elastic modulus (GPa)	200 (800 °C)	~260 (800 °C)
Fracture stress (MPa)	~130 (800 °C)	~370 (800 °C)
Relative irradiation creep rate (800 °C)	1	~0.1
Thermal conductivity (W/m K)	7.19 (200 °C)	12 (200 °C)
	3.35 (1000 °C)	20 (1000 °C)

[3] B.M. Ma, Nuclear Reactor Materials and Applications, Van Nostrand Reinhold Company, New York, 1983.
[4] K. Richter, C. Sari, J. Nucl. Mater. 184 (1991) 167–176.
[5] R. Thetford, M. Mignanelli, J. Nucl. Mater. 320 (2003) 44–53.
[6] C.M. Allison, G.A. Berna, R. Chambers, E.W. Coryell, K.L. Davis, D.L. Hagrman,D.T. Hagrman, N.L. Hampton, J.K. Hohorst, R.E. Mason, M.L. McComas, K.A. McNeil, R.L. Miller, C.S.

4.2 Reaction with water

Uranium nitride has the drawback of reacting with water, especially high temperature super-heated steam [13], which can be formed during severe accidents in PWRs.The reaction creates UO_2 and U_3O_8, which are less dense than uranium nitride.
$2\ UN + 4H_2O \Rightarrow 2UO_2 + 2NH_3 + H_2 + Energy$
This fuel expansion can cause the pin to burst. This problem will be initiated upon cladding failure that allows water ingress. There are a number of proposed solutions to this problem:

- Stronger cladding, such as silicon carbide cladding, which is less likely to leak
- Binding other elements in the fuel, such as uranium silicide or metallic additives such as yttrium and titanium [14] to prevent, to form composites and suppress the reaction,
- Coating the fuel with a waterproof coating to protect it from water
- Filling the gap between the fuel and the cladding with liquid metal. The cold water would solidify the liquid metal, protecting the fuel
- Filling the gap between the fuel and the cladding with a foam to prevent water from reaching the fuel

Because of the reaction with water and its compatibility with liquid metals, uranium nitride was at first mostly considered for use in liquid metal fast reactors (sodium [15], lead [16] and lead-bismuth fast reactors [17]). The higher thermal conductivity is also very relevant in fast reactors which have a high power density. The high density allows for even more compact cores, an asset for space power reactors [18].

4.3 Nitrogen in uranium nitride

Nitrogen only has two stable isotopes : ^{14}N and ^{15}N. ^{13}N and ^{16}N decay with constants of 9.96 minutes and 7.1 seconds.

^{14}N shows 99.636 % of nitrogen on Earth. It has 7 protons and 7 neutrons. ^{15}N accounts for the remainder. Fig 4.1a presents nitrogen 14 and 15's capture cross sections. One can see that ^{14}N is a pure 1/v absorber over the entire thermal and epithermal regions, and is more than 3 orders of magnitude more absorbant than ^{15}N. This is due to the fact that having 8 neutrons is energetically favorable.

Figure 4.1b represents nitrogen 14 and 15's elastic cross sections. We can see that the nitrogen 14's elastic scattering cross section drops over 1000-200,000 eV before having its first resonances, while ^{15}N's elastic cross section drops only after 100 keV and its resonances start at 1 MeV. Figure 4.1b represents nitrogen 14 and 15's inelastic scattering cross sections. The energy threshold for inelastic scattering is higher for ^{15}N, as having 8 neutrons is particularly stable.

Because of this high absorption cross section, uranium nitride has to be enriched in ^{15}N, up to 99.5-99.9 % [7]. This also reduces the amount of radioactive ^{14}C created by (n,p) reaction. Nitrogen enrichment could be done economically using cation-exchange resins [19].

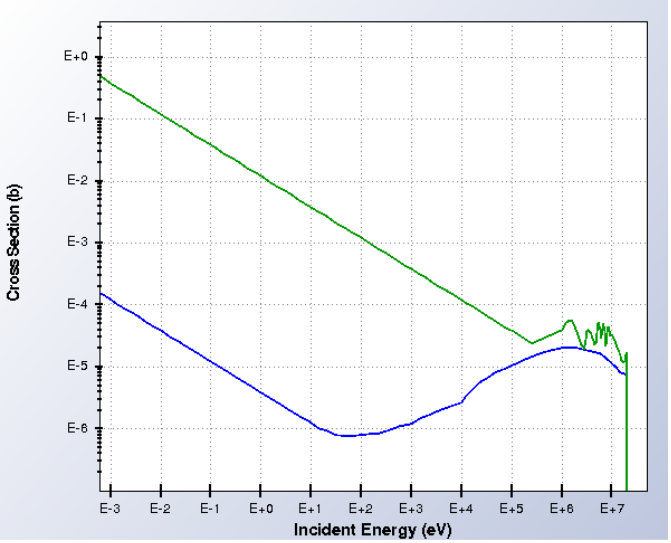

(a) ENDF/B-VII Capture cross section of nitrogen 14 (green) and 15 (blue) [3]

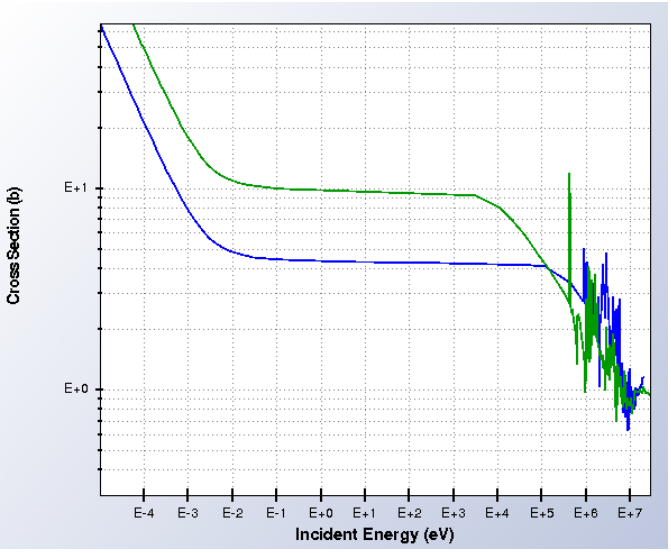

(b) ENDF/B-VII Elastic scattering cross section of nitrogen 14 (green) and 15 (blue) [3]

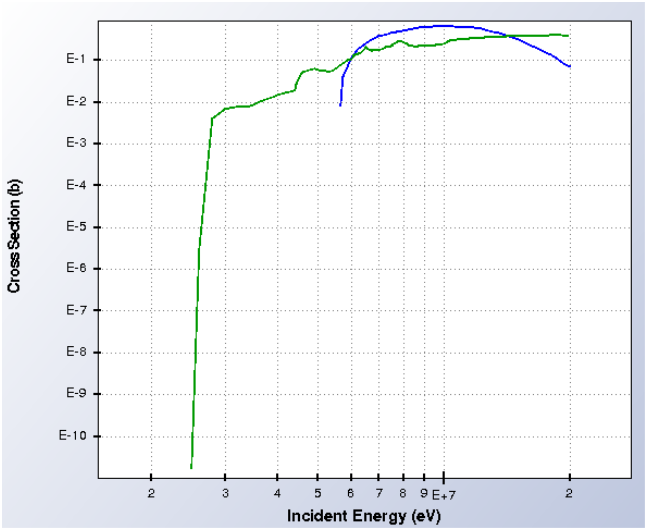

Figure 4.2: ENDF/B-VII Inelastic scattering cross section of nitrogen 14 (green) and 15 (blue) [3]

4.4 Density of uranium nitride for reactor applications

UN fuel has been shown to have more irradiation swelling than UO_2 fuel [20], but it has mostly been tested in fast reactors, and not as much in thermal reactors. In order to prevent this swelling, the fuel can be fabricated with a lower density. The cavities formed during irradiation will then interconnect and leak their gas outside the pellet, preventing swelling past a certain irradiation threshold. Previous studies advised 85 % density for the RRBWR reactor [7]. I assumed a density of 90 % of the theoretical density, so 12.9 g/cc, for our purpose. This value is possible even with previously mentioned concerns as the gap between the pellet and the cladding that I chose to use is bigger in proportion than in usual designs. Uranium nitride can readily be fabricated at such densities [21].

4.5 Previous experience with Uranium Nitride

Most of the nitride fuel previous irradiation experiments were carried out in Russia, which has used uranium nitride in the BOR-60 and BN-600 fast reactors [22], and as a driver fuel in the BR-10 fast reactor [21]. 1250 Helium bonded fuel pins were irradiated with a 1% fuel pin failure rate.

In the US, irradiation experiments were carried out in the liquid metal fast breeder reactor program, and a high failure rate was observed, mainly due to pellet cladding mechanical interaction (PCMI) [21]. Another irradiation campaign was led in thermal reactors in order to study uranium nitride for space nuclear reactor applications and no fuel failure was observed [21].

A detailed list of irradiation experiences of uranium nitride fuel throughout the world can be found in [21].

Chapter 5

Methodology

Given an AP1000 core shape - core diameter and number of assemblies -, the program numerically searches for the fuel pin configuration that can achieve the highest core power. To do that, I chose the two most important parameters with regards to thermal-hydraulics and mechanics: the fuel pin diameter and the pin-to-pin pitch-over-pin diameter ratio.

The fuel pin diameter was allowed to vary between 6.5 mm and 12.5 mm, and the pitch-over-diameter ratio between 1.1 and 1.55. This range encompasses square-lattice assemblies' common values [23]. The study is restricted to the values within these two ranges that can fit in an AP1000 core shape. From previous studies [24], I identified and included the number of spacer grids as an additional optimization parameter. Some results are only given over the pin diameter range 6.5 mm to 9.5 mm, as it was identified as the most promising.

For all these geometries, I used correlations and/or the EPRI developed, NRC-licensed code VIPRE-01 [25] to evaluate steady state operation and safety performances:

- Minimum departure from nucleate boiling ratio (MDNBR)
- Fuel bundle pressure drop
- Fuel temperature
- Flow instabilities
- Fretting and sliding wear at the spacer grid locations

For each core geometry, the power of the core was chosen so that it exceeded the reference design for each of these performances. Apart from the fuel temperature, these design limits are not fuel-dependent. Starting from an energy balance across the core:

$$\dot{m}_{core} c_p (T_{outlet} - T_{inlet}) = \dot{Q}_{core} \tag{5.1}$$

One can see that there are two ways to increase the core thermal power:

- Increase $\dot{m}_{core}$, the mass flow rate across the core
- Increase $T_{outlet} - T_{inlet}$, the temperature difference between the inlet and the outlet of the core

This served as my two optimization strategies. The algorithm to find the optimal core power is summarized in Figure 5.1. The same algorithms were implemented using correlations in a MATLAB tool modeling **a single channel**, and using a MATLAB-VIPRE interface, developed by [26], modeling **a full core**.

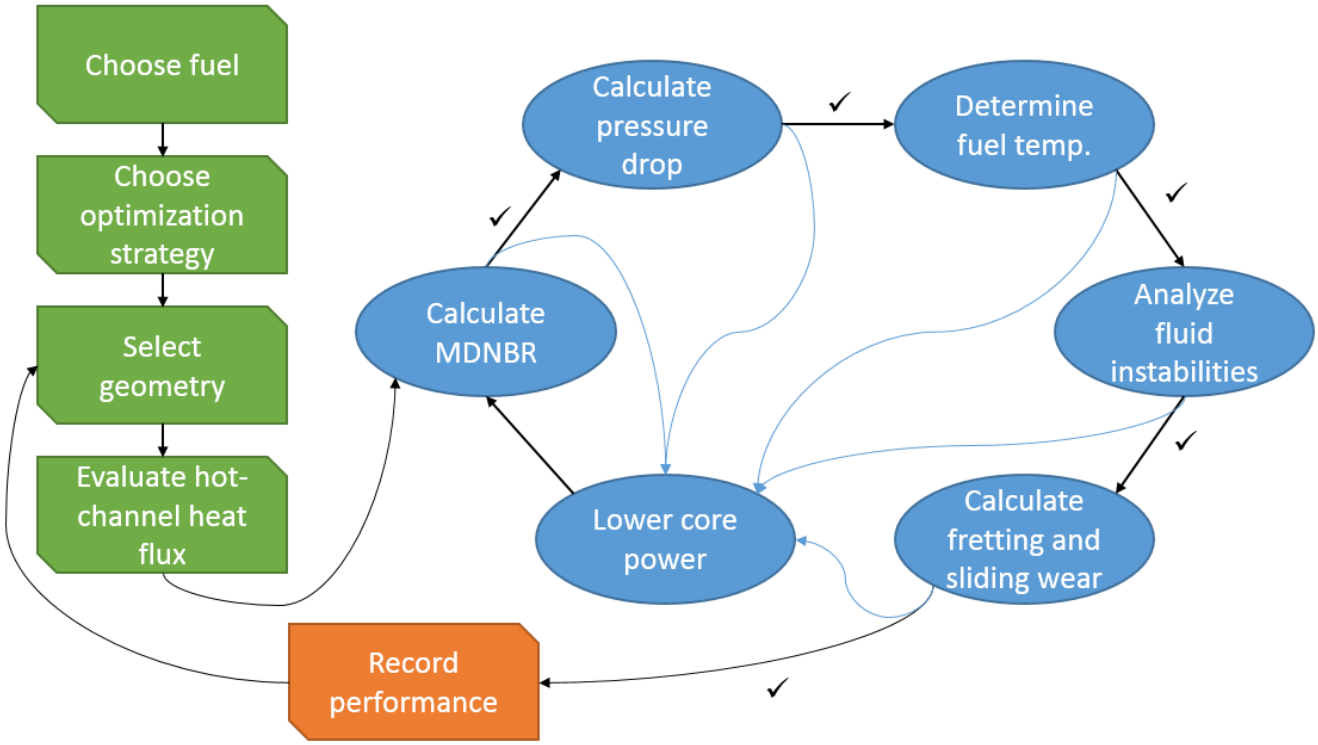

Figure 5.1: Geometry optimization algorithm for seeking the maximum power uprate in the MATLAB tool.

5.1 VIPRE and the VIPRE-MATLAB interface

VIPRE for Versatile Internals and component Program for Reactors from EPRI has been developed for nuclear power utility thermal-hydraulic analysis applications [25]. It is designed to help evaluate nuclear reactor core safety limits including minimum departure from nucleate boiling ratio (MDNBR), critical power ratio, fuel and clad temperatures, and coolant state in normal operation and assumed accident conditions. It predicts the velocity, pressure, and thermal energy fields, and the fuel rod temperatures for interconnected flow channels.

VIPRE input is a text document describing the core geometry and operating parameters. VIPRE outputs several text documents describing the core performances. Both input and output are very compact and prone to human error. This is why J. Malen [26] and his successors [27] created a MATLAB interface, which takes care of input generation and output treatment automatically.

I chose to complement the MATLAB tool with an implementation of the same algorithm in this interface because VIPRE models the entire core, and as a result can predict cross-flow velocities. These cross-flow

velocities can then be used to predict fretting and sliding wear.

5.2 Generating an AP1000-like geometry

Not all combinations of fuel pin diameters and pin pitch can fit in an AP1000 assembly. The AP1000 core is designed with 157 assemblies, each 14 ft long. The pitch and the number of pin per assembly define the size of the assembly. The pitch is part of my optimization process, the number of pin rows per assembly is thus adjusted to conserve the assembly size.

In the MATLAB script, the script chooses a number of pin rows per assembly such that the core surface is less than 4.5 % different from the reference core surface. In Figure 5.2a, one can see the number of fuel pin rows per assembly so that the assembly can fit in an AP1000 using these criteria. On the X-axis there is the pitch-over-diameter ratio (P/D) of the assemblies, and on the Y-axis there is the fuel pin diameter. I limited this parameter from 15 to 25 fuel rows per assembly, since below 15 rows results in too high of power per pin (thermal issue) and above 25 rows results in too thin of cladding (corrosion issue). In Figure 5.2b, one can see the core surface with these geometric parameters. The black regions represent the combination of pitch and number of rows that can not be fitted within an AP1000 core.

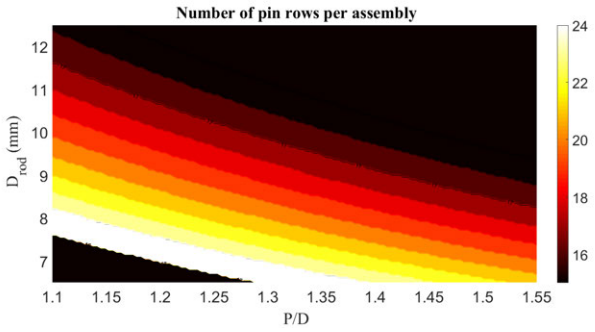

(a) Number of pin rows per assembly in MATLAB script

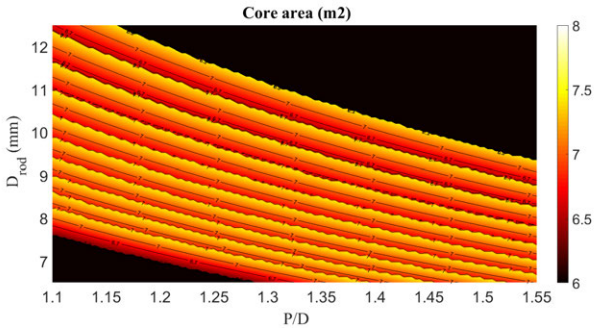

(b) Surface of the core in MATLAB script

Figure 5.2: Number of pin rows per assembly and core area when imposing an area constraint and a 157 assembly constraint for these pin diameters and pitch over diameter ratios

In the MATLAB-VIPRE interface, the core is built assembly by assembly starting from the center, and matches the core surface with a 5 per cent tolerance. In Figure 5.3a, one can see the number of fuel pin rows per assembly so that the assembly can fit in an AP1000 using this criterion. This method yields the core surfaces in Figure 5.3b.

In order to fit a new assembly design into a previously existing AP1000, one would need the assembly dimensions to be exactly the same. By selecting a fuel pin diameter or a pitch to diameter ratio close to the optimized values chosen, backfit capabilities can be achieved, and have similar performances to what is shown with an approximate geometry.

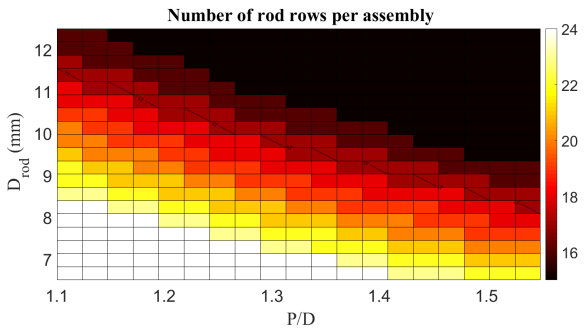

(a) Number of pin rows per assembly in VIPRE-MATLAB interface. The X axis is the pitch on diameter ratio, the y axis the pin diameter and the color indicates the number of pins

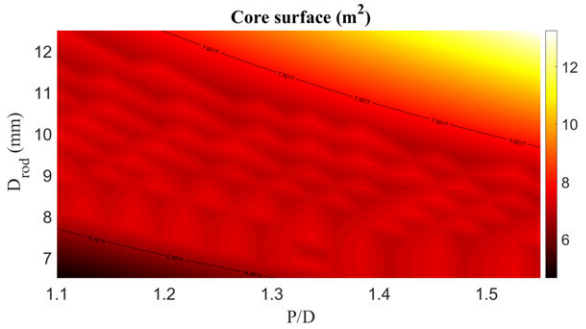

(b) Core surfaces in VIPRE-MATLAB interface

Figure 5.3: Number of pin rows per assembly and core area when imposing an area constraint and a 157 assembly constraint for these pin diameters and pitch over diameter ratios in the VIPRE-MATLAB interface

In VIPRE, in order to save computational ressources, non-peaking subchannels are lumped together. The methodology, developed by J. Malen [26], was implemented for 17 pin rows per assembly. For numbers of pin rows beyond 17, the user can either keep a constant number of unlumped channels (37 by default), and lump the rest of the channels in the core, or discretize one assembly, and lump the rest of the channels in the core. Both approaches have yielded similar results. The lumping of subchannels is shown in Figure 5.4 and 5.5.

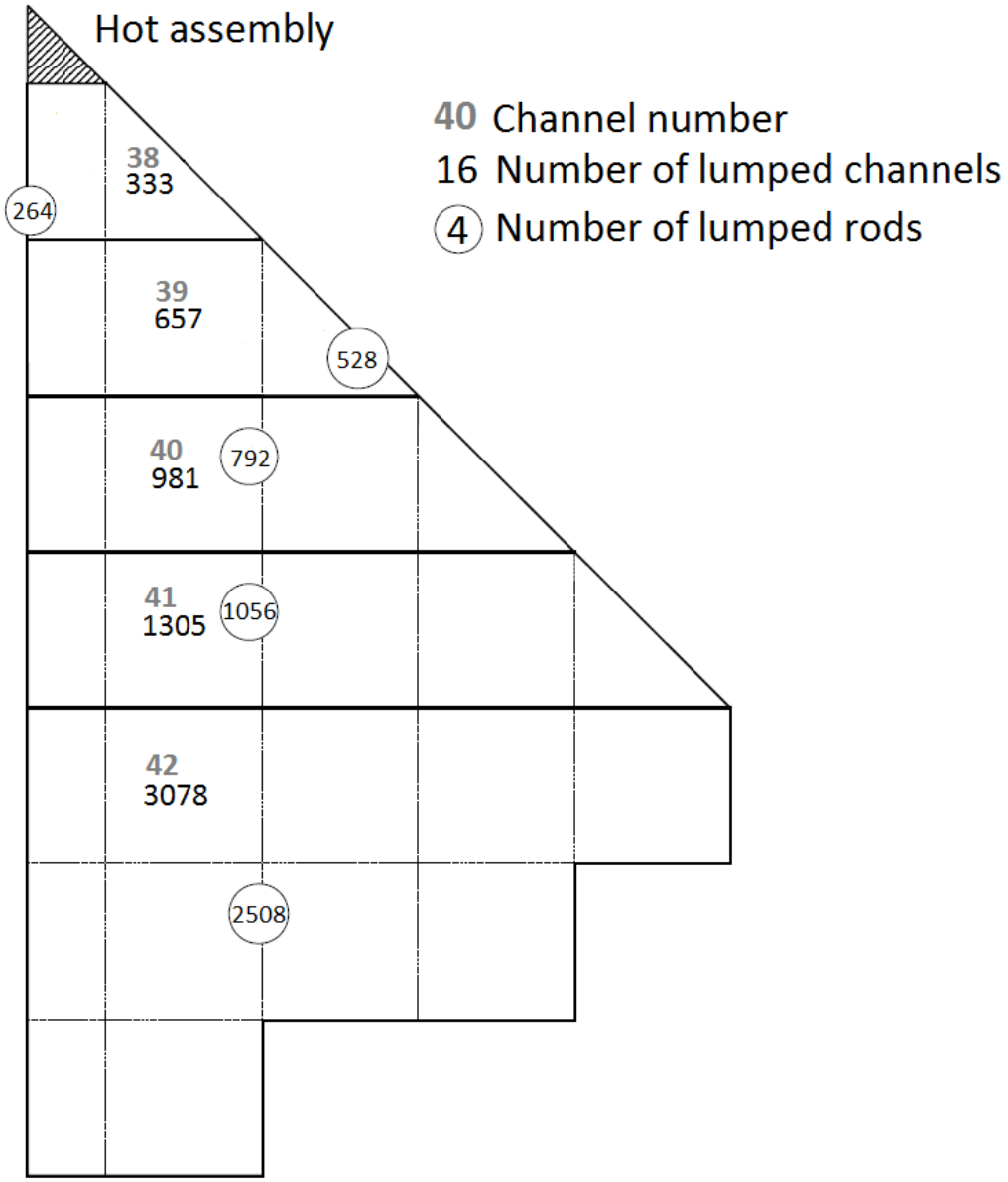

Figure 5.4: Lumping of most channels and rods in an AP1000-like core for use in VIPRE. Only the hot assembly is discretized

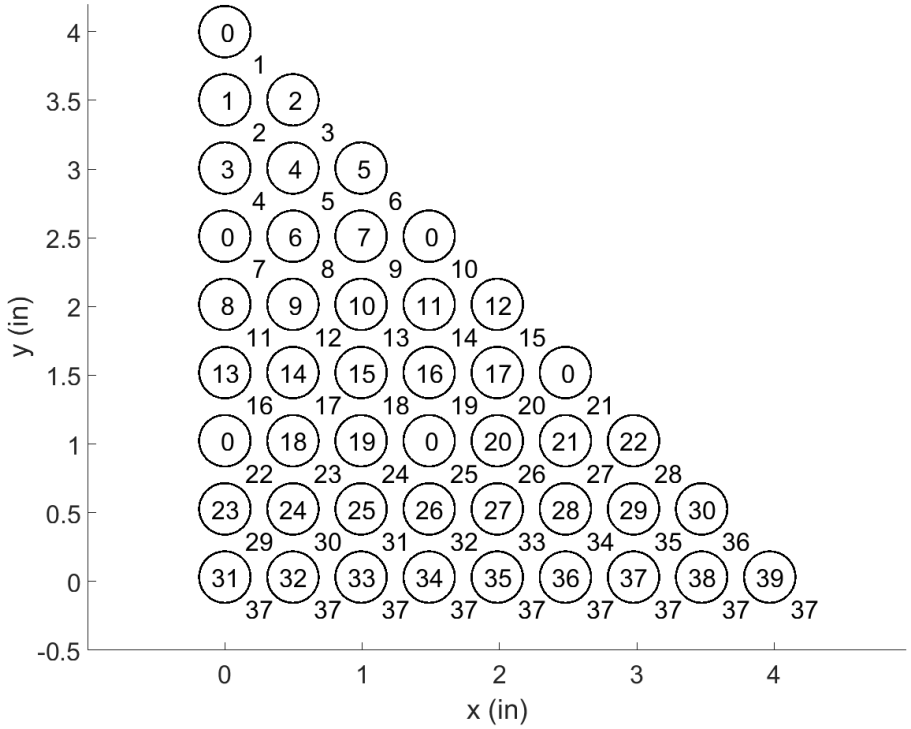

Figure 5.5: Discretization of the hot assembly in VIPRE. Only an eighth is modeled thanks to symmetries. Rod numbers are inside the rods, channel numbers outside. 0 indicates guide tubes for control rods. Channel 37 is the water gap, in contact with all lower rods and a lumped rod below.

5.3 Heat transfer mechanisms and correlations

In a regular PWR, in the hottest subchannel, the water enters subcooled at the bottom on the channel. It is then heated by forced convection, up until a point where subcooled nucleate boiling appears. It normally doesn't undergo saturated nucleate boiling as it's equilibrium quality remains negative. In the MATLAB script, only forced convection is modeled using the Dittus-Boelter correlation [23]. This is conservative as forced convection is a less efficient heat transfer mechanism than saturated nucleate boiling, with the same mass flux and geometry.

In VIPRE, all the heat transfer mechanisms that could intervene are taken into account. For cores that are simulated beyond regular PWR conditions, and for which power will have to be lowered at the next iteration, saturated nucleate boiling and if needed film boiling are modeled. Forced convection is modeled using the Dittus-Boelter correlation [23, 25], subcooled and saturated nucleate boiling are modeled with the Thom+Single phase correlation [25], film boiling with the Groenveld 5.7 correlation [25] and critical heat flux is estimated with the EPRI correlation [25].

5.4 Steady-state design limits

The steady state design limits on the thermal-hydraulics and mechanical behavior of the fuel bundle are summarized in table 5.1. These constrain the maximum achievable core power for each geometry in the two optimization strategies. They were developed with guidance from industry and MIT faculty by J. Malen [26] to provide sufficient safety margins and technical feasibility. Apart from the fuel temperature, these design limits are not fuel-dependent. I will therefore often present the results only for nitride-fueled bundles, even though the oxide will perform the same.

Table 5.1: Summary of performance objectives for uprated cores

Performance	MATLAB tool limit	VIPRE-MATLAB interface limit
MDNBR (-)	2.99	2.41
Pressure drop in core (MPa)	0.185	0.136
Fuel average temperature (oxide, °C)	1400	1400
Fuel centerline temperature (nitride, °C)	1700	1700
Fretting wear ratio (-)	1	1
Sliding wear ratio (-)	1	1
Maximal equilibrium quality (-)	0	0

The following characteristics are assumed of the core in the MATLAB tool:

- Radial peaking factor of 1.4
- Pin peaking factor of 1.
- Cosine axial flux profile

More conservative assumptions are not assumed because as there is no communication with other channels, a higher peaking can easily cause saturated boiling.

In the VIPRE-MATLAB interface, Figure 5.6 represents the radial power distribution, and the axial power profile is taken as a cosine.

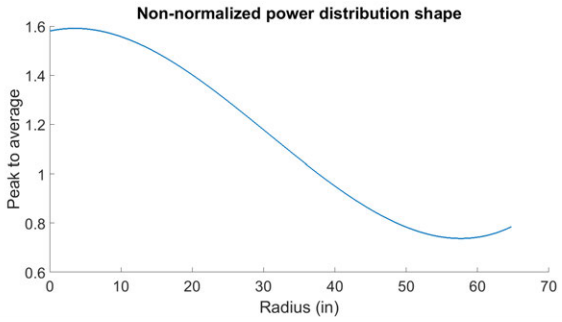

Figure 5.6: Radial power profile assumed in the VIPRE-MATLAB interface

5.4.1 Pressure drop in fuel bundle

As the AP1000 is already equipped with 4 of the largest pumps in the world, 7 meters high, 1.5 meters wide and around 91 tons, it is important for us to restrict the pressure drop in the core, in order not to propose an uprate that requires a pump head which will not be reached in the AP1000's lifetime.

Pressure drops in the core are created by friction between the coolant and the fuel rods, entrance and exit effects at the bottom and top of the core, and flow restrictions at the spacer grid locations. To model this phenomenon, for both tools, the Cheng and Todreas correlation [23] is used for the friction with the rods. For the spacer grids, the In model [23] is used. Four intermediate flow mixing grids are modeled between the four lower spacer grids. The mixing vanes on the IFMs and the spacers are modeled using the mixing coefficients from Chun and Oh [28].

The limit for pressure drop for all geometries is the **AP1000 performance in the core analysis script**.

Grid pressure drop correlations

Pressure drop at spacer grids are form drag-type pressure losses, and can be calculated using pressure loss coefficients. The pressure loss due to spacers is of the same order of magnitude as the pressure loss due to the friction along the rod.

Previously implemented in the script was Rehme's correlation : $\Delta p_s = C_v \cdot (\rho \cdot v_v^2/2) \cdot (A_s/A_v)^2$ With: C_v = modified drag coefficient, and v_v = average bundle fluid velocity away from the grid.

In square arrays, C_v varies from 9.5 at Re = 10^4 to 6.5 at Re = 10^5. This variation wasn't implemented.

For this thesis, the pressure drop model has been upgraded to a more recent correlation due to In [29]. This change was required to be able to model the pressure drop due to mixing vanes on the spacer grids, which the AP1000 possesses. The pressure drop is expressed using the velocity away from the grid.

$$\Delta p_{grid} = K_{grid}^{In} \cdot \frac{\rho v_v^2}{2} \tag{5.2}$$

The grid spacer loss coefficient K_{grid}^{In} is computed as the sum of three terms: the grid form loss, the grid friction loss and the rod friction loss within the spacer region. The first and third terms are of the same order of magnitude, one order of magnitude bigger than the second term. More details can be found in [23].

The effect of mixing vanes requires a fourth term [28]. This term is formulated by multiplication of an empirical form drag coefficient for abrupt flow blockage and a relative plugging of the flow cross-section by the mixing vanes [23]. It should account for around 15% of the pressure losses due to a spacer grid.

This correlation agreed within 10% of the experimental data used to validate it.

In Figure 5.7, 5.8a and 5.8b, I compare the pressure drops in the two models for the AP1000 grids and mixing vanes specifications. The Rehme pressure drop doesn't include the mixing vanes. The contribution of each term in the In and Chun pressure drop correlation is shown. The mixing vanes account for up to 30%

of the pressure drop, as compared with 15% mentioned in [23], because there are more mixing vanes than spacers, with four additional intermediary flow mixing grids. Figure 5.7 shows the In and Rehme pressure drops for the AP1000 nominal design, when varying the core power by changing the primary mass flow rate. The pressure drops vary quadratically with the mass flow in these correlations. The mixing vane pressure loss and the friction with the rod are the main pressure losses. In Figure 5.8a and 5.8a, I can see that the tighter the design the higher the pressure drop, and that the mixing vane effect is constant at a constant pitch over diameter ratio (P/D).

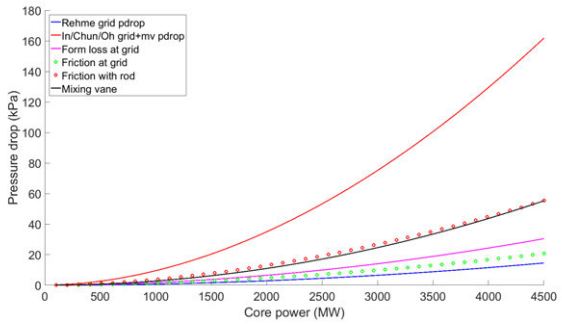

Figure 5.7: Pressure drop correlations in the AP1000 when varying the core power with the primary mass flow rate

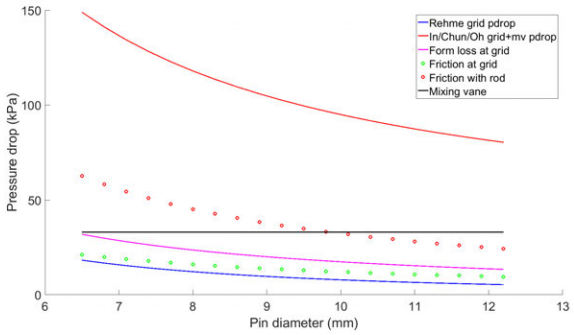

(a) Pressure drop correlations at a constant core power and pitch/diameter ratio, varying the pin diameter

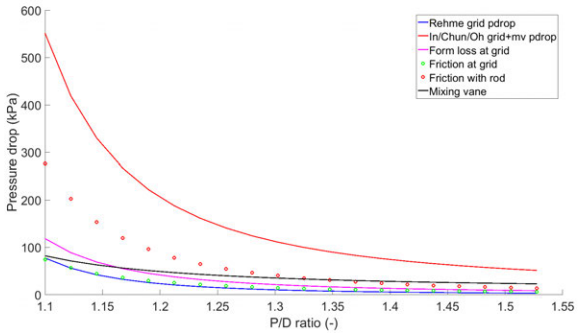

(b) Pressure drop correlations at a constant core power and pin diameter, varying the pitch on diameter ratio

Figure 5.8: Evaluating the pressure drop correlations' dependence on the channel geometry

5.4.2 Minimum departure to nucleate boiling ratio

The minimum departure to nucleate boiling ratio (MDNBR) is the ratio of the surface heat flux to the critical surface heat flux, at which the heat transfer mechanism switches from the efficient nucleate boiling to an inefficient film boiling. The cladding temperature then spikes, which can lead to cladding failure.

In both tools the W3L correlation [23] is used to determine the MDNBR. It is the W3 correlation developed by Westinghouse, improved to take into account the effects of L-type spacer grids. The following assumptions have been made in the MATLAB tool: no grid type modifier, a turbulent cross flow mixing parameter of 0.038 and a grid spacing parameter of 0.066. These values are conservative estimates [27]. In the VIPRE-MATLAB interface, I used the same parameters except a turbulent cross flow mixing parameter

of 0.042.

The limit for MDNBR for all geometries is the **performance of the nominal AP1000** in each code's model.

The non-uniform W3-L correlation

The W3 correlation is the most widely used in PWRs for the evaluation of DNB conditions. It can be applied to circular, rectangular and rod-bundle geometries. It was developed for axially uniform heat flux, but a correcting factor can be applied to account for non-uniform heat fluxes [23].

For an axially uniform heat flux, the critical heat flux is:

$$\begin{aligned} q''_{cr,u} = (2.022 - 0.06238p) + (0.1722 - 0.01427p)exp[(18.177 - 0.5987p)x_e] \\ [0.1484 - 1.596x_e + 0.1729x_e|x_e|)2.326G + 3271][1.157 - 0.869x_e][0.2664+ \\ 0.8357exp(-124.1D_e)][0.8258 + 0.0003413(h_f - h_{in})] \end{aligned} \tag{5.3}$$

where q_{cr} is in kW/m^2; p is in MPa; G is in kg/m^{2}s; h is in kJ/kg; and D$_e$ is in m, and the correlation is valid in the ranges:
-p (pressure) = 5.5–16 MPa
-G (mass flux) = 1356–6800 kg/m2s
-D_e (equivalent diameter) = 0.015–0.018 m
-x_e (equilibrium quality) = -0.15 to 0.15
-L (heated length) = 0.254–3.70 m
-the ratio of heated perimeter to wetted perimeter = 0.88–1.0.
Here the heated length validity range is exceeded with the 14ft/4.26m AP1000 assemblies. However as one can see the heated length parameter isn't in the critical heat flux formula, and a strong variation with this parameter is not expected so it is safe to extrapolate to 4.26m.

For a non-uniform axial heat flux, the uniform critical heat flux is divided by a factor F, $q_{cr,nu} = \frac{q_{cr,u}}{F}$.

$$F = \frac{C\int_0^Z q''(Z')\exp(-C(Z-Z'))\mathrm{d}Z'}{q''(Z)(1-\exp(-C(Z)))} \tag{5.4}$$

With C an experimental coefficient describing the heat and mass transfer effectiveness at the bubble-layer/subcooled-liquid–core interface.

Here, this integral can be integrated analytically because a cosine-shaped axial heat flux profile is assumed.

$$\int_0^Z q''(Z')\exp(-C(Z-Z'))\mathrm{d}Z' = (\frac{q'_{max}}{\pi D_{pin}})\frac{-\frac{\pi}{L}\cos(\frac{\pi Z}{L}) + C\sin(\frac{\pi Z}{L}) + \frac{\pi}{L}\exp(-CZ)}{(\frac{\pi}{L})^2 + C^2} \tag{5.5}$$

5.4.3 Fuel temperature

For oxide fuels, in order to keep fission gas release below 5%, I limit the average temperature to 1400°C [27]. Uranium oxide melts at 2800°C, and the fuel temperature peaks at the centerline, but limiting the fuel temperature to below 2800°C at the centerline is less restrictive than the previous criterion on the fuel average temperature.

For nitride fuels, current data on fission gas release shows limited fission gas release [7]. However, uranium nitride dissociates at 1700°C, this was chosen as the limit on the peak centerline temperature. In the MATLAB script, I assumed the materials thermal conductivity to be constant with temperature, and neglected the presence of an oxide film. I also only considered forced convection as a heat transfer mechanism. In PWRs, subcooled nucleate boiling appears in many channels, but since it is a more efficient heat transfer mechanism, only considering forced convection is a conservative assumption. The fuel centerline temperature is then:

$$T_{cl}(z) = T_{inlet} + q'_0[\frac{L_h}{\pi \dot{m} c_p}(\sin\frac{\pi z}{L_h} + \sin\frac{\pi}{2L_h}) + (\frac{1}{2\pi R_{co} h} + \frac{1}{2\pi k_c} log(\frac{R_{co}}{R_{ci}}) + \frac{1}{2\pi R_{gap} h_{gap}} + \frac{1}{4\pi k_f})\cos\frac{\pi z}{L_h}] \quad (5.6)$$

with q'_0 such that the lineic power is $q'_0 sin\frac{\pi z}{L_h}$, L_e the heated length, $\dot{m}$ the mass flow rate, c_p the fluid thermal capacity, R_{co} the cladding outer diameter, R_{ci} the cladding inner diameter, k_c the cladding thermal conductivity, $R_{gap} = \frac{R_{ci} + R_f}{2}$, R_f the fuel pellet radius and k_f the fuel thermal conductivity. The fuel thermal conductivity is taken constant. The error on fuel temperature is around 200°C, when comparing to VIPRE. This is significant, but in the regions that allow for an uprate, designs with smaller pins, this design limit not to be limiting

In the VIPRE MATLAB interface, the variation of thermal conductivity with temperature for uranium nitride, and oxide (default VIPRE) was taken into account, in Figure 5.9. Nitride fuel thermal conductivity is discussed more in detail in annex 1.

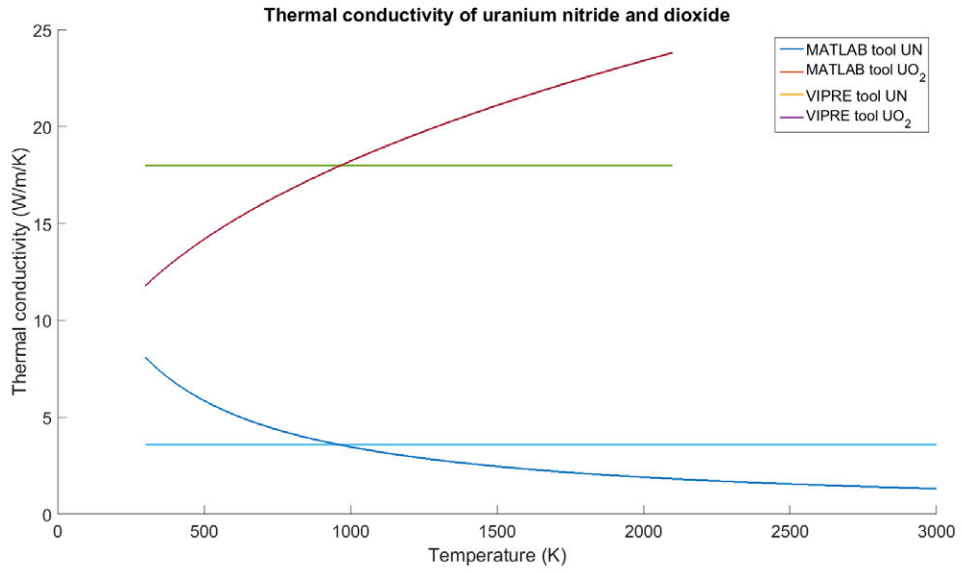

Figure 5.9: Thermal conductivity of uranium nitride and oxide in the two tools

5.4.4 Equilibrium quality

While subcooled nucleate boiling is allowed as a heat transfer mechanism in PWRs in the US, saturated nucleate boiling is not. In MATLAB only one channel is modeled. Therefore all heat added to this channel remains within the channel. If the channel power is too high, the coolant in the channel will boil. This limits the pin peaking factor to 1, which is not conservative.

In the VIPRE-MATLAB interface, there was no criterion on channel saturated boiling implemented. I implemented one, and because cross-flows between channels are modeled, I could model realistic pin peaking. VIPRE outputs the channel equilibrium quality and the power was lowered for all designs until it was beneath zero.

5.4.5 Fretting wear

Fuel rods are initially held tight by the ten spacer grids along the fuel bundle. But as springs are exposed to a high neutron fluence, the springs get looser and fretting appears at the spacer grid locations. Fretting results from combined rubbing and impaction between the fuel rod support and the cladding surface. This can wear out the cladding and eventually cause leakage of fission gases into the coolant. This mechanism is responsible for 65% of fuel failures in the US [30].

For the vibrations due to axial flow, the Paidoussis correlation was used, and for the vibrations due to cross-flow, the Pettigrew and Goreman correlations were used, described in [27, 31] and below. The MATLAB tool assumes the cross-flows in the core to be proportional to the core power, and constant axially. The VIPRE-MATLAB interface uses the cross-flows output by VIPRE. The VIPRE-MATLAB interface has a stronger scaling of fretting wear with core power than the MATLAB tool.

The limit for fretting wear and sliding wear for all geometries is the **performance of the nominal AP1000** in each code's model.

Fretting wear models: how to quantify fretting wear

It is very difficult to quantify a wear rate, so it is assumed that fretting wear to be proportional to the power dissipated by the vibrating rod [31]. Only the first vibration mode is considered. The power dissipated by the first vibration mode is:

$$\dot{W}_{fretting} = 32 \cdot \pi^3 \cdot \xi_1 \cdot f_1^3 \cdot L_s \cdot m_t \cdot y_{rms}^2 \tag{5.7}$$

I assumed that the wear rate is independent of time. This is not conservative as vibrations can increase when the cladding is slightly worn, or if the springs relax with irradiation. To determine this time-dependence accurately, one would need to model the cladding-grid interaction very finely, with a finite element code. However, it is the industry's belief that after a short period of break-in, the wear-rate is somewhat constant for most of its life, until they get close to failure [27]. Because the reference design, the AP1000 fuel pins, should withstand fretting wear, any design with a lesser fretting wear rate in this semi-permanent regime should be more likely to resist.

The total wear is then $Q = \dot{W}_{fretting} \cdot K_{rod} \cdot T$, with K_{rod} a coefficient which I'll assume to only depend on the materials and not on the geometry, and T the time the assembly spends in the core. To qualify a design's fretting wear, the script compares

$$\frac{Q_{new-design}}{Q_{nominal}} = \frac{\dot{W}_{\text{fretting, new design}} \cdot K_{rod} \cdot T}{\dot{W}_{\text{fretting, nominal}} \cdot K_{rod} \cdot T} \tag{5.8}$$

Here the cycle length is kept constant between the designs, as only uprates were investigated, not longer cycle lengths, and K_{rod} was assumed to only depend on the cladding and grid materials.

$$\frac{Q_{new-design}}{Q_{nominal}} = \frac{(32\pi^3 \xi_1 f_1^3 L_s m_t y_{rms}^2)_{new-design}}{(32\pi^3 \xi_1 f_1^3 L_s m_t y_{rms}^2)_{nominal}} = \frac{(f_1^3 L_s m_t y_{rms}^2)_{new-design}}{(f_1^3 L_s m_t y_{rms}^2)_{nominal}} \tag{5.9}$$

The damping ratio, ξ_1, is assumed to be constant. The fluid is the same in the two cases, but the spring's constant and the linear mass of the rod are different, so this hypothesis is made mainly to simplify the model. L_s or δ_{grid} is the distance between spacers, which can vary in my study.

The rod first natural frequency can be found by considering that the rod vibration amplitude is null where the rod is held, at every spacer grid.

$$f_1 = \frac{\pi}{2\delta_{grid}^2} \sqrt{\frac{E_{mod,clad} I}{m_t}} \tag{5.10}$$

E is the young modulus of the cladding, I the inertia moment and m_t the lineic mass.

Fretting wear models: sources of vibration

The rod vibration can be caused by turbulence in parallel flow and in the cross-flow because as it creates random pressure fluctuations around the rod. Turbulence is a random phenomenon and it is convenient to measure the displacements they cause by the root mean square response. I then assume that the total rms displacement is the sum of the response to cross flow induced vibrations and the response to axial flow induced vibrations.

$$y_{rms}^{total} = y_{rms}^{axial} + y_{rms}^{cross} \tag{5.11}$$

According to Au-Yang [31] the RMS rod response to cross-flow turbulence can be written as :

$$\langle y^2(x) \rangle = \sum_{\alpha} \frac{L_s G_p(f_\alpha) \psi_\alpha^2(x) J_{\alpha\alpha}(f_\alpha)}{64\pi^3 m_t^2 f_\alpha^3 \xi_\alpha} \tag{5.12}$$

with α the mode index, $J_{\alpha\alpha}$ the "joint acceptance", L_s the correlation length, G_p the random pressure power spectral density (PSD), $\psi_\alpha(x)$ the mode shape and m_t the linear mass. The joint acceptance is the probability that a structure originally vibrating in the nth mode will remain in the nth mode under the excitation of the forcing function. Only the first mode is considered, and J_{11} was taken to be 0.64 for a simply supported tube or $\frac{2\lambda}{L_s}$ for a bundle [31]. The correlation length is assumed to be equal to the distance between two spacers. Indeed, the cross-flow is uncorrelated between above and below a spacer, as one can

see when plotting cross-flows in VIPRE.

The random PSD was determined through experiments to be:

$$G_p = C_R D(\frac{1}{2}\rho_{fl} V_{cross}^2)^2 \tag{5.13}$$

C_R is a random lift coefficient, found in [31].

For axial flow turbulence induced vibration, the Paidoussis correlation [31] is used:

$$y_{max,axial} = 5e - 5DK\alpha^{-4}(\frac{u^{1.6}\epsilon^{1.8}Re^{0.25}}{1+u^2})(\frac{D_h}{D})^{0.4}(\frac{\beta^{0.67}}{1+4\beta}) \tag{5.14}$$

with

- K = 5 for turbulent flow
- $\alpha = \pi$ for simply supported rods
- $u = V_{axial} L_s \sqrt{\frac{\rho_{fl} A_o}{E_{cl} I_{cl}}}$
- V_{axial} peak axial velocity
- A_o outer rod cross sectional area
- $\epsilon = L_s/D$
- Re Reynold's number
- D_h: hydraulic diameter
- $\beta = \frac{\rho_{fl} A_o}{m_t}$
- ρ_{fl} coolant density
- m_t total linear mass

The rod response distribution is assumed to follow a normal distribution, in which case the RMS response is close to a third of the maximum value. $y_{rms,axial} = \frac{y_{max,axial}}{3}$

5.4.6 Sliding wear

Sliding, or adhesive, wear occurs where the grid support springs and rod rub against one another in a sliding movement. Connor's model, described in [27, 31], is used. The sliding wear rate is equal to the product of the normal contact force between the rod and support spring, F_n and the total sliding distance, S_d.

$$\dot{W}_{sliding} = F_n \cdot S_d \tag{5.15}$$

$$F_n = \frac{3\pi D y_{rms}}{\mu(\frac{L_s}{A_{cl}E_{cl}} + \frac{D^2 L_s^2}{E_{cl}I_{cl}})} \tag{5.16}$$

with μ a friction coefficient and A_{cl} the cladding cross-sectional area.
The sliding distance S_d is given by $\pi f_1 g$, with g the diametral gap between the cladding and the support.

The cumulative sliding wear at time T is

$$Q_{sliding} = K_{rod} \cdot \dot{W}_{sliding} \cdot T = K_{rod} \cdot F_n \cdot \pi \cdot f_1 \cdot g \cdot T \tag{5.17}$$

5.5 Algorithm optimization

If a design cannot accommodate a higher power than 1,000 MW and the script tries all core powers starting at an initial guess of 5,000 MW by steps of 100 MW, then the script is going to take 40 iterations to find the design's maximal power of 1,000 MW. However, if the initial guess is 1,400 MW instead of 5,000 MW, then the script will only take 4 iterations to find the design's maximal power of 1,000 MW, a reduction by a factor of 10 of computation time.

So instead of a uniform initial guess for the core power, the idea is to change the initial guess based on previous calculations. By running the script on a coarse grid for the geometrical parameters and saving the results, I can then make good initial guesses that will help us compute very quickly a much finer grid over the same parameter ranges.

If the initial guess is too low, despite taking some margin, then the code reports it, and the user can retry with a higher margin, or update the initial guess function and then retry. This approach, and changing serial calculations into vector calculations in MATLAB each allowed for a factor of ten reduction in computation time.

5.6 Original contributions

5.6.1 MATLAB core design script

- I implemented a new strategy to increase the core power, by reducing the core inlet temperature at a constant mass flow rate
- I created a 'trends' mode, to run all geometries at a fixed power and see what the trends are for the various performances (mDNBR, pressure drop, fuel temperature...)
- I created a 'nominal' and a 'selected core' mode, to run the nominal geometry or a given geometry from an outside file with minimal changes to input parameters
- I replaced the Rehme spacer grid pressure drop model by the In model, in order to be able to model the mixing vanes with the additional Chun and Oh model
- I created a module that assigns a number of pins per assembly when the pin diameter and pitch on diameter ratio have been chosen. It tries to conserve the core area.
- I implemented the W3-L correlation to take into account the effect of spacer grids on mDNBR
- based on the VIPRE results, the correlation used to determine cross-flow in the fretting and sliding wear analysis was modified.

- I vectorized all calculations, and pre-allocated arrays, gaining a factor of 10 on calculation time
- I solved analytically the non-uniform W3-L factor's integral, which was previously done numerically in all 43 axial nodes of the subchannel, diminishing by a factor of 100 the calculation time
- the algorithm optimization mentioned in the previous section

5.6.2 VIPRE-MATLAB interface

- I added the number of spacer grid as a simulation parameter
- I implemented an alternative strategy to raise the core power : rather than raise the primary mass flow rate, I lower the primary inlet temperature
- I created a 'nominal' and a 'selected core' mode, to run the nominal geometry or a given geometry from an outside file with minimal changes to input parameters
- I changed the core assembly pattern, to fit the AP1000 core shape
- I changed the way the core power was distributed among pins, to avoid excessive peaking
- I changed the correlations for heat transfer mechanisms back to the VIPRE default ones, which are more numerically stable, with less exponential terms
- I enabled different assembly sizes, not just 17 pin rows but from 15 to 25 pin rows per assembly

Chapter 6

Geometry Optimization Results

6.1 Trends for core performances

In this section, I will present the performance of all the considered geometries in this study, with an AP1000 core shape. I will consider only the case with 10 spacers. This allows us to visualize the effects of the geometry on the core thermal-hydraulic and mechanical behavior. It also allows to compare the MATLAB script to the VIPRE-MATLAB interface. They will be presented as color maps. The color indicates the performance (power, pressure drop...) of a given geometry.

6.1.1 Linear power at constant core power

Linear power is a determining factor for MDNBR and fuel temperature. It depends on the number of pins and the core power for a given fuel height. I plot it on Figure 6.1a and 6.1b assuming 264 fuel rods every 289 rods. The more numerous the fuel rods, the lower the linear power. The pitch, product of P/D and diameter, defines the number of pins at constant surface. The layers are due to the discrete values of the number of pin rows per assembly.

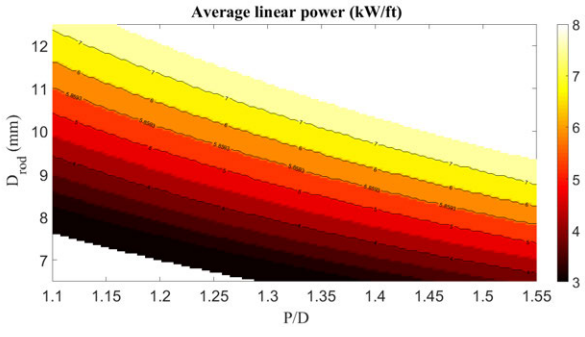

(a) Linear power at constant core power in MATLAB tool

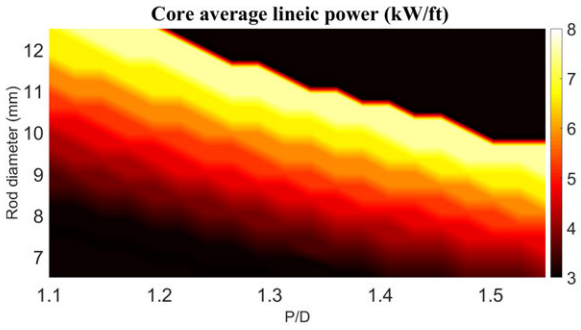

(b) Linear power at constant core power in VIPRE-MATLAB interface

Minimum Departure from Nucleate Boiling Ratio

Figure 6.2 presents the trend for the evolution of the MDNBR at a constant power, taking into account the geometry constraints. One can see that the lowest MDNBRs, the closest to the limit, are for high pitches and large pins. In fact, the first order influence of MDNBR is clearly the core average linear power, which is expected.

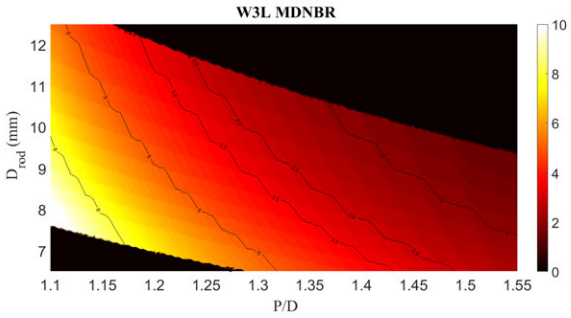

Figure 6.2: MDNBR for constant power over a range of geometries, MATLAB tool

6.1.2 Pressure drop across the fuel bundle

Figure 6.3 shows the trend for the evolution of the pressure drop at a constant power, taking into account the geometry constraints. It appears that the tighter the designs, the larger the pressure drop. There is also a change in pressure drop induced by the number of pin rows.

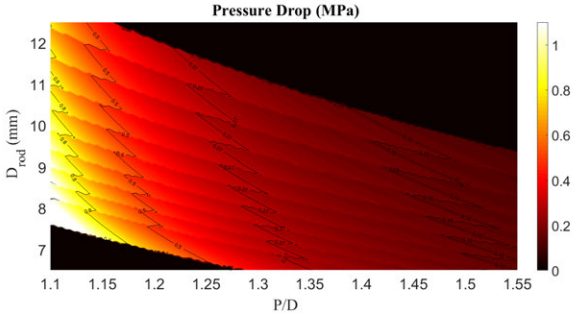

Figure 6.3: Pressure drop for constant power over a range of geometries, MATLAB tool

6.1.3 Fuel temperature

Figure 6.4a shows the average fuel temperature at a constant reference power (3400 MW_{th}) for the peaking pin in an oxide-fueled core, in an AP1000 geometry. The number of pins is not constant. Figure 6.4b shows the fuel centerline temperature in the peaking pin of a nitride-fueled cores for the same power. Larger pins are the hottest. The bigger the P/D ratio, the lower the amount of fuel pins, and therefore the higher the pin power and temperature. Overall, it seems unlikely that a fuel temperature constraint will limit an uprate for nitride fuels, but that is possible for oxide fuels.

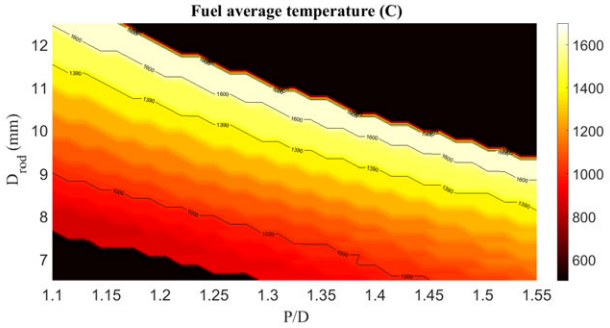

(a) Average fuel temperature of oxide-fueled pins in matlab tool with AP1000 surface constraints

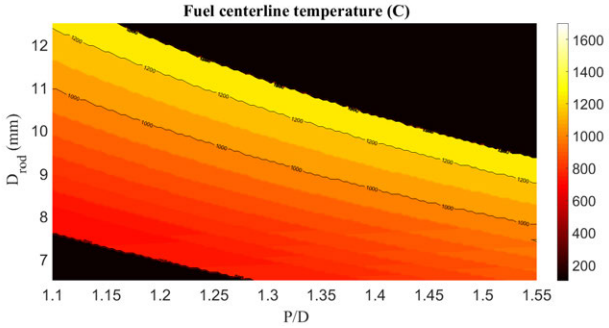

(b) Fuel centerline temperature of nitride-fueled pins in matlab tool with AP1000 surface constraints

6.1.4 Fretting wear

Figure 6.5 shows the trend for the evolution of the fretting wear at a constant power, taking into account the geometry constraints. The tighter the pitch and the smaller the pins, the stronger the fretting wear is. We can also see the variation in fretting wear that the change of the number of pin rows per assembly induces seems to be significant, which may induce discontinuities in the power maps.

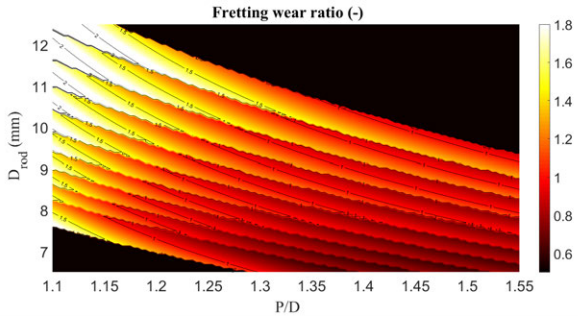

Figure 6.5: Fretting wear for constant power over a range of geometries, MATLAB tool

6.1.5 Sliding wear

Figure 6.6 presents the trend for the evolution of the sliding wear at a constant power, taking into account the geometry constraints. Similar to fretting wear, the tighter the pitch and the larger the pins, the stronger the sliding wear is. The variation in sliding wear that the change of the number of pin rows per assembly induces seems to be significant, which may induce discontinuities in the power maps.

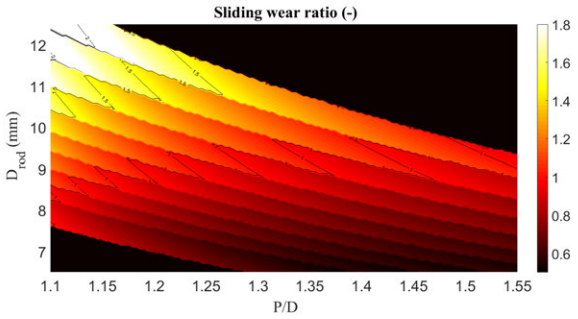

Figure 6.6: Sliding wear for constant power over a range of geometries, MATLAB tool

6.2 Geometry optimization for power uprates

In this section we will present the results for the geometry optimization to achieve a maximum core power.

6.2.1 Optimization strategy 1: Increasing mass flow rate

Figure 6.7a and 6.7b show the maximum achievable power using nitride fuels in the strategy involving an increase of the primary mass flow rate. Both tools predict a uprate of 400 MWth. Comparing the limits in Figure 6.8 and 6.9, it appears that the fretting wear and the MDNBR are more limiting in the VIPRE-MATLAB interface, and the pressure drop is more limiting in the MATLAB tool, but both tools are in general agreement. I expect that the fuel temperature limit is not reached on the relevant domain.

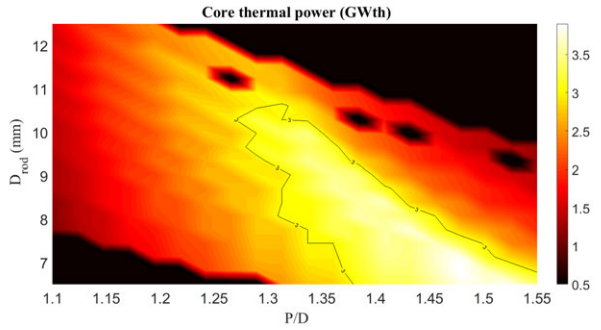

(a) Maximum achievable power with uranium nitride fuel in strategy 1 using MATLAB tool

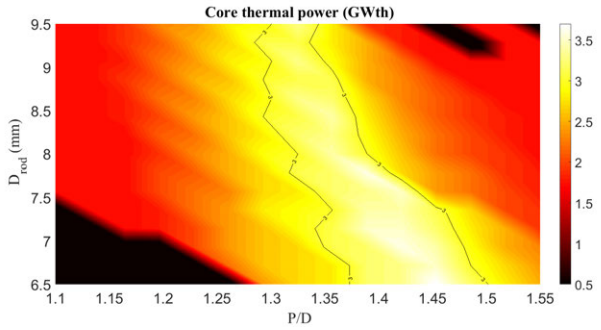

(b) Maximum achievable power with uranium nitride fuel in strategy 1 using VIPRE-MATLAB tool

In Figure 6.8 presenting the cores' performances in the MATLAB tool, MDNBR is limiting for designs with high pitches, the iso-MDNBR are at constant pitch size. Pressure drop is limiting for lower pitches and fretting wear for intermediate pitches. Fuel centerline temperature is never limiting. The same conclusions can be drawn for the VIPRE-MATLAB interface in Figure 6.9.

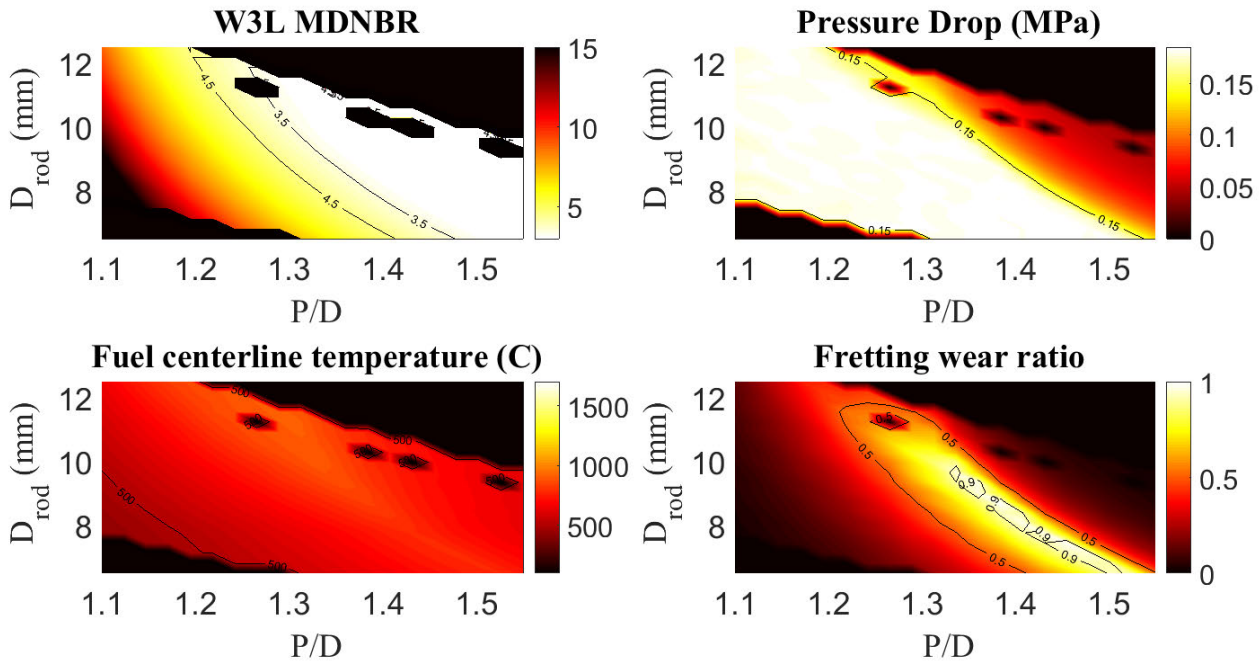

Figure 6.8: Thermal hydraulic and mechanic performances of maximum power cores, MATLAB tool

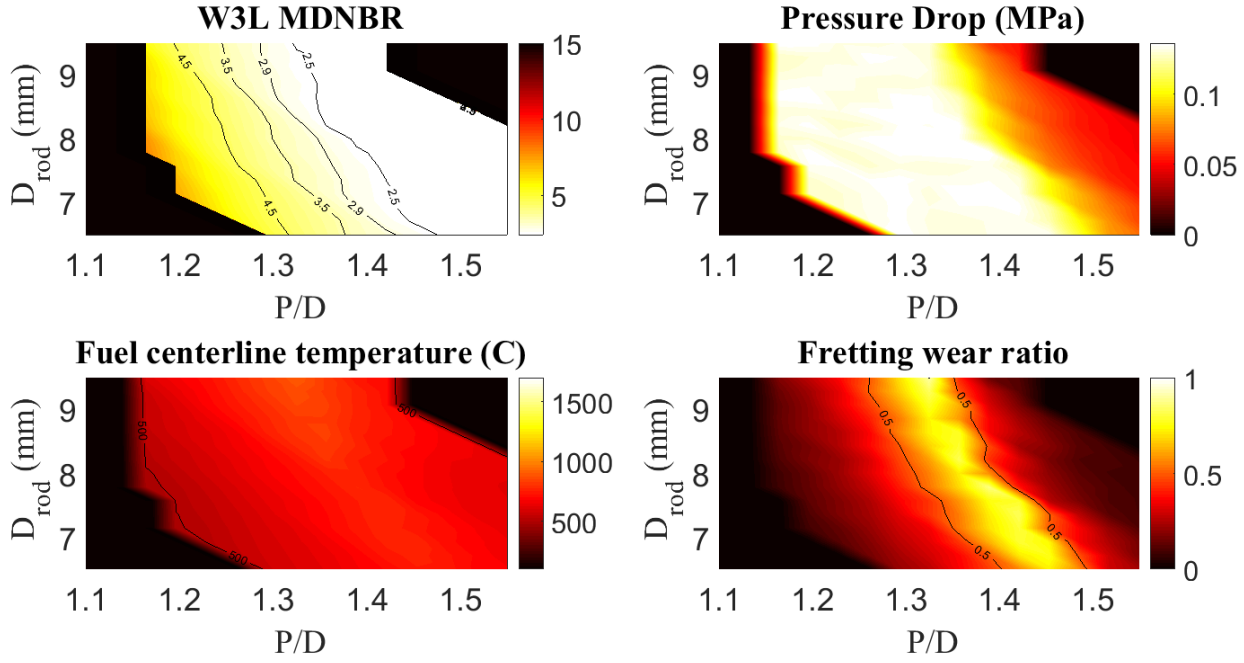

Figure 6.9: Thermal hydraulic and mechanic performances of maximum power cores, MATLAB-VIPRE interface

6.2.2 Optimization strategy 2: Decreasing core inlet temperature

In this strategy the possible uprate is limited to 1.4 GW_{th}, or an inlet temperature of 257°C. This is because the steam cycle assumed breaks down at this core inlet temperature. However no geometry reach this limit

in the MATLAB script, see Figure 6.10a and in the VIPRE-MATLAB interface, see Figure 6.10b.

The dark zones are for some geometries due to incompatibilities between the pin geometry and the AP1000 core shape with assemblies having from 15 to 24 pin rows. For other geometries, the absence of viable power is due to the fact that in this strategy, the core mass flow rate is the nominal mass flow rate, and this choice makes for a high fretting wear or pressure drop for some geometries. Therefore, for all inlet temperatures, a core with those geometries doesn't meet the limits.

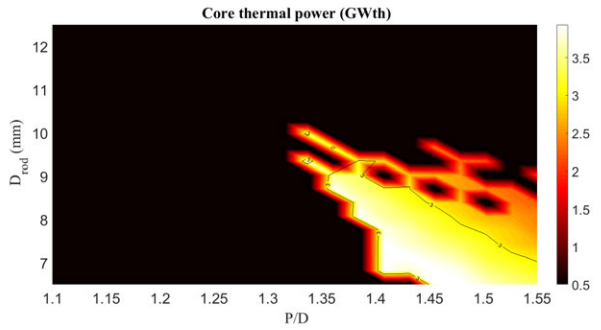

(a) Maximum achievable power with uranium nitride fuel in strategy 2 using MATLAB tool

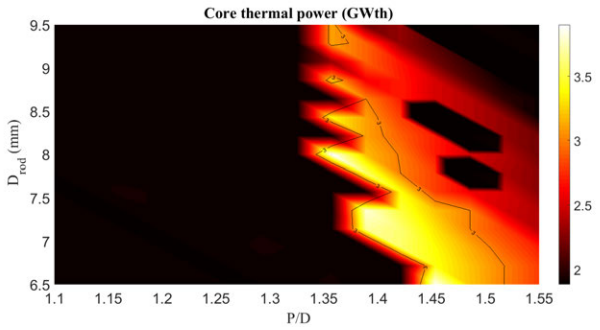

(b) Maximum achievable power with uranium nitride fuel in strategy 2 using VIPRE-MATLAB interface

Figure 6.11 shows that in the MATLAB tool the MDNBR is the limiting factor for most designs, and that pressure drop is also limiting for some optimal designs. Fuel centerline temperature is not limiting. In Figure 6.12 indicates that with the VIPRE-MATLAB interface, fretting wear is the most limiting. MDNBR is also close to the nominal performance for designs with the highest power. This was to be expected because the dependence of fretting wear on the core inlet temperature is very weak.

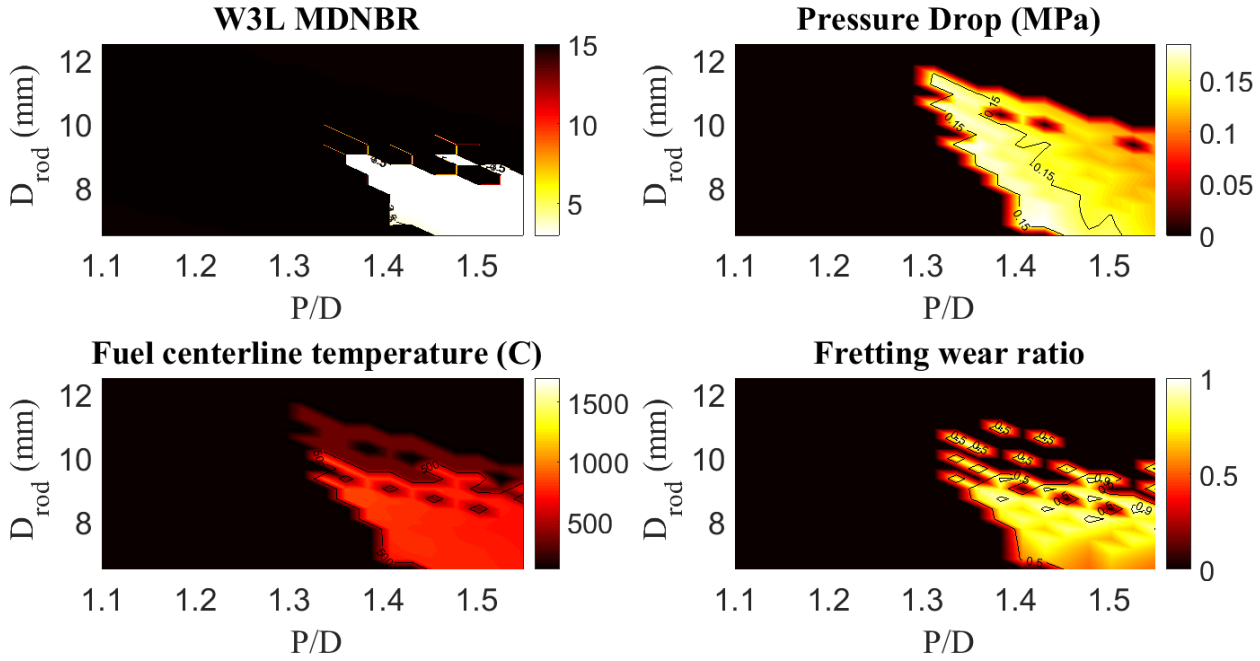

Figure 6.11: Thermal hydraulic and mechanic performances of maximum power cores with nitride fuel, MATLAB tool

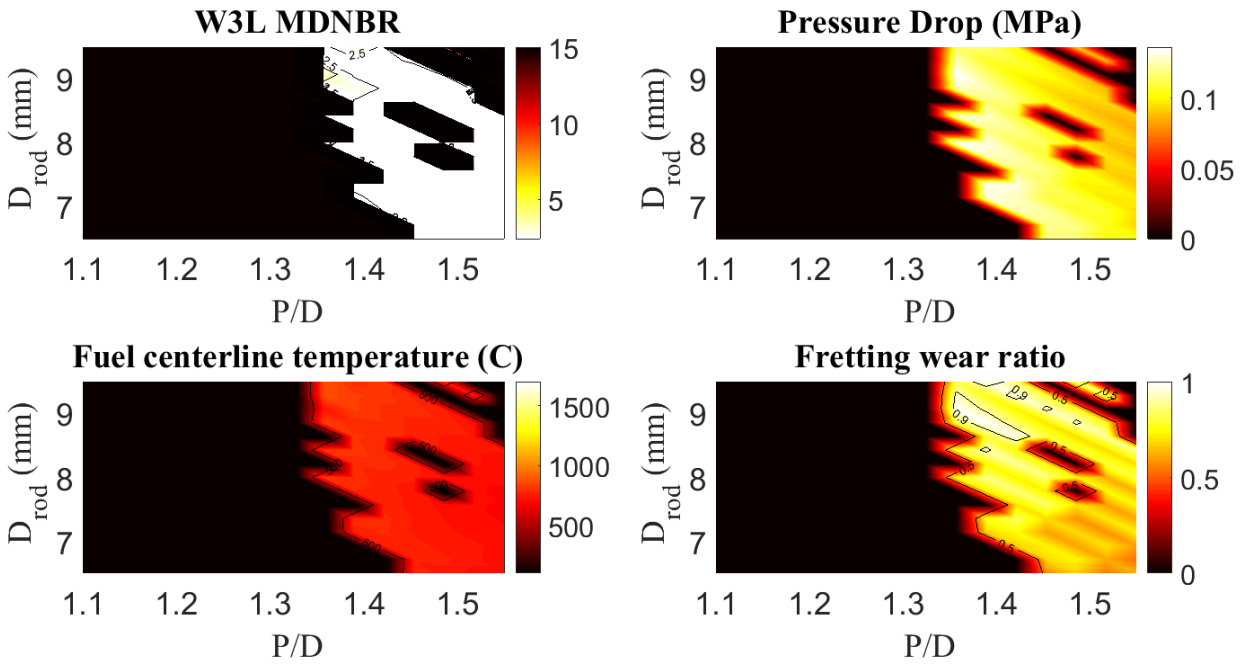

Figure 6.12: Thermal hydraulic and mechanic performances of maximum power cores with nitride fuel, MATLAB-VIPRE interface

In this strategy, in order to increase the core thermal power, I have modified the core inlet temperature. In order for heat to be transferred from the primary loop to the secondary loop, I need to make sure that the steam generator operating temperature is still lower than the core inlet temperature. This strategy forces a lower steam generator temperature, therefore a lower steam generator saturation pressure, and modifies the thermodynamic efficiency of the power conversion system. I will study this effect in the next section.

6.3 Effects on steam cycle of modifying the core inlet temperature

6.3.1 Core inlet temperature optimization strategy

In the power optimization strategy involving lowering the core inlet temperature, the steam cycle should be modified. Indeed, the heat transfer in the steam generators is driven by the temperature difference between the primary and secondary loops. If the primary fluid has to exit the steam generator at a lower temperature, then the secondary fluid also has to be at a lower temperature. Since the steam generator turns the secondary fluid from liquid to vapor, this means that the saturation pressure, or steam generator steam pressure, will have to be lower. This will lower the steam cycle thermodynamic efficiency.

6.3.2 First order estimate of change in secondary loop operating parameters

Nuclear power plants use a Rankine cycle to convert the heat produced by the core into electricity. In Figure 6.13, we can see that the primary fluid is heated by the core, then flows into a steam generator, in

which it evaporates a secondary fluid, before going back into the core through a pump. The secondary steam will condense in a turbine, producing electricity.

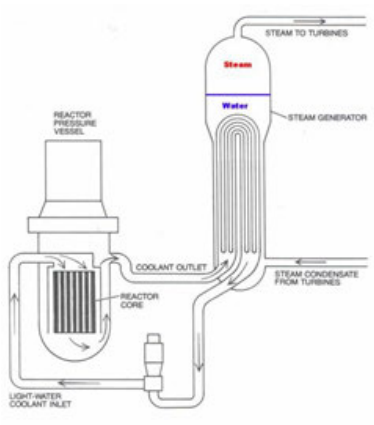

Figure 6.13: Flow pathways of primary and secondary loops [4]

In the steam generator, the primary fluid flows in tubes, surrounded by the secondary fluid, which heats up, and then boils into steam. In the primary loop, the heat transfer mechanism is convection, in the tube it's conduction through the metal and in the secondary system it's nucleate boiling.

The flow of heat energy per unit area can be approximated by

$$\ddot{q} = \frac{\Delta T}{\frac{r_i \log(\frac{r_o}{r_i})}{k} + \frac{1}{h_p(\dot{m}_p, T_p, P_p)} + \frac{1}{h_s(\dot{m}_s, T_s, P_s)}} \tag{6.1}$$

with ΔT the temperature difference between the primary core inlet and the secondary steam, k the tube thermal conductivity, r_i and r_o the tube inner and outer radii, h_p the heat transfer coefficient in the primary fluid, and h_s the heat transfer coefficient in the secondary fluid. Nucleate boiling and conduction in a metal are more effective heat transfer mechanism than convection in a single phase flow.

At first order, I can further approximate the flow of heat per unit area by $\ddot{q} = \frac{\Delta T}{\frac{1}{h_p(\dot{m}_p, T_p, P_p)}}$. This will set the steam generator outlet temperature, and therefore its pressure. I assume no super-heating of the steam.

6.4 Steam cycle

In order to estimate the effect of lowering the steam generator saturation pressure on the thermodynamic efficiency of the cycle, I need to model a steam cycle for the power plant. Nuclear power plant steam cycles include a number of reheaters, high and low pressure turbines and other components. I chose to model the AP600 steam cycle, in Figure 6.14, as its characteristics were readily available and the two reactors are fairly similar.

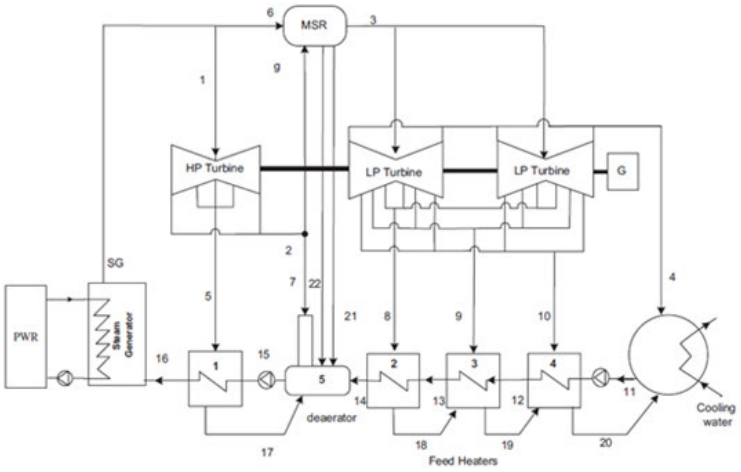

Figure 6.14: Schematic diagram of the AP600 nuclear power plant steam cycle [5]

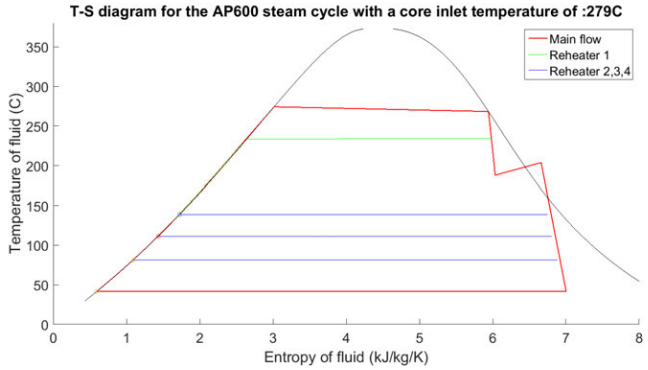

Figure 6.15: T-S diagram of steam cycle at nominal core inlet temperature

I modeled the steam cycle in MATLAB using a system's approach. The turbines and the pumps have an isentropic efficiency of 0.84 and 1. The state-points in this cycle are summarized in table 6.1. Pressure drop is only modeled in the steam generators and the MSR. It is scaled with mass flux using the Dittus-Boelter correlation [23].

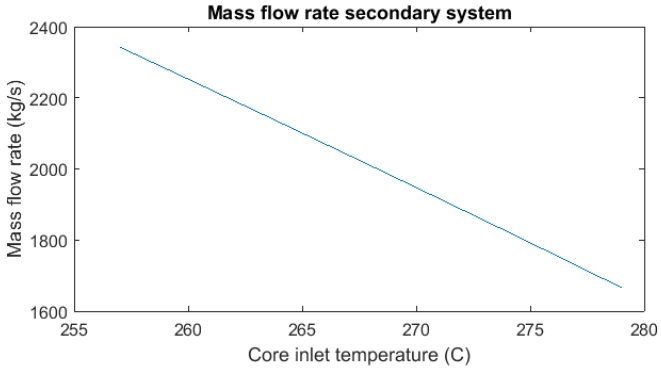

Figure 6.16: Mass flow rate in the secondary loop vs core inlet temperature

The increase in the core power is handled by raising the secondary mass flow rate, see Figure 6.16. Because of the strong scaling of the pressure drop in the steam generators with the secondary mass flow rate, it is necessary to use a third steam generator to lower the pressure drop (for both optimization strategies). Also, the lower pressure in the turbines would require a large turbine.

At a core inlet temperature of 279°C, the TS diagram for the cycle is represented in Figure 6.15. The

Table 6.1: Nominal steam cycle state points with a core inlet temperature of 279°C

N°	Temperature (°C)	Pressure(bar)	Steam Quality(-)	Mass flow rate(kg/s)
1	268.3	53.6	1	1666.1
2	188	12	0.89	1537.4
3	203.9	11	>1	1277.8
4	41.5	0.08	0.84	1134.4
11	41.5	0.08	0	1277.8
12	61.4	30	0	1277.8
13	80.9	30	0	1277.8
14	100.6	30	0	1277.8
15	140.2	58.8	0	1666.1
16	170.8	58.8	0	1666.1
5	233.9	30	0.94	128.7
6	268.3	53.6	1	43.5
7	188	12	0.89	53.1
8	133.9	3.5	0.96	50.3
9	111.4	1.5	0.93	47.7
10	81.3	0.5	0.89	45.4
17	233.8	30	0	128.7
18	138.9	3.5	0	50.3
19	111.4	1.5	0	98.0
20	81.3	0.5	0	143.4
21	268.3	53.6	0	43.5
22	188	12	0	162.9

topmost line is the steam generator. The liquid turns to vapor in the steam generator, and the temperature is the saturation pressure, which is lowered by the pressure drop in the steam generator. The first slope on the right is the high pressure turbine, the notch is the moisture separator and re-heater, and the last slope is the low pressure turbine.

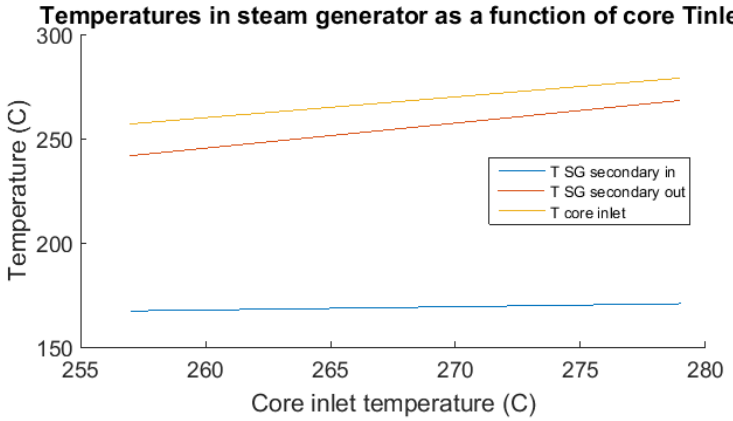

Figure 6.17: Steam generation saturation temperature with varying core inlet temperature

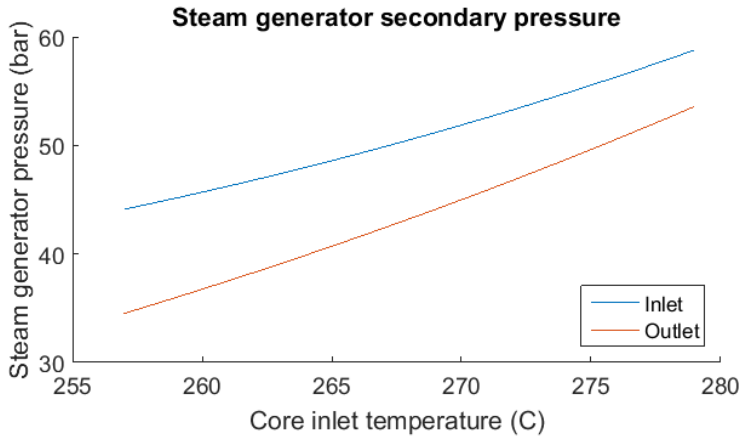

Figure 6.18: Pressure at the inlet and outlet of steam generator as a function of core inlet temperature

In Figure 6.17, the scaling law for the steam generator secondary outlet temperature with the core inlet temperature is shown. As the core inlet temperature decreases, the temperature difference between the two fluids has to increase as the amount of heat that has to be exchanged increases. Subsequently, on Figure 6.18, we can see the secondary side corresponding pressures. As the core inlet temperature decreases, the secondary mass flow increases and the pressure drop between the inlet and outlet of the steam generator on the secondary side increases.

Finally, Figure 6.19 gives the efficiency of the steam cycle with varying inlet temperature. The efficiency goes from a nominal 32.3% to 30% at a reduced core inlet temperature of 257°C. This is a decrease of 1% per 10°C of core inlet temperature, which is the expected order of magnitude [32].

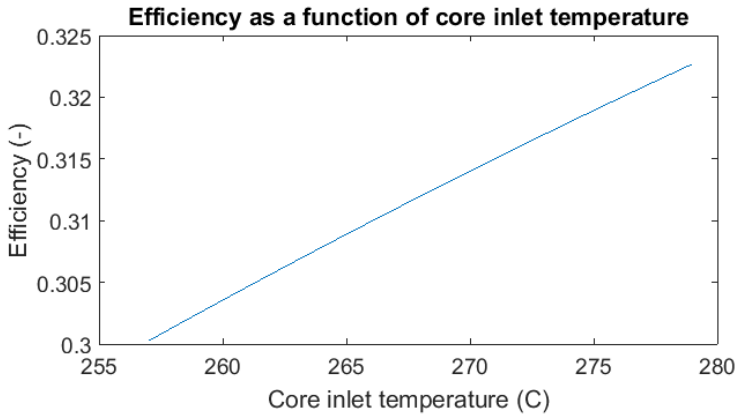

Figure 6.19: Efficiency of steam cycle with core inlet temperature

6.5 Increasing the primary mass flow rate optimization strategy

In the power optimization strategy involving increasing the core mass flow rate, the amount of energy that has to be extracted from the primary loop has increased, but the temperature in the steam generator hasn't changed. The solution to extract more energy can be to increase the mass flux in the secondary system, and possibly add an extra steam generator. This requires more pump work in the primary loop compared

to the previous strategy, but the overall effect of this strategy on the thermodynamic efficiency of the plant is smaller than in the previous scenario.

6.6 Potential for an electric power uprate

Taking into account the effect of the increased pump consumption in the secondary side, and in the primary side for the first strategy, and the decreased steam cycle efficiency for the second strategy, Figure 6.20a and Figure 6.20b show the electric power output over the geometry range for the strategy of increasing the core mass flow rate. Figure 6.21a and 6.21b show the electric power power output for the strategy involving decreasing the core inlet temperature. The possible uprates are 150/110 MWe (MATLAB/VIPRE) for strategy 1 and 145/130 MWe (MATLAB/VIPRE) for strategy 2.

Such uprates may not require an additional steam generator even with the increased secondary mass flow rate, but probably a bigger high-pressure turbine, because of the decreased steam generator saturation pressure in the case of strategy 2.

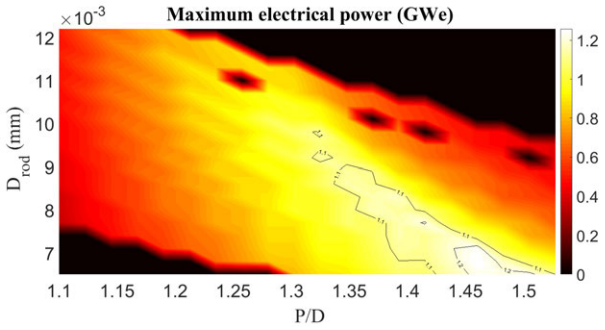

(a) Maximum achievable electric power with uranium nitride fuel in strategy 1 using MATLAB tool

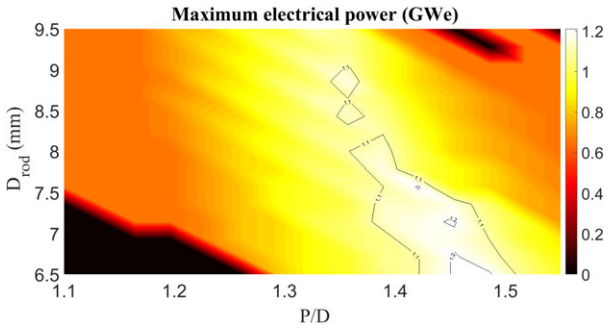

(b) Maximum achievable electric power with uranium nitride fuel in strategy 1 using VIPRE-MATLAB interface

Figure 6.20: Achievable electric power uprates by increasing the primary mass flow rate

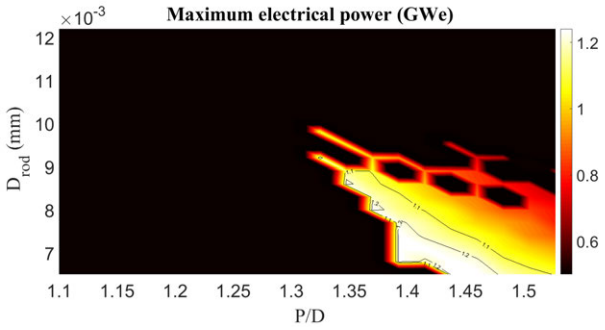

(a) Maximum achievable electric power with uranium nitride fuel in strategy 2 using MATLAB tool

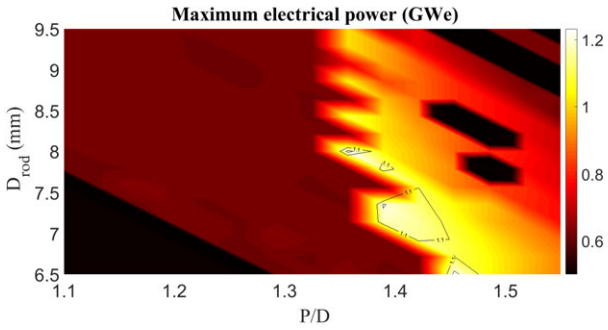

(b) Maximum achievable electric power with uranium nitride fuel in strategy 2 using VIPRE-MATLAB interface

Figure 6.21: Achievable electric power uprates by decreasing the core inlet temperature

6.6.1 Selection of an optimized design

With similar uprate potentials, I chose to use the an optimized design with a decreased core inlet temperature. Indeed, I chose a bundle design with a moderation ratio (Hydrogen/Heavy Metal) the closest to the nominal design. This ratio is determinant for transient behavior. Its characteristics as well as the AP1000's are summarized in table 6.2, and these cores' performances are summarized in table 6.3. The evaluations were made with the VIPRE-MATLAB interface, the less simplified and more accurate tool. Further assembly design is described in section 7.2.

Table 6.2: Nominal and optimized design parameters

	Core power (GWe/GWth)	D_{pin} (mm)	P/D	Pitch (mm)	Lattice pin rows	Channel H/HM	Core inlet temp. (°C)	Lineic power (kW/ft)
AP1000 nominal oxide	1.1/3.4	9.5	1.326	12.6	17	3.46	279.4	5.85
Optimized design nitride	1.24/3.95	8	1.3571	10.9	20	2.94	271.2	4.94

Table 6.3: Nominal and optimized design thermal-hydraulic and mechanical performances (VIPRE-MATLAB interface)

	MDNBR	Pressure drop (MPa)	Fretting wear ratio (-)	Sliding wear ratio (-)	Fuel centerline temp. (°C)	Fuel avg temp. (°C)
AP1000 nominal (UO_2)	2.42	0.136	1	1	1533	940
AP1000 nominal (UN)	2.42	0.136	1	1	664	568
Optimized design (UN)	2.42	0.134	0.76	0.64	632	550

6.6.2 Axial plots of core performances

Assuming a cosine power shape, I obtain from VIPRE the following axial plots. Figure 6.22 shows the fuel average temperature in a oxide-fueled AP1000, at 3400 MWth, and the nitride-fueled optimized design, at 3950 MWth, for the hottest channel (fuel temperature wise). The optimized design is colder, mainly because of the nitride fuel higher thermal conductivity, but also because of the smaller pin diameter. Both designs are far from the dissociation temperature limit for uranium nitride. The flat portions represent the upper and lower plenum, which do not contain fuel and do not produce power.

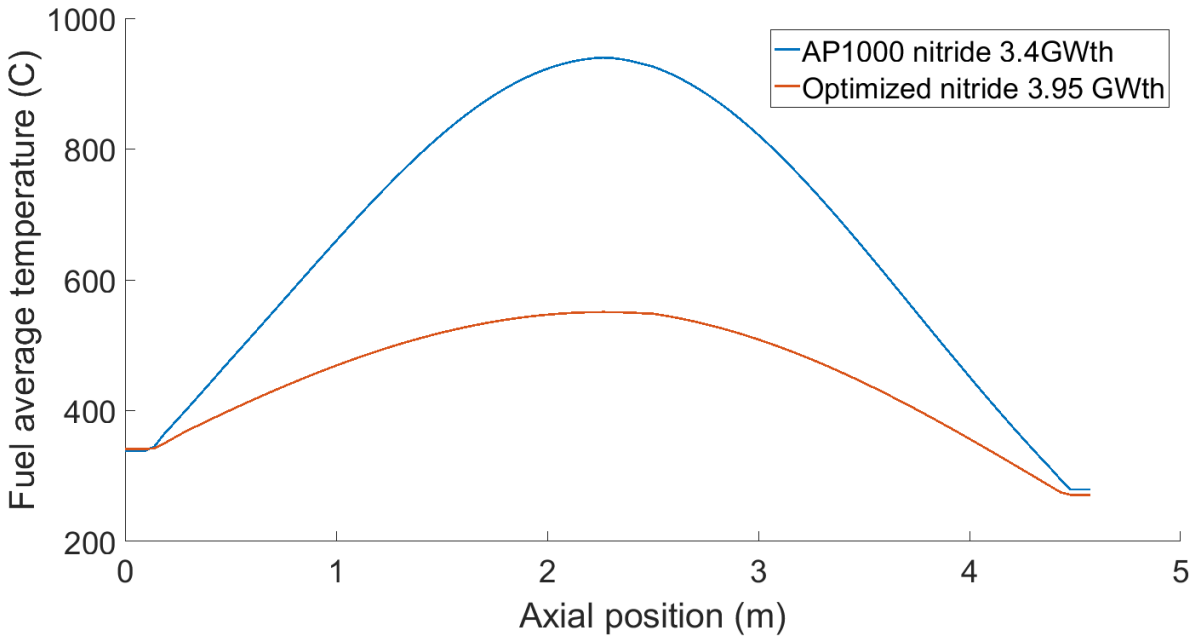

Figure 6.22: Average fuel temperature axial profile in nominal AP1000 with oxide fuel, 3.4GW$_{th}$ power, and optimized design with nitride fuel, 3.95GW$_{th}$ power, VIPRE

Figure 6.23 shows the pressure drop in the hottest channel (coolant enthalpy wise). Because both design operate at similar mass flow rates, their pressure drop are similar. The vertical segments are due to the grid spacers.

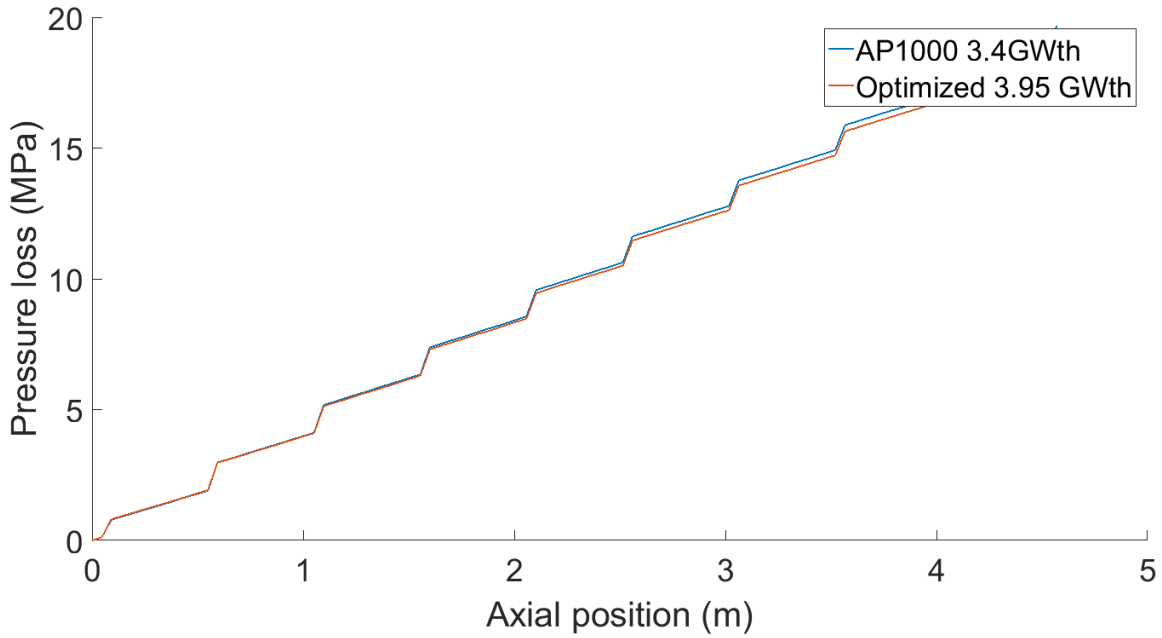

Figure 6.23: Pressure drop axial profile in nominal AP1000 with oxide fuel, 3.4GW$_{th}$ power, and optimized design with nitride fuel, 3.95GW$_{th}$ power, VIPRE

Figure 6.24 shows the fluid steam quality in the hottest channel (coolant enthalpy wise). In the hottest

channel, the coolant starts boiling, and the steam quality goes above zero. Then mixing with other channels takes place and the steam quality decreases, as it moves to other channels. The quality remains low, as the equilibrium quality is below 0 (subcooled boiling).

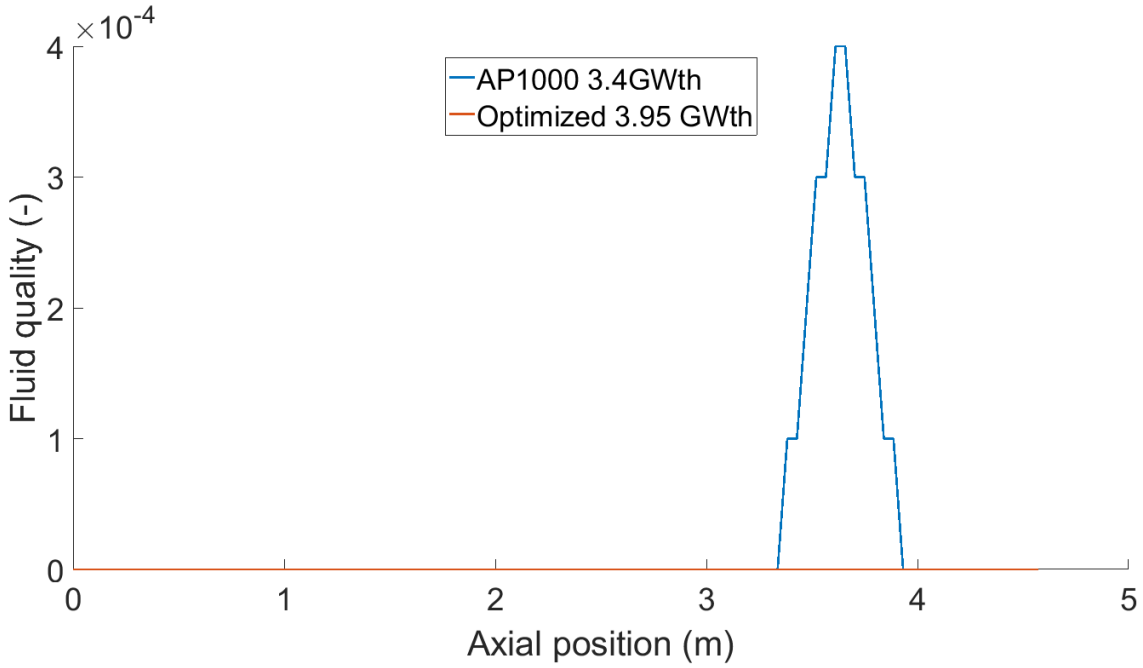

Figure 6.24: Steam quality axial profile in nominal AP1000 with oxide fuel, 3.4GW_{th} power, and optimized design with nitride fuel, 3.95GW_{th} power, VIPRE

Chapter 7

Neutronics Analysis: Assembly

7.1 Cross sections generation

7.1.1 CASMO4E : a deterministic lattice physics code

The main code that was used for cross section generation is CASMO4E. Its output can be easily fed into SIMULATE3 and SIMULATE3k, which are a full core nodal codes and a transient code.

CASMO4E [33] is a multigroup two-dimensional transport code for burnup calculations on BWR and PWR assemblies. It was developed by Studsvik. It uses the method of characteristics to solve the transport equation. Nuclear data for CASMO4E comes from ENDF-VI, and it is collected into 70 energy groups. CASMO4E uses the predictor-corrector approach to predict the evolution of nuclide densities in depletion calculation.

7.1.2 SERPENT-2 : a continuous energy Monte Carlo reactor physics burnup calculation code

Serpent [34] is a three-dimensional continuous-energy Monte Carlo reactor physics burnup calculation code, developed at VTT Technical Research Center of Finland since 2004. Serpent 2 includes new features such as multi-physics applications and OpenMP parallel computation. Its main features are spatial homogenization and group constant generation for deterministic reactor simulator calculations and detailed assembly-level burnup calculations.

In the calculations using SERPENT-2, the ENDF/B-BVII evaluated data files was used. SERPENT-2 was run primarily to check CASMO4E results.

7.1.3 Flux in nitride fueled assemblies

Figure 7.1 compares the neutron flux in a nitride fueled assembly with the same assembly loaded with oxide fuel. The uranium enrichment is the same. However as UN is denser than UO_2, there is more fuel in the first case, which is why the spectrum is faster.

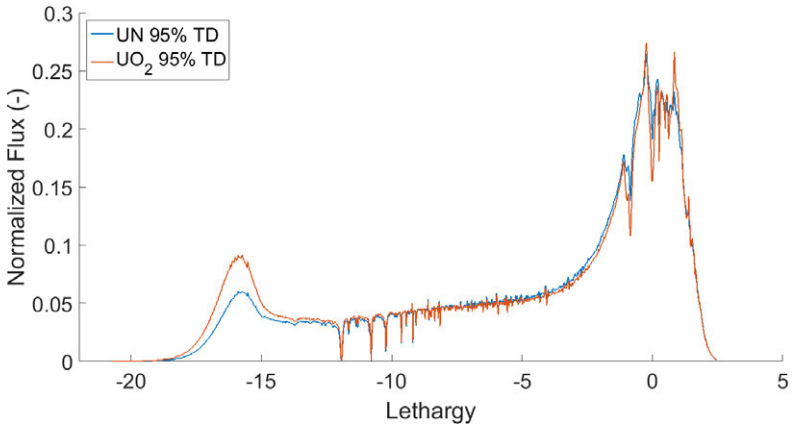

Figure 7.1: Comparison between fluxes in assemblies loaded with UN (99% ^{15}N) and UO_2 in SERPENT2

7.1.4 Replacing N15

CASMO4E uses the ENDF-VI library which does not contain the cross sections for ^{15}N. In order to keep using CASMO4E, which allows us to use SIMULATE and then SIMULATE3k for transient calculations, I looked at replacing ^{15}N with another nuclide, which would have the same behavior in the core, and if necessary adjust the number densities in CASMO4E. ^{14}N is not a good candidate as its ratio of scattering to absorption cross section is very different from ^{15}N's. Because of simple shell model considerations, I first looked at ^{16}O as a candidate, as it has the same number of neutrons, 8, which is a magic number.

Figure 7.2a shows elastic scattering and absorption cross sections for ^{15}N and ^{16}O. Figure 7.2b shows absorption cross sections for ^{15}N and ^{16}O. ^{16}O is one order of magnitude more absorbent than ^{15}N.

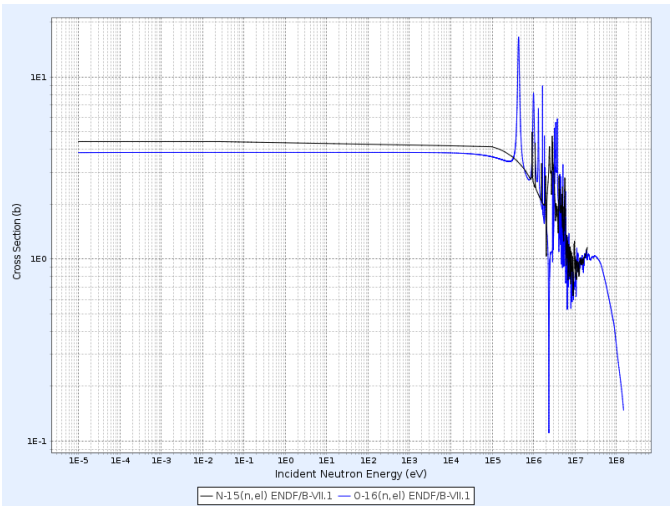

(a) ENDF/B-VII Elastic scattering cross section of nitrogen 15 and oxygen 16 [35]

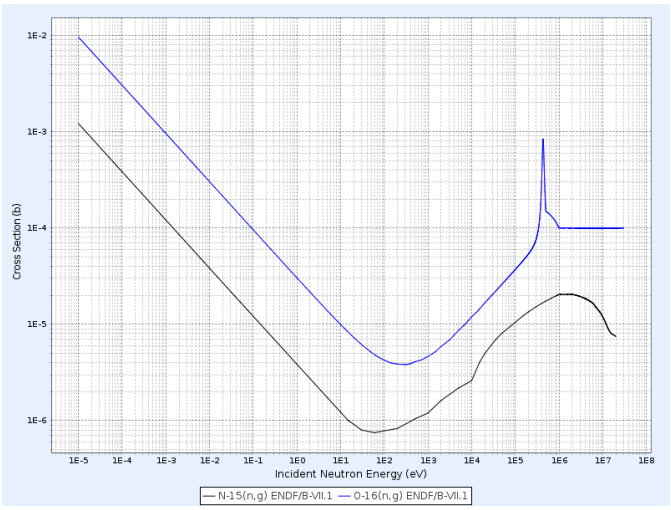

(b) ENDF/B-VII Absorption cross section of nitrogen 15 and oxygen 16 [35]

In order to adjust the macroscopic total cross sections, I then looked at 1 group cross sections. To condense the cross section I used the flux from a reference 17x17 assembly loaded with UN 99.9% enriched in N15, modeled in SERPENT 2 7.3. The ratio of 1 group total cross sections is then $\frac{\sigma^{tot}_{1gN15}}{\sigma^{tot}_{1gO16}} = 1.044$. A more

rigorous approach would have been to use an SPH factor to do the equivalence between the two nuclides. However that was not implemented due to time constraints.

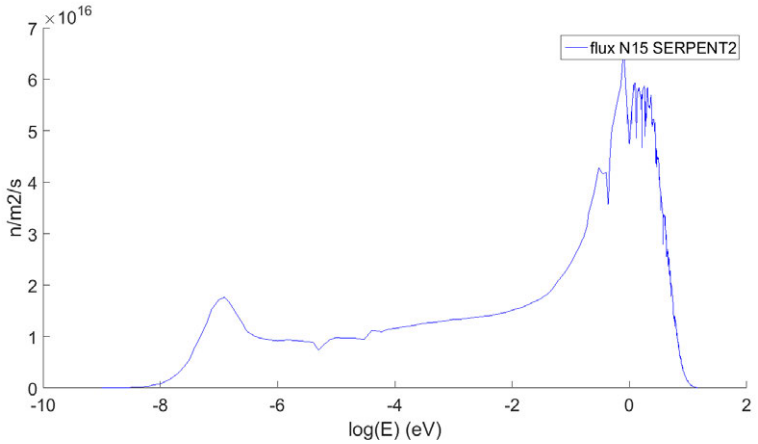

Figure 7.3: Flux in a 17x17 reference assembly [6] loaded with uranium nitride at 0 MWd/kg burnup

The reactivity, Figure 7.4, reaction rates and flux, Figure 7.5 and 7.6 and isotopic compositions, Figure 7.4 when replacing nitrogen 15 in the fuel composition by oxygen 16 in SERPENT2 were checked. The reactivity difference stays below 100 pcm for a depletion burnup up to 80 MWd/kg. Uncertainty reported by SERPENT 2 is below 4 pcm. The fractional error on reaction rates for fission on U235, capture and fission on U238 are below 0.6 %. Two group inverse velocity and diffusion coefficients were also checked.

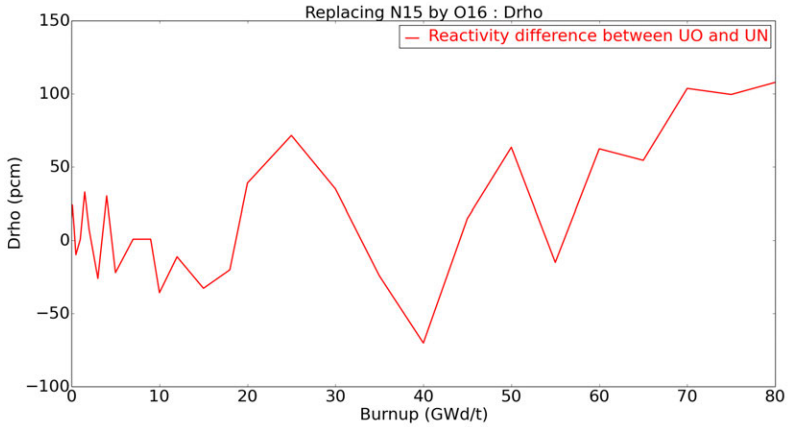

Figure 7.4: Difference in reactivity as a function of fuel burnup between UN and UO equivalent in SERPENT 2 for a reference assembly

7.2 Control rod placement and design

As shown in Figure 7.1, the flux in a uranium nitride core is faster. The neutrons' energies are higher. Control rods are made up of neutron-absorbing isotopes. There are various possibilities, such as boron carbide (B_4C, Boron 10 is the neutron-absorbing isotope, and makes up for 20% of all boron) or silver-indium-cadmium (AIC) for black control-rods or tungsten and stainless steel for gray control rods, that are

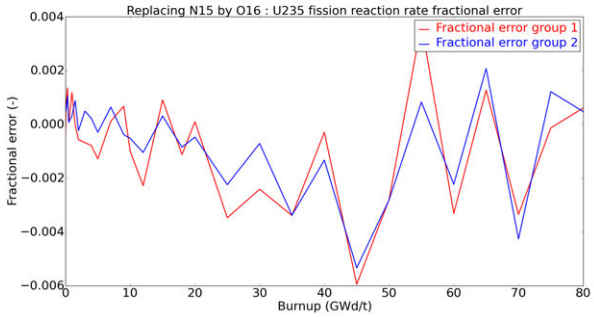

(a) U235 fission reaction rate fractional error

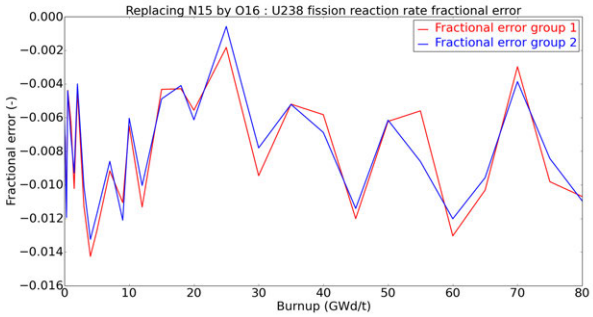

(b) U238 fission reaction rate fractional error

Figure 7.5: U235 and U238 fission rates fractional errors as a function of fuel burnup between UN and UO equivalent in SERPENT 2 for a reference assembly

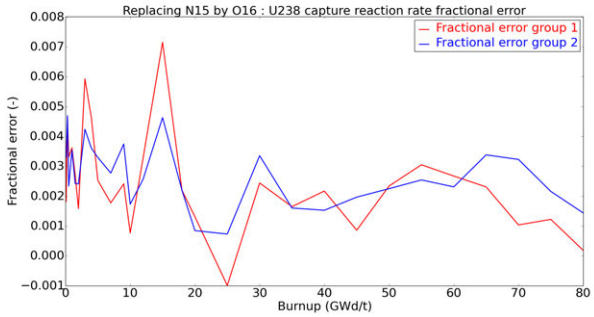

(a) U238 capture reaction rate fractional error

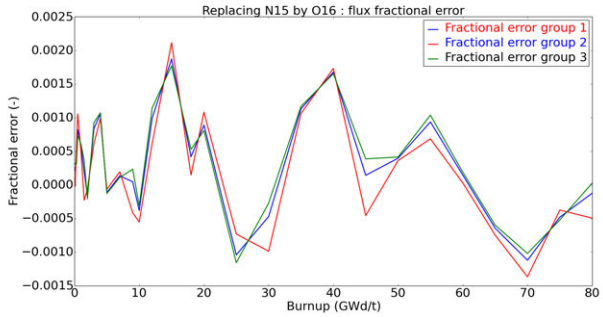

(b) Flux fractional error

Figure 7.6: U238 capture rate and 3 group flux fractional errors as a function of fuel burnup between UN and UO equivalent in SERPENT 2 for a reference assembly

partially transparent to neutrons. For all of these nuclides, and especially for B_4C, the majority of the neutrons absorbed are at thermal energies. Control rods are therefore less efficient with uranium nitride fuel. To maintain enough control rod worth, I chose to increase the proportion of control rods in assemblies from 8.3% in the AP1000 to 9.3% for my assembly design. This can be seen in Figure 7.7a. I also chose to use B_4C rather than AIC and tungsten in the AP1000, as boron 10 is the most absorbing nuclide. Alternatively, the B-10 enrichment in B_4C could have also been pursued.

Having a 20 pin rows assembly meant that I needed a large guide tube (4 pin spaces) in the center to house measurement instruments. I have attempted to use similar guide tubes for the control rods, but the power peaking was too strong. I ended up using a large guide tube for the instruments, and 4 smaller guide tubes per quadrant for the control rods. They were placed to avoid proximity between the water rods, to limit power peaking.

7.3 Burnable poison concentration and placement

Burnable poisons are nuclides that have a high neutron absorption cross section, and that are added to some fuel pins in order to limit excess reactivity at beginning of cycle, and control the reactivity swing over the cycle. There are four main types of burnable poisons available: PYREX, WABA, Gadolinium and IFBA.

PYREX are annular pins made of boron carbide. They are fitted inside empty control rod tubes. They do not displace fuel. WABA for Wet Annular Burnable Absorber are also annular pins, they are also fitted in the empty control rod tubes, but contain moderator in their center. They deplete faster than B_4C pins but slower than IFBAs. They can be withdrawn after one cycle, and therefore leave no residual reactivity penalty.

Gadolinium is mixed inside the fuel. It is essentially Gd-155 that is transmuted to Gd-156 and Gd-157 after capturing neutrons. However since Gd-157 also has a significant absorption cross-section, it leaves a residual reactivity penalty. Higher gadolinium concentration depletes slower. It also reduces the fuel thermal conductivity.

IFBAs for Integrable Fuel Burnable Absorbers, are coatings of Zirconium di-boride, ZrB_2, on the fuel pellets. They can be placed on a high number of fuel rods, to reduce pin peaking. They can also be axially zoned, to reduce axial peaking. They deplete rather fast compared to the previous burnable poisons, as the coating thickness is usually less than 0.0025 cm [36]. Boron neutron capture produces helium that increases the fuel pin pressure.

I chose to use IFBA and gadolinium nitride in this project. I couldn't use IFBA alone. Because the optimized design has smaller fuel pins, there is a smaller gaps between the pellet and the cladding, so less space to have an IFBA coating. Using uranium nitride also makes the reactor spectrum faster, so the absorption cross-section for boron-10 is decreased. Having IFBA too thick or too enriched in boron-10 could lead to fuel failure from over-pressure. I chose a maximum boron-10 content of 0.64 mg/cm. This was chosen to have the same ratio $\frac{NB_{10}/cm}{V_{gap}+V_{plenum}}$ as the AP1000 first core [37] and a typical PWR [6].

The optimized assembly is shown in figure 7.7a. The inner large instrument guide tube created a lot of difficulties in creating a low-peaking assembly design. Because it is such a large amount of water, the pins nearby see a very high thermal flux, and their power peaks strongly. I solved the issue by placing gadolinium pins with a lower U^{235} enrichment (10 % lower than the other pins) on the immediate neighborhood, and pins with fuel+gadolinium on the diagonals. Then I avoided using similar big guide tubes for the control rods, and used guide tubes scaled with the fuel pin diameters, from the nominal AP1000 assembly guide tube diameter. The IFBA pins were placed to reduce peaking.

For the AP1000 assembly, in Figure 7.7b,I have placed gadolinium pins at locations where there is the most moderation: next to the instrument guide tube in the center, between the two close control rod guide tubes, and at the corner of the assembly. These locations would have had high pin peaking, with a gadolinium pin they don't peak. Then I placed IFBA pins to reduce peaking.

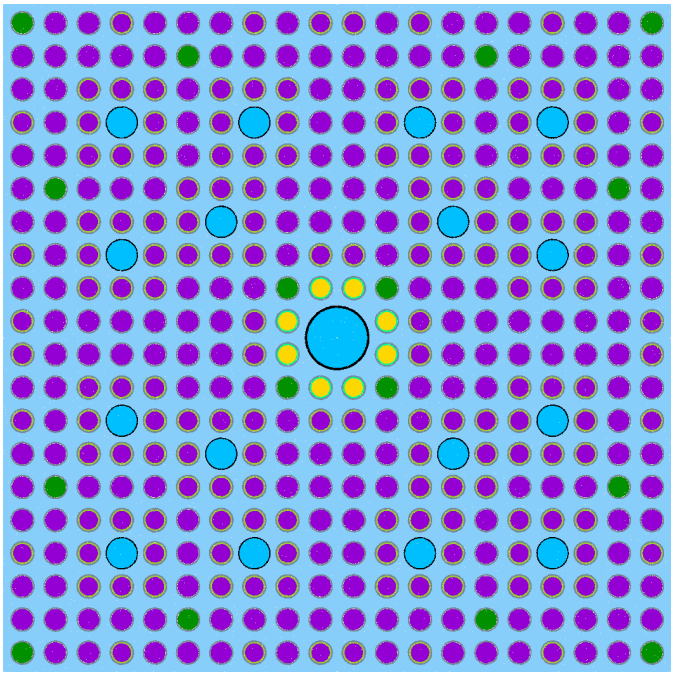

(a) Full assembly geometry for the optimized 20 by 20 assembly. Gad pins are in green, in yellow with a reduced U235 enrichment. IFBA pins have an green inner ring (exaggerated)

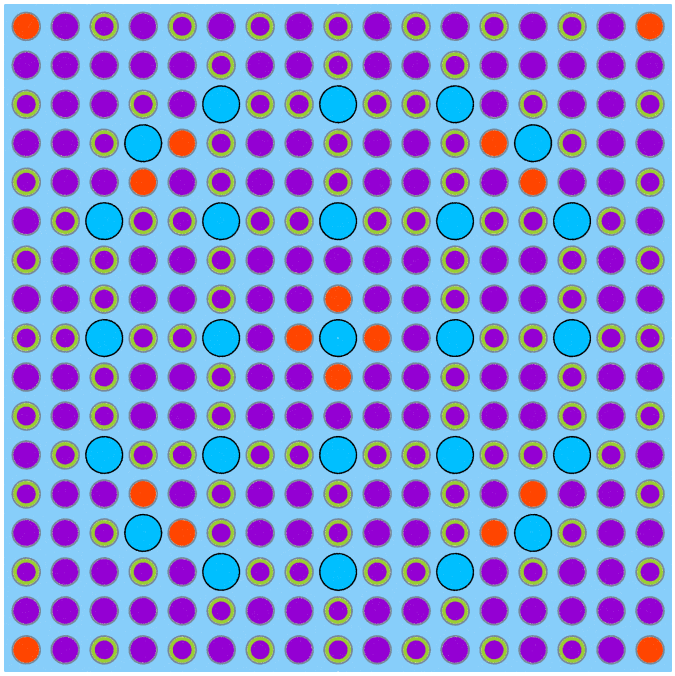

(b) Full assembly geometry for the nominal AP1000 17 by 17 assembly. Gad pins are in orange. IFBA pins have a green inner ring (exaggerated). The control rod pattern is from the AP1000 design control document [37]

7.4 Summary of burnable poison loading

For the reference oxide assembly and the optimized nitride assembly, I have generated 5 different burnable poisons loadings. They are summarized in Table 7.1. For these 5 loadings, I have generated cross-sections for a variety of U^{235} enrichments, for a total of 96 different assembly types.

Assembly type	Number IFBAs (prop.)	IFBA content per pin (mg/cm)	Number Gd pins (prop.)	Gd w%
AP1000 oxide 0	0	0	0	0
AP1000 oxide 2	104 (0.36)	0.84	16 (0.055)	2
AP1000 oxide 4	104 (0.36)	0.84	16 (0.055)	4
AP1000 oxide 6	104 (0.36)	0.84	16 (0.055)	6
AP1000 oxide 8	104 (0.36)	0.84	16 (0.055)	8
Opt. nitride 0	0	0	0	0
Opt. nitride 2	160 (0.4)	0.64	24 (0.06)	2
Opt. nitride 4	160 (0.4)	0.64	24 (0.06)	4
Opt. nitride 6	160 (0.4)	0.64	24 (0.06)	6
Opt. nitride 8	160 (0.4)	0.64	24 (0.06)	8

Table 7.1: Summary of burnable poisons loadings used

7.5 Reflectors

The thickness of the core shroud is proprietary information, and the same goes for the structure of top and bottom internals. These are critical in modeling the radial, top and bottom reflectors. The AP1000 baffle/shroud is known to be thicker than for regular PWRs, and a model by CASL [38] assumed 1.5 inches of 304 stainless steel, versus 0.85 inches for regular PWRs. I assumed 1.5 inches of 347 stainless steel, pre-built in CASMO4E and very similar. For top and bottom reflectors, I assumed the same internal structure as in a previously modeled regular PWR [6].

7.6 Reactivity curves for these assemblies

I have depleted these assemblies in CASMO4E. The results are shown in Figure 7.8. From these curves, one can know when each assembly's power is going to peak once placed inside the core. The higher the K_∞ peak, the more the assembly's power is going to peak, increasing the core radial peaking. Burnable poisons are used to reduce the K_∞ swing, the difference between the peak and initial value of K_∞.

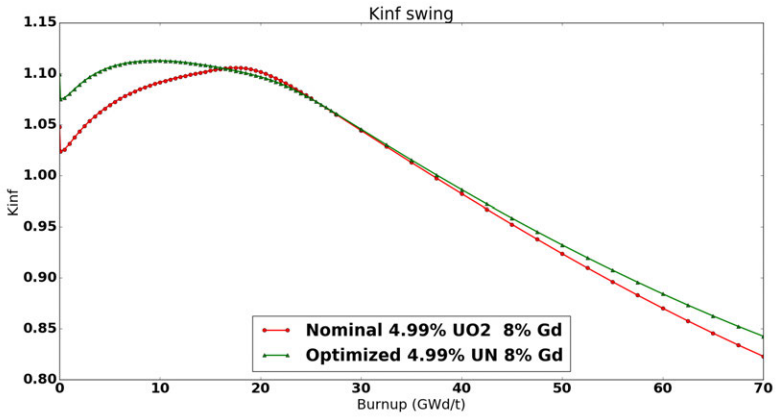

Figure 7.8: K_∞ of the 4.99% enriched nominal oxide and optimized nitride assemblies with burnup. Nitride fuel is more dense, so more fissile material is present inside the assembly and it stays critical longer

Chapter 8

Neutronics Analysis: Core

In CASMO4E, I have modeled in 2D and resolving the pins and channels of the assemblies using 70 energy groups. I cannot model the entire core this way. A 2D calculation would be too inaccurate, and a 3D calculation in 70 groups or with a fine geometry would be too costly. I model the entire core using a two-group nodal method. Each assembly is separated into 30 nodes axially and 4 nodes horizontally. The two-group cross sections for these nodes have been generated by CASMO4E and assembled in a library. SIMULATE-3 [39] uses these cross sections to solve the transport equation over the nodal mesh.

8.1 SIMULATE 3

SIMULATE-3 [39] is an advanced two-group nodal code for the analysis of both PWRs and BWRs. The code is based on the QPANDA neutronics model which employs fourth-order polynomial representations of the intra-nodal flux distributions in both the fast and thermal groups. It can perform 3D depletion, calculate reactivity coefficient and control rod worths. From the nodal flux values and the intra-assembly flux profiles generated by CASMO4E, it can reconstruct the pin powers, and determine the peaking factors.

8.2 Loading plan

The core is made of 157 assemblies. These assemblies stay in the core for 2 to 3 cycles, and the position of each assembly inside the core at each cycle is given by a loading plan. I have been aiming for a 500 days cycle length. This means 18 month cycles, including one month of refueling. I designed a loading plan for the optimized design and a loading plan for the nominal design, they are shown in Figure 8.2 and 8.1. They have been conceived on the same basis. All the assemblies starting with "TY" are fresh assemblies. At each cycle, at all of these locations, an assembly of "TYPE N" is placed in the locations marked "TY N". The assemblies are described in Table 8.1 for the oxide core and Table 8.2 for the nitride core. At the beginning of every cycle, those now once-burned assemblies are moved to another location. For example, a location marked "L-03" means that the assembly that was in column L row 3 during the previous cycle will move to this location for the next cycle.

Here there are 13 different types of fresh assemblies, described in table 8.1, in order to allow for more freedom in optimizing the core loading pattern. Once a "good" loading plan was found, I limited the number of different types of assemblies for simplicity. In the next section, I will describe what are the criteria to make a good loading plan.

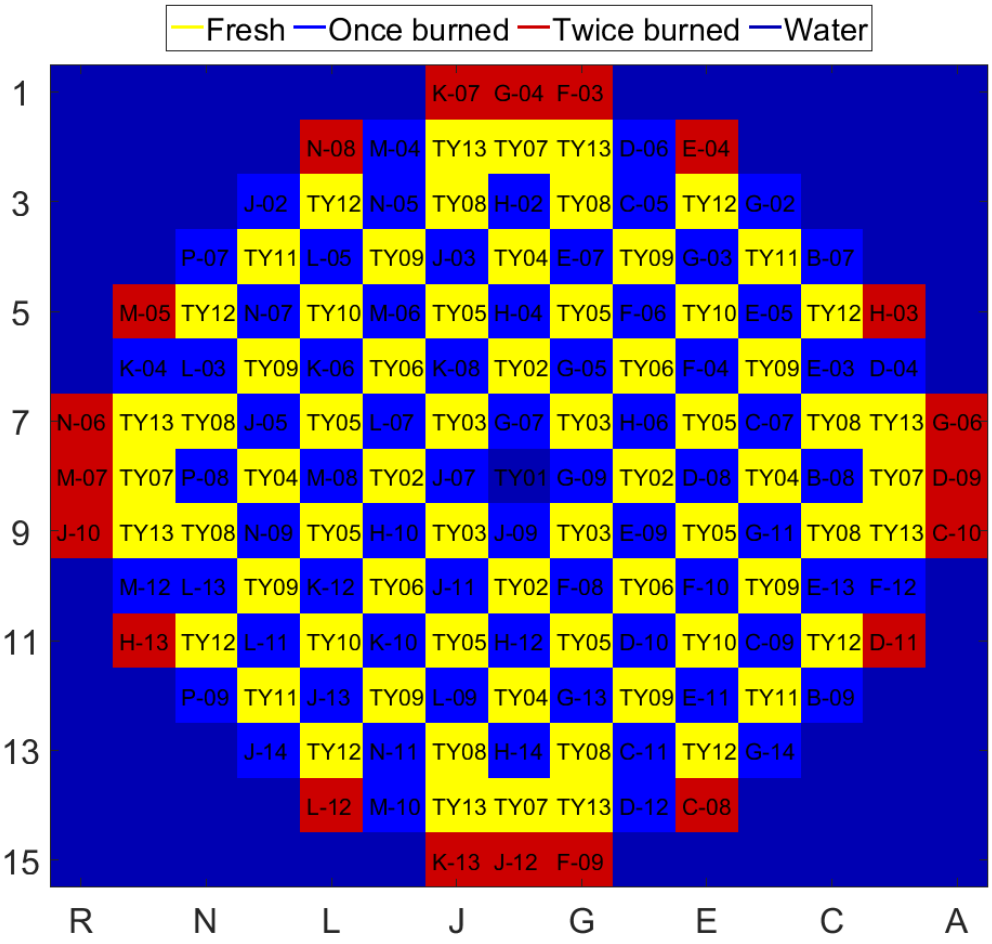

Figure 8.1: Loading pattern with 68 feed assemblies for the UO_2 AP1000

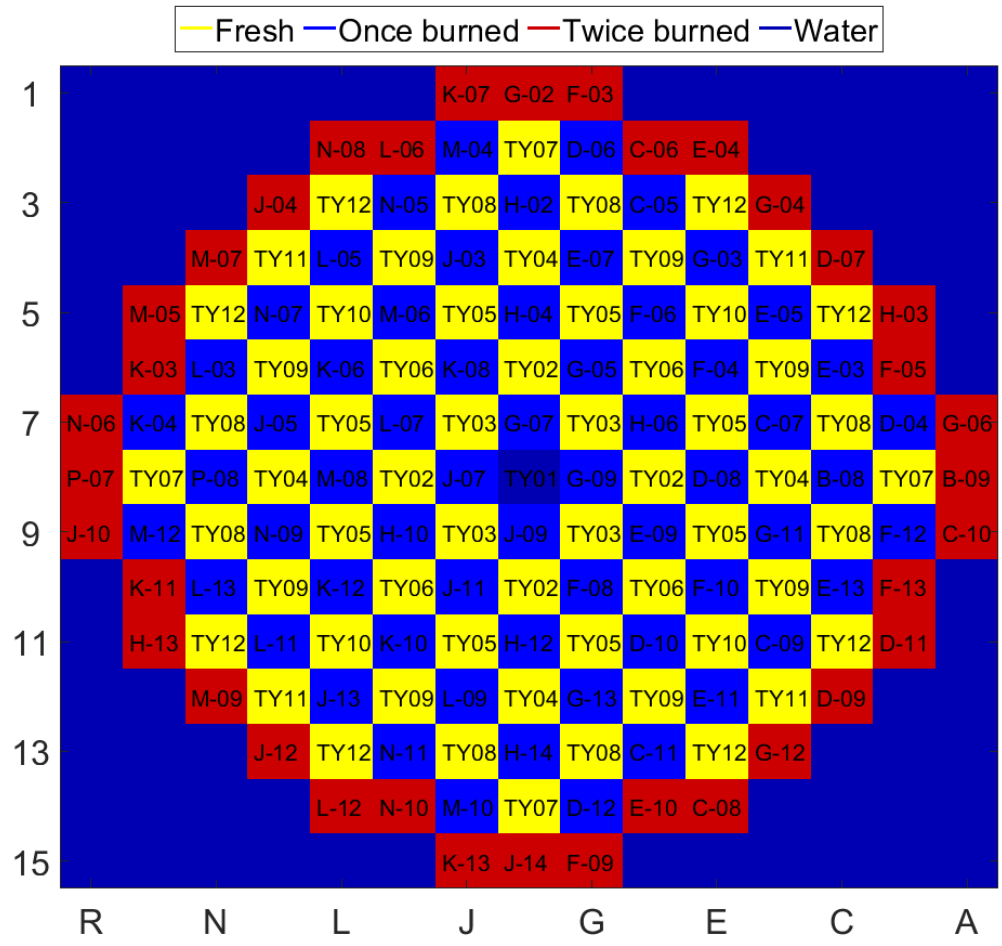

Figure 8.2: Loading pattern with 60 feed assemblies for the UN optimized AP1000

Table 8.1: Axial description of the assemblies in the oxide nominal core.

^{235}U enrichment (weight %) **Gd enrichment (weight %)**	0-20 cm	20-60 cm	60-366 cm	366-406 cm	406-426.72 cm
TYPE 1	3.3	3.3	3.3	3.3	3.5
	0.0	6.0	6.0	6.0	0.0
TYPE 2	3.3	4.8	4.6	4.8	3.5
	0.0	4.0	8.0	4.0	0.0
TYPE 3	3.3	4.8	4.6	4.8	3.5
	0.0	4.0	8.0	4.0	0.0
TYPE 4	3.3	4.8	4.6	4.7	3.5
	0.0	4.0	6.0	4.0	0.0
TYPE 5	3.3	4.8	4.3	4.6	3.5
	0.0	4.0	6.0	4.0	0.0
TYPE 6	3.3	4.8	4.3	4.8	3.5
	0.0	4.0	6.0	4.0	0.0
TYPE 7	3.3	4.8	4.7	4.8	3.5
	0.0	2.0	2.0	2.0	0.0
TYPE 8	3.3	4.8	4.7	4.8	3.5
	0.0	2.0	4.0	2.0	0.0
TYPE 9	3.3	4.8	4.7	4.8	3.5
	0.0	2.0	4.0	2.0	0.0
TYPE 10	3.3	4.8	4.7	4.8	3.5
	0.0	2.0	4.0	2.0	0.0
TYPE 11	3.3	4.8	4.7	4.8	3.5
	0.0	2.0	2.0	2.0	0.0
TYPE 12	3.3	4.8	4.7	4.8	3.5
	0.0	2.0	2.0	2.0	0.0
TYPE 13	3.3	4.8	4.7	4.8	3.5
	0.0	2.0	4.0	2.0	0.0

Table 8.2: Axial description of the assemblies in the nitride optimized core

^{235}U enrichment (weight %) **Gd enrichment (weight %)**	0-20 cm	20-60 cm	60-366 cm	366-406 cm	406-426.72 cm
TYPE 1	3.3	3.5	3.5	3.5	3.3
	0.0	6.0	6.0	6.0	0.0
TYPE 2	3.3	3.8	4.3	3.8	3.3
	0.0	4.0	8.0	4.0	0.0
TYPE 3	3.3	3.8	4.3	3.8	3.3
	0.0	4.0	8.0	4.0	0.0
TYPE 4	3.3	3.8	4.2	3.8	3.3
	0.0	4.0	6.0	4.0	0.0
TYPE 5	3.3	3.8	4.2	3.8	3.3
	0.0	4.0	6.0	4.0	0.0
TYPE 6	3.3	3.8	4.2	3.8	3.3
	0.0	4.0	6.0	4.0	0.0
TYPE 7	3.3	4.9	4.99	4.9	3.3
	0.0	2.0	2.0	2.0	0.0
TYPE 8	3.3	4.4	4.5	4.4	3.3
	0.0	2.0	4.0	2.0	0.0
TYPE 9	3.3	4.4	4.4	4.4	3.3
	0.0	2.0	4.0	2.0	0.0
TYPE 10	3.3	4.4	4.4	4.4	3.3
	0.0	2.0	4.0	2.0	0.0
TYPE 11	3.3	4.9	4.99	4.9	3.3
	0.0	2.0	2.0	2.0	0.0
TYPE 12	3.3	4.9	4.99	4.9	3.3
	0.0	2.0	2.0	2.0	0.0
TYPE 13	3.3	4.4	4.5	4.4	3.3
	0.0	2.0	4.0	2.0	0.0

8.3 Summary of constraints on the loading plan

Licensing requirements impose a channel peaking factor F_{Δ_h} ($=\frac{P_{channel}}{P_{average}}$) of less than 1.55. This is meant to avoid departure from nucleate boiling in a channel. To meet this limit, the assembly peaking factor needs to be low, and the pin peaking factor in the assembly also needs to be low. I had a pin peaking factor of 1.09 at a burnup of 10 MWd/kg, so the assembly peaking factor had to be lower than 1.42 at 10 MWd/kg.

In addition, the overall peaking factor, or heat flux hot channel factor F_Q, which takes into account the axial peaking, has to be kept below 2.6 [37, 40]. This is not a licensing requirement, more like a PWR core design best practice. For the nitride core, one must realize that the F_Q constraint was mostly designed to avoid too high fuel temperatures, which is not an issue with uranium nitride and its high thermal conductivity.

Another constraint is linked to the burnup. For pins with zircaloy cladding, the local burnup shouldn't exceed 62 MWd/kg, as part of NRC regulation. This was meant to avoid fuel failure. The AP1000 uses ZIRLO© cladding, with a higher corrosion resistance. I aimed to remain below 70 MWd/kg. This precluded me from using a 56 feed loading plan for the optimized core, which had up to 72 MWd/kg local burnup.

As previously mentioned, I aim for a cycle length of 500 effective full power days (EFPD). In a PWR, the cycle ends when the core can no longer achieve criticality. This means that despite withdrawing all control rods and bringing the boron concentration in the water to 0 ppm, a chain reaction can't be sustained in the fuel, mainly because of the depletion of U^{235}, and the absorption of neutrons by fission products which have built up. By replacing a fraction of the fuel, it can achieve criticality once again.

Other licensing limits, such as having a negative moderator temperature coefficient for example, will be discussed below.

8.4 Core performances

Table 8.3 summarizes the performances of the optimized core loaded with uranium nitride and an oxide-fueled AP1000. The UN-fueled core required a lower feed, and a lower enrichment to reach the same cycle length, while performing an uprate of 500 MWth. While the thermal hydraulics study prohibits a further uprate, with a higher enrichment and/or a higher feed and if fuel performance allows it, cycle lengths of 24 months could be reached with the uprated power.

Table 8.3: Summary of optimized and nominal core performances

	Power (MWth)	Cycle lth (EFPD)	Feed avg enr.(w%)	Feed	Max Bu (MWd/kg)	Max axl peak.	Max rad peak.	Max $F\Delta_h$	Max $F\Delta_Q$
Opt. UN AP1000	3950	501	4.35	60	66	1.25	1.42	1.55	1.89
Nom. UO_2 AP1000	3400	501	4.53	68	66.3	1.23	1.42	1.54	1.84

8.4.1 Average fuel temperature

Average fuel temperature is influenced by power peaking (much less so than maximum fuel temperature) but mostly by the evolution of the fuel thermal conductivity. Uranium nitride's thermal conductivity is thought to increase with irradiation. As a result, the fuel gets exceptionally cold during operations, around 660K. The fuel average temperature is shown in Figure 8.3.

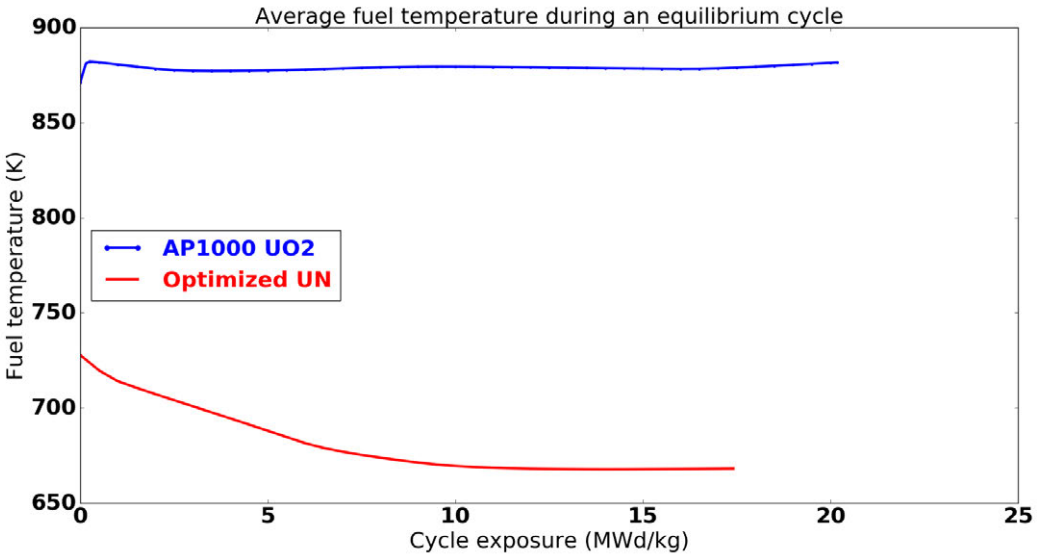

Figure 8.3: Fuel temperature during an equilibrium cycle for the optimized UN core and an UO_2 AP1000

8.4.2 Plutonium content

Throughout the cycle, U^{238} nuclei capture neutrons, forming U^{239}, which successively decays to Np^{239} then Pu^{239}. Pu^{239} is fissile, and at the end of a cycle about half the fissions come from Pu^{239}. Knowing the plutonium content will help us analyze the evolution of the reactivity coefficients. Plutonium content is displayed in Figure 8.4. The nitride core has more plutonium because it has a lower feed.

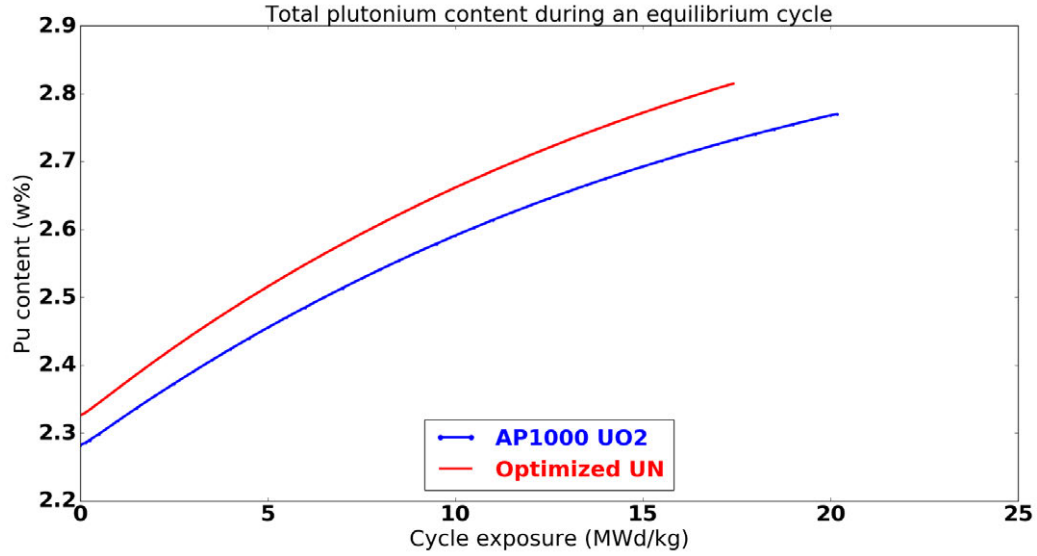

Figure 8.4: Plutonium content during an equilibrium cycle for the optimized UN core and an UO_2 AP1000

8.4.3 Moderator temperature coefficient

The moderator temperature coefficient is the change in core reactivity when the temperature changes by 1 °C. When it is positive at full power conditions, the core is considered unsafe, because a higher power increases the coolant temperature, which further increases the power. When it is negative, the core is considered safe, which is one of the PWR core licensing requirements. A higher power increases the coolant temperature, bringing the power down. NRC regulation requires the moderator temperature coefficient to be negative at full power for licensing purposes. In Figure 8.5 it appears that the moderator temperature coefficient in both core remains negative. The UN core is more under-moderated, so despite its higher boron concentration it's moderator temperature coefficient is lower.

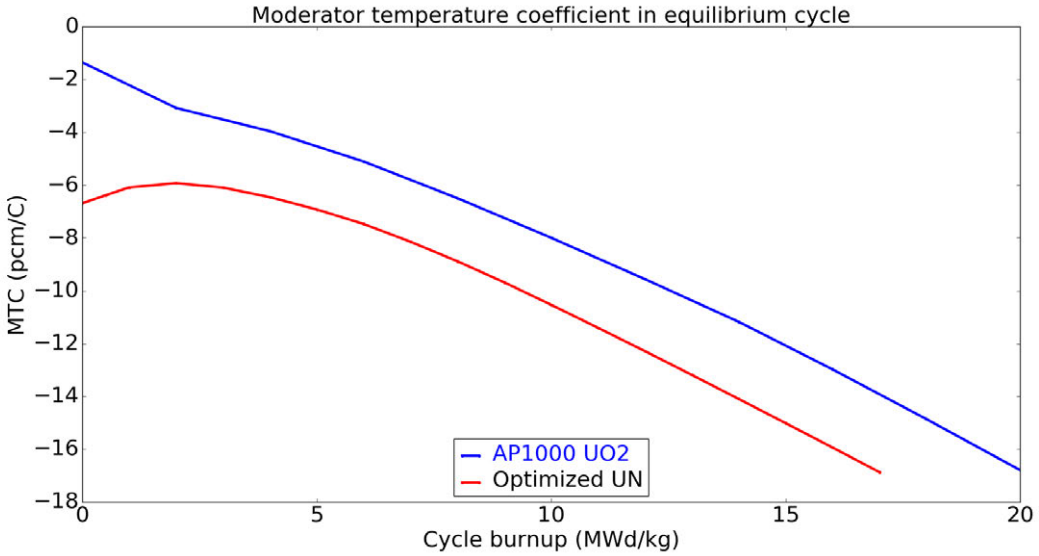

Figure 8.5: Moderator temperature coefficient during an equilibrium cycle for the optimized UN core and an UO_2 AP1000

8.4.4 Power coefficient

The power coefficient measures the change in reactivity when the core power increases or decreases. To meet licensing requirements, it is required that it be negative. Figure 8.6 demonstrates that both designs meet this requirement.

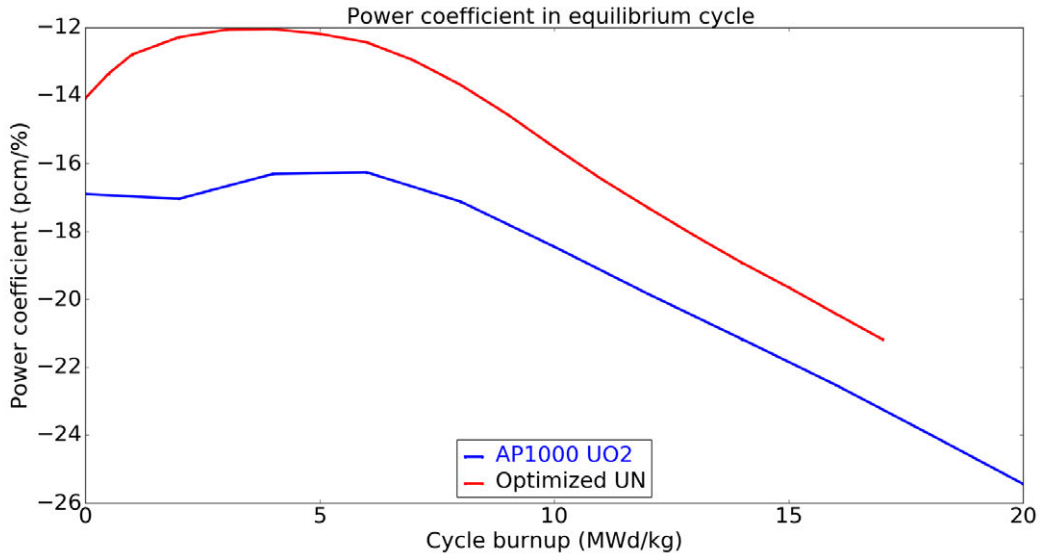

Figure 8.6: Power coefficient during an equilibrium cycle for the optimized UN core and an UO_2 AP1000

8.4.5 Doppler coefficient

The Doppler coefficient measures the decrease in reactivity when the temperature increases and the U^{238} resonances widen, capturing more neutrons. It is part of the fuel temperature coefficient, which also includes thermal expansion. It is plotted in an equilibrium cycle in Figure|8.7. It first increases because gadolinium is depleting in all the fuel pins. Gadolinium is a strong absorber and contributes significantly to resonant absorption. It becomes more and more negative as burnup increases because fission products build up and their absorption resonances contribute to the Doppler coefficient. It is lower for the nitride-fueled core because there is more fuel in the core, so when the resonances in the fuel widen, the absorption effect is stronger. However, both the lower fuel temperature and the higher plutonium content mitigate this.

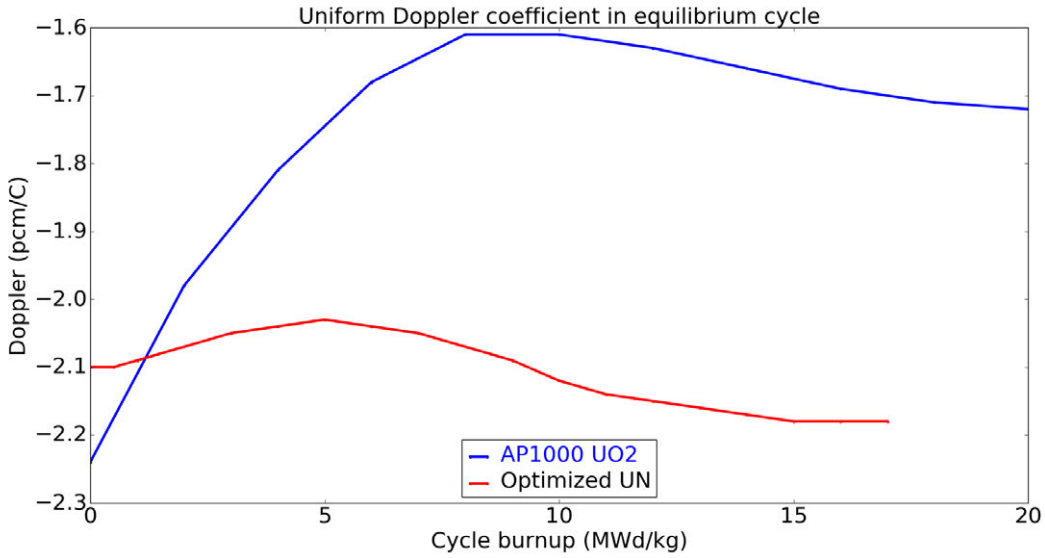

Figure 8.7: Doppler coefficient during an equilibrium cycle for the optimized UN core and an UO_2 AP1000

8.4.6 Shutdown margin

Figure 8.8 presents the core shutdown margin for the optimized core and the nominal core. Both cores use B4C control rods, which are very absorbing, while a typical PWR uses AIC control rods. NRC regulation imposes a -1300 pcm shutdown margin, which is met by both cores. It seems that I overshot the shutdown margin with B4C, and I could consider using AIC rods. The AP1000 has 69% of its assemblies that house control rod clusters, when the reference PWR has 27%. The oxide core performs much better mainly because the nominal assembly has more control rod guide tubes than the optimized design.

The shutdown margin is defined as $\Delta k_{HFP \to HZP} + 0.9(\Delta k_{all\ rods\ in} - \Delta k_{most\ valuable\ rod\ in})$. The 10% margin is meant to account for uncertainties.

The shutdown margin follows the same behavior as the Doppler coefficient. The $\Delta k_{HFP \to HZP}$ is the main contributor to this behavior, as between HZP and HFP only the fuel temperature changes.

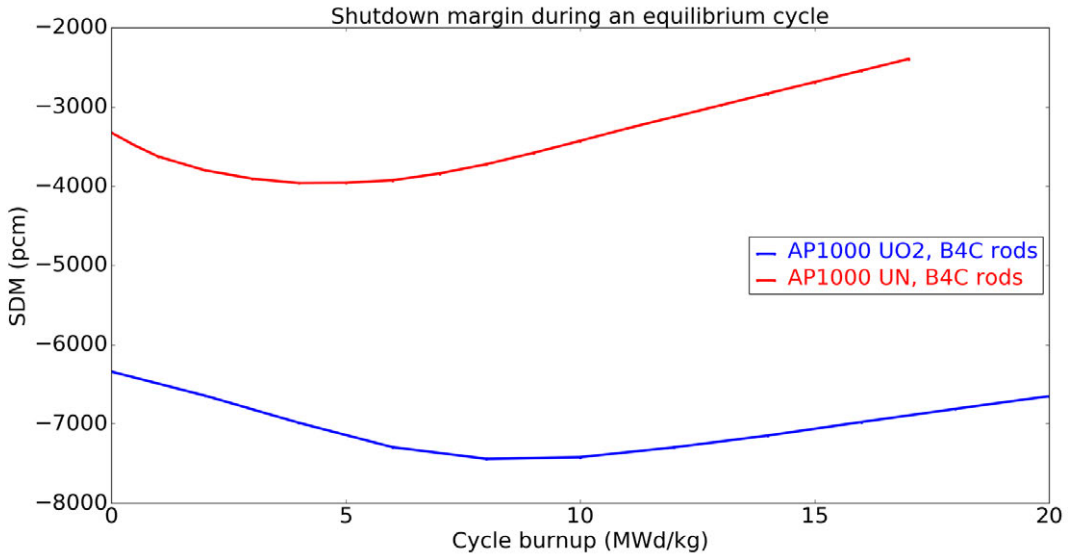

Figure 8.8: Shutdown margin during an equilibrium cycle for the optimized UN core and and an UO_2 AP1000. The two cores are equipped with B_4C control rods

8.4.7 Boron letdown curve

Boron, in the form of boric acid in the coolant, is used in PWRs to compensate for the excess reactivity in the core. As the fuel burns, less boron is needed. When the boron concentration reaches zero, the reactor must either shutdown or lower the core temperature increase reactivity. To keep the moderator coefficient negative, MIT faculty advise to keep boron concentration below 1550 ppm. Indeed, if there is too much boron, when the coolant loses density due to raising in temperature, the loss of moderation can be compensated by a loss of boron absorption.

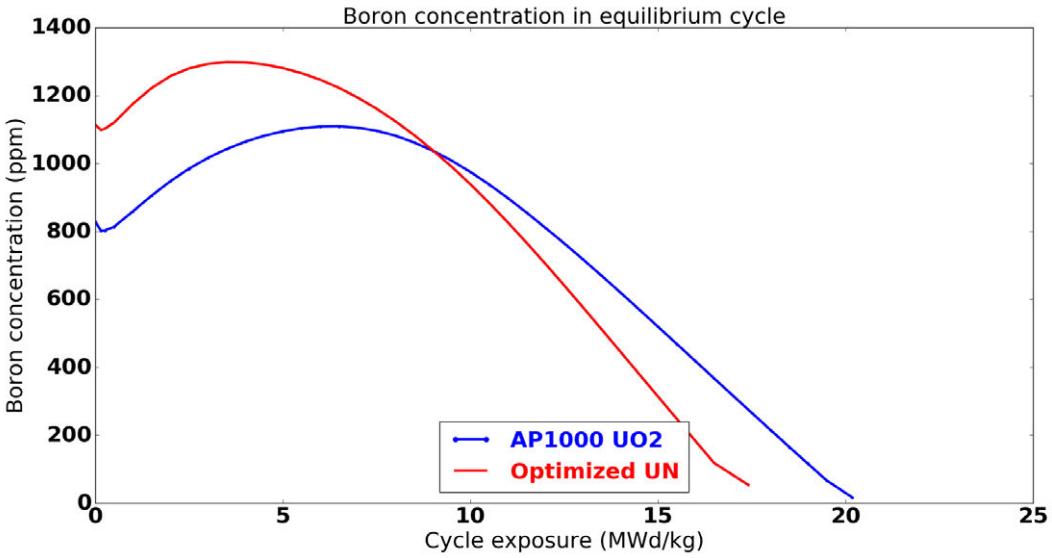

Figure 8.9: Boron letdown curve during an equilibrium cycle for the optimized AP1000 UN core and a UO_2 AP1000

8.5 Expected transient behavior

In this section, I will qualitatively analyze the reactivity insertion accident by rod withdrawal. First, let's compare some relevant characteristics of the two cores.

8.5.1 Prompt neutron lifetime

The prompt neutron lifetime is the time it takes for a prompt neutron generated by a fission to induce another fission. This time is mostly spent between scatters off hydrogen atoms, in which the neutron loses energy. Figure 8.10 shows that the prompt neutron lifetime is 40% smaller in the optimized design. This is because the optimized design has a lower H/HM ratio than the nominal one, see Table 6.2. This lower ratio means that a thermal neutron will find a fissile atom faster, and have less collisions in the moderator. Overall, the spectrum with nitride fuel is faster, as shown in Figure 7.1.

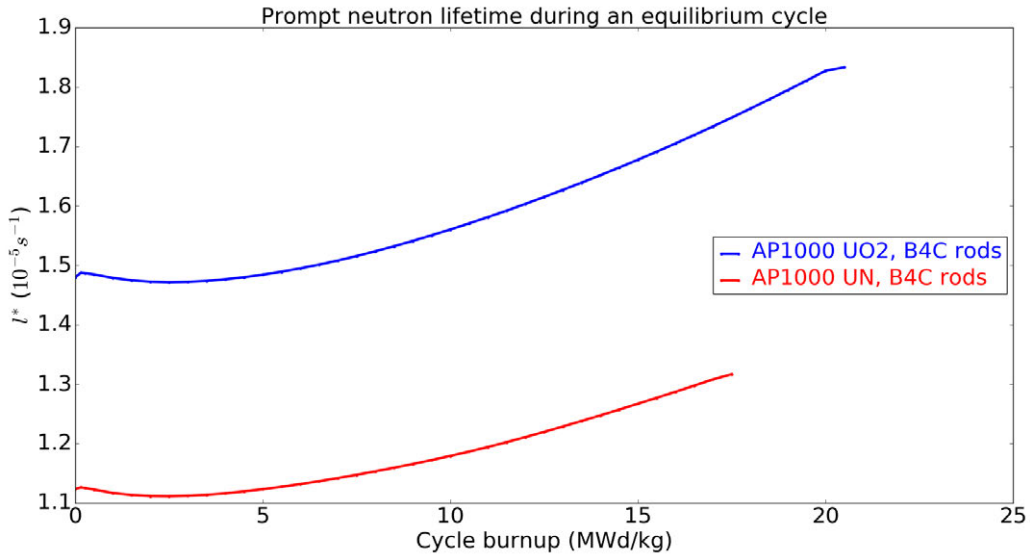

Figure 8.10: Prompt neutron lifetime during an equilibrium cycle for the optimized AP1000 UN core and a UO_2 AP1000

8.5.2 Delayed neutron fraction

The delayed neutron fraction is the proportion of neutrons that are created by fission products a few seconds after a fission, rather than immediately like with prompt neutrons. They are essential to control a reactor, as they increase the reactor period from hundredths of milliseconds to seconds, making it controllable. Figure 8.11 displays the delayed neutron fractions are very close for both cores. The delayed neutron fraction diminishes with burnup because plutonium is built by neutron capture on U^{238}, and the delayed neutron fraction of plutonium is significantly less than for U^{238}.

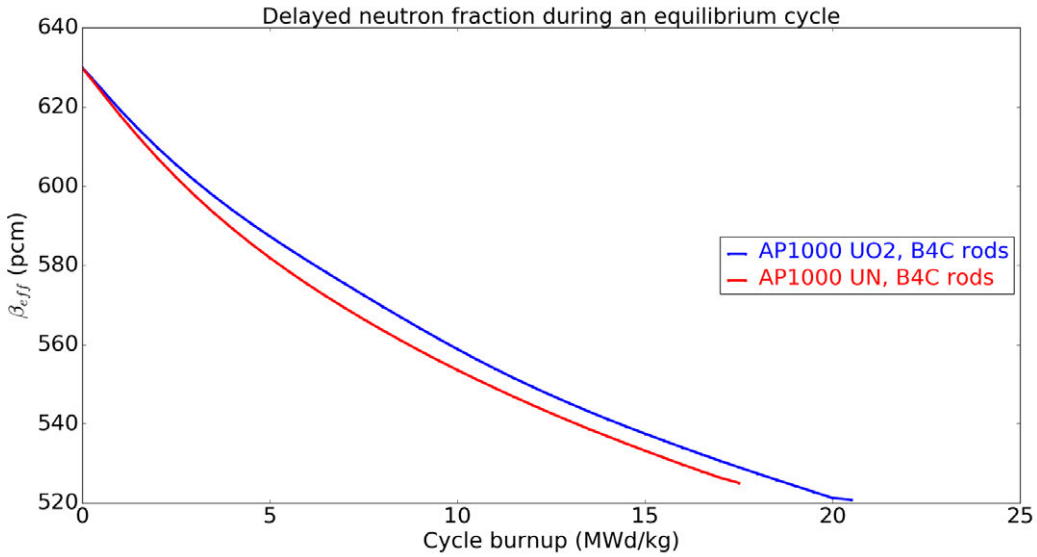

Figure 8.11: Delayed neutron fraction during an equilibrium cycle for the optimized AP1000 UN core and a UO_2 AP1000

8.5.3 Highest control rod worth

The highest rod worth is the maximum of the amounts of reactivity inserted in the core if a control rod is ejected from the core. The most valuable control rod is usually placed in the core location with the highest flux. Figure 8.12 exhibits that the nitride core has a lower most valuable rod worth. This is because the flux spectrum in the nitride core is faster, so the thermal absorption from B_4C, the control rod material, is less important. For both cores the rod worths are fairly small despite using B_4C control rods. This is because I have simplified my analysis of the AP1000 control rod placements and considered that all rods could be used to shut down the core. I did not use any grey rods like in the AP1000 nominal design. Because of that, 69% of the assemblies house control rod clusters that can participate in a shutdown, when an usual PWR [6] has 27%.

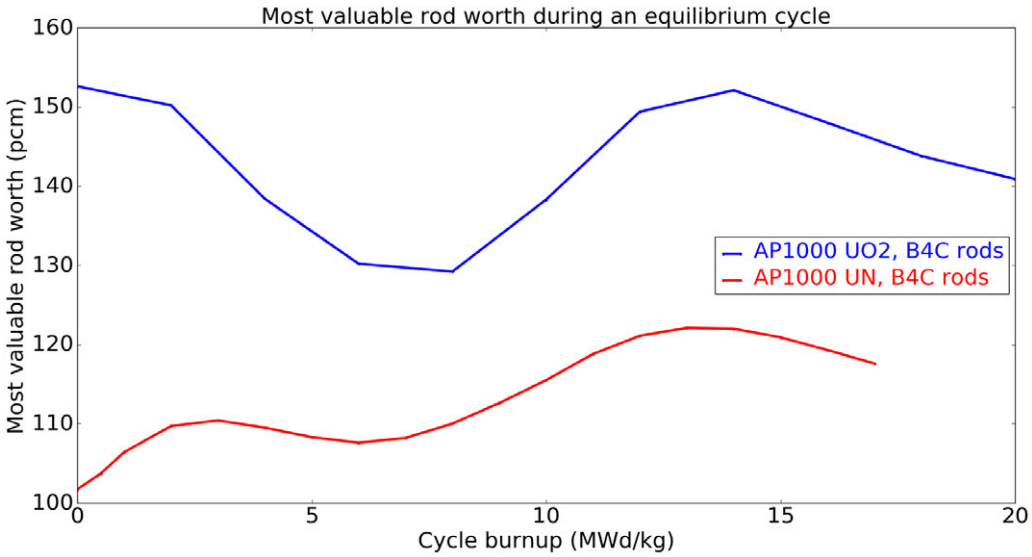

Figure 8.12: Most valuable rod during an equilibrium cycle for the optimized AP1000 UN core and a UO_2 AP1000

8.5.4 Summary of expected behavior during a reactivity insertion accidents

The lower prompt neutron lifetime has very little effect on the reactor period if the core doesn't go prompt-critical. Given the most valuable rod worth and the delayed neutron fractions, the oxide and nitride cores will not go prompt-critical during a reactivity insertion accident caused by a rod ejection. Even if I made different assumptions on the role of each control rod cluster, and considered grey rods,the ratio of the current highest rod worth to delayed neutron fraction is still of 1 to 6, so new assumptions will not turn the rod ejection RIA into a prompt-critical scenario.

On these grounds, it can be expected the behavior during RIA below prompt-criticality transients of both cores to be fairly similar.

On the other hand, reactivity insertion accidents that induce prompt criticality are more complicated to

predict. They are however the ones that have to be considered for licensing purposes. A core may fail these transients if the cladding fails after the power excursion, due to reaching a high temperature. For ZIRLO cladding, the onset of the high temperature exothermal reaction with water is the limiting condition. Let's try to give an insight into these transients by detailing the relevant fuel and cladding properties, and using the Fuchs-Nordheim model.

We start from the point kinetics equation, and ignore the delayed neutrons contribution because of the prompt-criticality.

$$\frac{dP}{dt} \approx \frac{\rho(t) - \beta}{l^*} P(t) \tag{8.1}$$

With P(t) the power, ρ the reactivity, β the delayed neutron fraction and l^* the prompt neutron lifetime.

Let's assume that the transient is so fast that no heat is transferred from the fuel. We will only look at the influence of the fuel properties.

$$T_{fuel} = T^0_{fuel} + \frac{1}{C_p} \int P(t) dt \tag{8.2}$$

I'll also assume a Doppler feedback coefficient independent of temperature.

$$\rho(T_{fuel}) = \rho(T^0_{fuel}) - \alpha(T_{fuel} - T^0_{fuel}) \tag{8.3}$$

One can show that the peak fuel temperature during the transient and the peak power during the transients are:

$$T^{peak}_{fuel} = \frac{(\rho_{rod} - \beta)}{\alpha} + T^0_{fuel} \tag{8.4}$$

$$P^{peak} = \frac{C_p(\rho_{rod} - \beta)^2}{2l^*\alpha} + P^0 \tag{8.5}$$

The peak fuel temperature is independent of the neutron lifetime and heat capacity. Still assuming that no heat is transferred to the cladding, the fuel temperature at the end of the transient is:

$$T^{end}_{fuel} = \frac{2(\rho_{rod} - \beta)}{\alpha} + T^0_{fuel} \tag{8.6}$$

Therefore, the total amount of energy that has been gained by the fuel is:

$$C_p \Delta T = \frac{C_p 2(\rho_{rod} - \beta)}{\alpha} \tag{8.7}$$

Comparing the oxide and nitride fuel:

$$\frac{(C_p\Delta T)_{oxide}}{(C_p\Delta T)_{nitride}} \approx \frac{\frac{80 \cdot 330}{1.8e-5}}{\frac{110 \cdot 230}{2.1e-5}} = 1.38$$

This means that under these assumptions the amount of energy transferred to the cladding is much lower for the nitride fuel. The cladding is also colder in the steady state conditions because of the lower coolant

temperature of the optimized core.

Because of the higher thermal conductivity and the lower heat capacity of the nitride fuel, this energy will be transferred to the cladding faster. In addition, the cladding in the optimized design in 0.52mm thick, whereas the cladding in the nominal design is 0.57 mm thick. Also, the pin internal pressure could be higher for one of the fuels. This was not taken into account as fuel performance wasn't part of this study.

Taking into account all the previous arguments, the optimized design is expected to fare better than the nominal one in reactivity insertion accidents that induce prompt-criticality.

8.5.5 Summary of expected behavior during a loss of flow accident

A loss of flow accident can occur if the four primary pumps fail/trip simultaneously. This can happen during a loss of off-site power. In this scenario, the control rods drop in the core, because of the pump trip, shutting down the reactor. But the fuel still produces heat, because of the residual heat from the decay of fission products. In the AP1000, natural circulation of the coolant, aided by passive systems, ensures that the core is sufficiently cooled for 72 hours without requiring external intervention.

The optimized design has the same pressure drop as the nominal design at the nominal mass flow rate. So in the first few seconds of the transient, the behavior of the two cores are expected to be similar.

In the longer term, the core power is 15% higher for the optimized design. However natural circulation is enhanced by a colder secondary side, the usual cold source in the natural circulation loop. With regards to additional passive safety provided by cold pressurized water tanks, these may have to be resized to make up for the increase in decay heat generation.

8.5.6 Summary of expected behavior during a loss of coolant accident

A loss of coolant accident (LOCA) happens if the pressure vessel or the primary circuit breaks. I will consider a large break LOCA. In this scenario, the coolant pressure rapidly diminishes in the core. In seconds, the control rods drop in the core, shutting it down. Before this, the negative moderator density coefficient has already started decreasing the power. The core is then uncovered for dozens of second before pumps or passive systems re-flood the core.

In those phases, studies led using TRACE to show the dependence of the cladding temperature on the thermal conductivity [41] show that the higher the fuel thermal conductivity the lower the cladding temperature, and the higher the thermal energy stored in the core the higher the peak cladding temperature. Nitride fuel will have less thermal energy in the fuel because of a lower heat capacity and also a higher thermal conductivity.

In addition, the amount of coolant in the core is approximately 11.9 tons for the nominal oxide design, and 12.7 for the optimized nitride design. This means that if the flow rate through the large break is the same for both cores, the nitride core will be uncovered later during the LOCA, which lower the peak cladding temperature.

These considerations, as well as a lower linear heat generation rate, and a much lower fuel temperature during steady state for the optimized nitride-fueled core, point towards a better performance of the nitride-fueled core during a large break LOCA.

Chapter 9

Economics study

Finally, with the core loadings required to get an 18 month cycle length for the two reactor designs using the two fuels, I can compare the fuel cycle costs. In this study, I will neglect the back-end fuel cycle costs. I use the UxC fuel calculator, available online [42], and use the SWU, conversion and U_3O_8 that it provides. These values describe the uranium market in January 2017. The ^{15}N enrichment cost and fuel fabrication price are from a Westinghouse publication on accident tolerant fuels [43]. They are summarized in Table 9.1.

Table 9.1: Summary of economic input assumptions

U_3O_8 price ($ /lb)	22.5
Conversion price ($ /kgU)	5.85
SWU price ($ /SWU)	47
N^{15} price ($/kg N^{15})	1,130
N^{15} price ($/kg U)	71.2
Fabrication Price ($/kgU)	275

In table 9.2, I show the fuel cycle costs for the two cores. The nitride fuel cost ends up more expensive by 0.17 $ / MWhr electric (+5%). This is mostly due to the ^{15}N enrichment cost. This increase in fuel cost is minor compared to the increase in revenue with the 150 MWe uprate. 0.17 $ / MWhr is much smaller than average electricity prices, in dozens of dollars per MWhr [44].

Table 9.2: Summary of the 18 months fuel cycle summary

	Fuel	Pellet density (g/cm^3)	# Feeds	Average enrichment	Power (GWe)	Reload cost ($M)	N^{15} cost ($/MWhr)	Fuel cycle cost ($/MWhr)(% diff.)
AP1000 nominal oxide	UO_2	10.46	68	4.53	1.1	44	0	3.30 (ref.)
Optimized design nitride	UN	12.9	60	4.35	1.25	52	0.19	3.47 (+5%)

Chapter 10

Conclusion

10.1 Key points

- To investigate an uprate in PWRs using uranium nitride, two strategies were tested: increasing the primary mass flow rate and decreasing the core inlet temperature
- They both yielded similar uprate potentials, around 150 MWe with optimized geometries. The fuel did not matter for the thermal-hydraulics and mechanics study
- Increasing the primary mass flow rate incurs uprating the primary pumps, decreasing the core inlet temperature diminishes the efficiency of the steam cycle
- An optimized design with a decreased inlet temperature and nitride fuel was able to perform the uprate for a cycle length of 18 months with only 60 fresh assemblies per cycle and a 4.5% enrichment
- For a nominal AP1000 oxide-fueled core it takes 68 fresh assemblies and a 4.6% enriched fuel
- Transient performances in reactivity insertion, loss of flow and loss of coolant accidents are expected to be better for the nitride-fueled core
- The front-end fuel cycle costs are higher for the nitride core by 5%, but this is increase is minor compared to the additional revenue from the uprate

10.2 Discussion

Challenged by low natural gas prices, nuclear power plants have to improve their economic performances. To do so, the reactor can be operated at a higher power, or for longer cycles. The current fuel, UO_2, with the current ^{235}U enrichment limit, 5%, cannot accommodate either. I have therefore chosen to study the uprate capabilities when using uranium nitride. Uranium nitride is 30% denser, so 30% more fissile material can be placed in the core. I have investigated the incorporation of UN in the AP1000, the Gen-III+ reactor by Westinghouse, a design bound to dominate the nuclear industry in the coming decades.

In order to improve or maintain the steady-state thermal-hydraulic and mechanical behavior despite a power uprate, I have performed a parametric study of relevant performances, MDNBR, pressure drop etc, in a range of core geometries. I analyzed two strategies for power uprates. The first one had the primary mass flow rate increase, with the same coolant temperature increase in the core as the nominal design, and the second one had the inlet temperature decrease, with the same core outlet temperature and the same primary mass flow rate as the nominal design. I found that smaller pins with a similar pitch-to-diameter ratios were offering significant margins for uprates while improving the core steady state performances. The second optimization strategy proved to be more promising, with uprate possibilities of up to a 1GWth. However, geometries optimized for thermal-hydraulics have lower fuel content because of the higher pitch-to-diameter ratio.

I then considered the effects on the steam cycle of the two optimization strategies. Both strategies require an additional steam generator. When lowering the core inlet temperature, I also need to lower the steam generator saturation pressure. This will require larger components, such as a larger turbine. The efficiency of the steam cycle also diminishes, at the rate of 1% per 10 degrees C of core inlet temperature.

Afterwards, I designed an AP1000-like 157 assemblies core with the optimized for steady state thermal-hydraulics design. In order to keep both 157 assemblies and the same core surface with smaller pitches, I used 23 pin rows assemblies rather than the nominal 17. I created IFBA loading patterns to minimize peaking and optimize the reactivity shift. I allowed for more control rod positions because of the slightly harder flux with uranium nitride. I built a high reload fraction loading plan to improve cycle performances. I calculated the equilibrium cycle performances, and found that to reach a cycle length of 18 months with uranium nitride, I have to limit the uprate to 550 MWth in the previously thermal-hydraulics-optimized geometry. I were able to maintain a negative moderator temperature coefficient and a sufficient shutdown margin. Transient behavior and fuel performance studies are part of future studies.

To conclude, I demonstrated the possibility for a significant uprate, around 150 MWe / 550 MWth, in the AP1000 using uranium nitride. It requires an optimized bundle geometry, but the assembly size remained constant. The bundles can therefore fit in the same core. If achieved by decreasing the core inlet temperature, it would also require changes to the steam cycle, such as possibly a third steam generator and a bigger high pressure turbine to handle the lower steam generator saturation pressure. If achieved by increasing the primary mass flow rate, primary pumps need to be uprated and a third steam generator may also need to be added.

Chapter 11

Future Work

By demonstrating the possibility of uprates in the AP1000 using uranium nitride, this project has opened up many possibilities for further research in what could be a game-changing fuel for the nuclear industry, both inside and outside the United States.

11.1 Two-year fuel cycle length

Currently, in the US regulated electricity markets, where four AP1000 are being constructed, it is desirable to move to a two-year refueling scheme compared to the current 18-month refueling scheme. It allows nuclear power plants to increase plant availability and revenue while decreasing cost. Uranium Nitride is an enabling technology that allows nuclear utilities to meet the restrictive 5% U-235 enrichment limit even with those longer refueling scheme. Southern Nuclear Company is currently interested in using Uranium Nitride. The parametric study could be extended to examine which geometries can reach such cycle length, and if there is a potential for a simultaneous power uprate.

11.2 Plutonium burning with Uranium Nitride

After the Fukushima disaster in Japan, which led to the shutdown of all of its nuclear power plants, the nuclear fuel reprocessing facility in Japan continued to separate Plutonium from the spent nuclear fuel. In order to burn this excess plutonium, HITACHI, one of the main nuclear vendors in Japan, is designing a boiling water reactor for burning of their excess Plutonium inventory. Uranium nitride as a 30% denser fuel offers interesting possibilities for burning plutonium. This would build up on previous MIT studies for BWRs [7], and PWRs [6, 45].

11.3 Studying design basis accidents and other transients

As I have chosen to use the Studsvik codes, CASMO4E and SIMULATE3, I can easily use our results to study reactivity insertion accidents using SIMULATE3K. Of particular interests are the loss of on-site power,

and therefore loss of primary pumps, and the large break loss of coolant accident, which will require another code. As passive safety is the main selling feature of the AP1000, it should be maintained while performing an uprate. One could make sure that natural circulation of the coolant will prevent the melting of the fuel. This may require re-sizing of the safety injection pressurized tanks and the passive heat removal systems.

11.4 Effects on steam-cycle of various uprates

In order to achieve an uprate, the power conversion scheme has to be modified. I chose to mainly modify the secondary mass flow rate in one uprate strategy, and also the steam generator saturation pressure in the other one. The current steam cycle can accommodate a small uprate, and I chose to add a steam generator to achieve bigger uprates. Determining the threshold for this change would be of interest to determine the optimal uprate with regards to economics. A hybrid strategy, combining increasing the core mass flow rate and decreasing the core inlet temperature, would allow us to reach even higher uprates.

I modeled with a systems approach the AP600 steam cycle, adapted it and then perturbed a few parameters and obtained the effect on the efficiency. This efficiency can be improved by re-optimizing the steam cycle with the perturbed parameters. This could further increase the uprate on electric power.

11.5 Extending the parametric study beyond thermal-hydraulic steady state performances

After the thermal-hydraulic and mechanical study, I have chosen an optimized bundle design, created a core loading pattern and tested its neutronic performances. The transients will also be ran on that design. However, the core loading pattern is most likely valid for other assembly designs. So the evaluation of the neutronic performances could also be led as a parametric study. This would allow for multi-objective performance, to look at both thermal-hydraulic performance, power and transient performances. Other parameters, such as the uranium nitride density or the pellet-cladding gap size would then come into play.

11.6 Fuel performance study of uranium nitride

The dependence of uranium nitride thermal conductivity and other physical parameters on fuel burnup isn't well known, except by the Russian industry which has been using uranium nitride for experiments in the BOR-60 and BN-600 fast reactors [22], and as a driver fuel in the BR-10 fast reactor [21]. The sensitivity of these properties on synthesis methods, fabrication parameters and impurity levels of uranium nitride has brought great variance in the few measurements [21]. These properties could be measured by irradiating UN samples in the MIT reactor for example.

As mentioned in section 4.2, uranium nitride reacts with water and expands to burst the cladding open. This reaction could be studied experimentally in an experimental loop. Proposed methods to suppress this reaction, such as creating composites could also be investigated.

Bibliography

[1] P. Guenoun, G. Daines, G. Giudicelli, B. Hiscox, K. Shirvan, T. J. McKrell, and M. S. Kazimi, "Poster presented at MIT Energy Night," 2015.

[2] http://www.world-nuclear-news.org/NN-Final-module-installed-at-Sanmen-2-0401165.html Accessed: 2016-06-01.

[3] "National Nuclear Data Centre Evaluated Nuclear Data File (ENDF) retrieval & plotting." http://www.nndc.bnl.gov/sigma/Accessed:2016-04-20.

[4] http://allthingsnuclear.org/dlochbaum/cracked-steam-generator-tubes-at-san-onofre Accessed: 2016-06-05.

[5] M. Darwish, F. M. Al Awadhi, and A. O. Bin Amer, "Combining the nuclear power plant steam cycle with gas turbines," *Energy*, vol. 35, 2010.

[6] N. C. Andrews, "Application of Advanced Fuel Concepts for use in Innovative Pressurized Water Reactors," *MIT PhD Thesis*, 2015.

[7] B. Feng, M. S. Kazimi, and B. Forget, "Feasibility of breeding in hard spectrum boiling water reactors with oxide and nitride fuels," *MIT-NFC-TR-124*, 2011.

[8] "World-nuclear.org, an article on uranium supplies from December 2016." http://www.world-nuclear.org/information-library/nuclear-fuel-cycle/uranium-resources/supply-of-uranium.aspx, accessed January 25th 2017.

[9] "Capacity factors for utility scale generators not primarily using fossil fuels, by the US Energy Information Administration." http://www.eia.gov/electricity/annual/html/epa_04_08_b.html, accessed January 25th 2017.

[10] "Background on Power Uprates for Nuclear Plants," 2015. http://www.nrc.gov/reading-rm/doc-collections/fact-sheets/power-uprates.html Accessed: 2016-06-10.

[11] "Clean power plan: Opportunities for nuclear power," 2015. https://www.epa.gov/cleanpowerplan/fact-sheet-clean-power-plan-opportunities-nuclear-power Accessed: 2016-06-10.

[12] http://www.westinghousenuclear.com/New-Plants/AP1000-PWR Accessed: 2016-06-01.

[13] J. Antill and B. L. Myatt, "Kinetics of the Oxidation of UN and U(CO) in Carbon Dioxide, Steam and Water at Elevated Temperatures," *Corrosion Science*, vol. 6, pp. 17–23, 1966.

[14] C. Alexander, "Metal-actinide nitride nuclear fuel," *US Patent 4,624,828*, 1986.

[15] T. Kawakita, K. Ikeda, S. Moro, M. Saito, and H. Sekimoto, "Feasibility Study on Nitride Fuel Core and Recycling System Toward Self-Consistent Nuclear Energy System," *Progress in Nuclear Energy*, vol. 40, pp. 597–606, 2002.

[16] E. Adamov and al., "The next generation of fast reactors," *Nuclear Engineering and Design*, vol. 173, pp. 143–150, 1997.

[17] Z. Su'ud and H. Sekimoto, "Design and Safety Aspect of Lead and Lead-Bismuth Cooled Long-Life Small Safe Fast Reactors for Various Core Configurations," *Journal of Nuclear Science and Technology*, vol. 32, pp. 834–845, 1995.

[18] S. Demuth, "SP 100 Space Reactor Design," *Progress in Nuclear Energy*, vol. 42, pp. 323–359, 2003.

[19] X. Ding and al., "High enrichment of N15 isotope by ion exchange for nitride fuel development," *Progress in Nuclear Energy*, vol. 50, pp. 504–509, 2008.

[20] B. Feng, A. Karahan, and M. S. Kazimi, "Steady-state fuel behavior modeling of nitride fuels in FRAPCON-EP," *Journal of Nuclear Materials*, vol. 427, 2012.

[21] M. Pukari, "Experimental and theoretical studies of nitride fuels," *Doctoral Thesis KTH Royal Institute of Technology*, 2013.

[22] "Nuclear fuel cycle in Russia," 2016. http://www.world-nuclear.org/information-library/country-profiles/countries-o-s/russia-nuclear-fuel-cycle.aspx Accessed: 2016-06-12.

[23] M. S. Kazimi and N. E. Todreas, *Nuclear Systems volume 1: Thermal-hydraulic fundamentals 2nd edition*. CRC Press 978-1-4398-0888-7, 2011.

[24] C. Shuffler, "Optimization of Hydride Fueled Pressurized Water Reactor Cores," *MIT master thesis*, 2004.

[25] EPRI-NP-2511-CCM-A, REVISION 3, "VIPRE 01: Thermal Hydraulic Code for Reactor volume II Users Manual,"

[26] J. Malen, N. Todreas, and A. Romano, "Thermal Hydraulic Design of Hydride Fueled PWR Cores," *MIT master thesis MIT-NFC-TR-062*, 2004.

[27] C. Shuffler, J. Trant, J. Malen, and N. Todreas, "Thermal hydraulic analysis for grid supported pressurized water reactor cores," *Nuclear Engineering and Design*, vol. 239, 2009.

[28] T. Chun and D. S. Oh, "A Pressure Drop Model for Spacer Grids with and without Flow Mixing Vanes," *Journal of Nuclear Science and Technology*, vol. 35, 1998.

[29] W. K. In, D. S. Oh, and T. H. Chun, "Pressure Drop Correlation for a PWR Fuel Assembly with Mixing Vane," *Proceedings of the Korean Nuclear Society Spring Meeting Cheju, Korea*, 2001.

[30] "IAEA, Review of Fuel Failures in Water Cooled Reactors, no. NF-T-2.1." http://www-pub.iaea.org/MTCD/Publications/PDF/Pub1445_web.pdf, accessed January 25th 2017.

[31] M. K. Au Yang, *Flow induced vibration of power and process plant components.* ASME 0791801667, 2001.

[32] D. Feng, P. Hejzlar, and M. S. Kazimi, "Thermal-hydraulic design of high-power-density annular fuel in PWRs," *Nuclear Technology*, vol. 160, 2007.

[33] Studsvik Scandpower, "CASMO-4 A FUEL ASSEMBLY BURNUP PROGRAM User's manual," *SSP-09/443-U Rev 0.*

[34] J. Leppanen, "Serpent – a continuous-energy monte carlo reactor physics burnup calculation code," 2015.

[35] "Nuclear data center at KAERI." http://atom.kaeri.re.kr/ Accessed: 2016-04-20.

[36] R. Simmons, N. Jones, F. Popa, D. Mueller, and J. Pritchett, "Integrable fuel burnable absorbers with ZrB2 in pressurized water reactors," *Nuclear Technology*, vol. 80, 1988.

[37] M. Hone, S. Skidmore, M. Misvel, and E. Resch, "AP1000 Core Reference Report," *WCAP-17524-NP*, 2012.

[38] F. F. et al., "AP1000 PWR Startup Core Modeling and Simulation with VERA-CS," *Advances in Nuclear Fuel Management 2015*, vol. CASL-U-2015-0132-00, 2015.

[39] Studsvik, "SIMULATE-3 Advanced Three-Dimensional Two-Group Reactor Analysis Code," *SSP-09/447 - University release*, 2009.

[40] USNRC HRTD Rev 0508, "Westinghouse Technology Systems Manual: Section 2.2 Power Distribution Limits,"

[41] K. A. Terrani, D. Wang, L. J. Ott, and R. O. Montgomery, "The effect of fuel thermal conductivity on the behavior of LWR cores during loss-of-coolant accidents," *Journal of Nuclear Materials*, vol. 448, p. 512–519, 2014.

[42] "Ux Consulting company fuel cost calculator." https://www.uxc.com/p/tools/FuelCalculator.aspx, accessed January 24th 2017.

[43] J. Secker, F. Franceschini, and S. Ray, "Accident tolerant fuel and resulting fuel efficiency improvements," *Advances in Nuclear Fuel Management V*, 2015.

[44] "Wholesale electricity prices, by the US Energy Information Administration." https://www.eia.gov/electricity/wholesale/, accessed January 25th 2017.

[45] N. Andrews, K. Shirvan, and M. S. Kazimi, "Viability of uranium nitride fueled high-conversion PWR," *Progress in nuclear energy*, 2015.

[46] US Nuclear Regulatory Commission, "FRAPCON-3.5: A computer code for the calculation of steady-state, thermal-mechanical behavior of oxide fuel rods for high burnup," *NUREG/CR-7022, Vol. 1, Rev. 1.*

[47] R. Vandervoort, W. Barmore, and C. Chne *Transactions of the Metallurgical Society of AIME*, vol. 242, 1968.

[48] "MATWEB material property data." http://www.matweb.com/search/datasheettext.aspx?matguid=61c13d461c3748d284bc89b15342f856.

Annex 1: Thermal Conductivity of Nitride Fuels

11.7 Uranium nitride

In the thermo-mechanical part of our study of uprates in uranium nitride cores, we must ensure that the uprates do not bring the fuel temperature past the uranium nitride dissociation point, at 1700°C. In the neutronic part of our study, we need to know the temperature of the fuel, to Doppler-broaden the resonances in the cross-sections and to take into account fuel expansion.

For these reasons, we must know the temperature dependence of the thermal conductivity of uranium nitride. There have been multiple determinations, shown in figure 11.1. We have chosen to use Rogzkin model to be consistent with previous fuel performance studies at MIT [7].

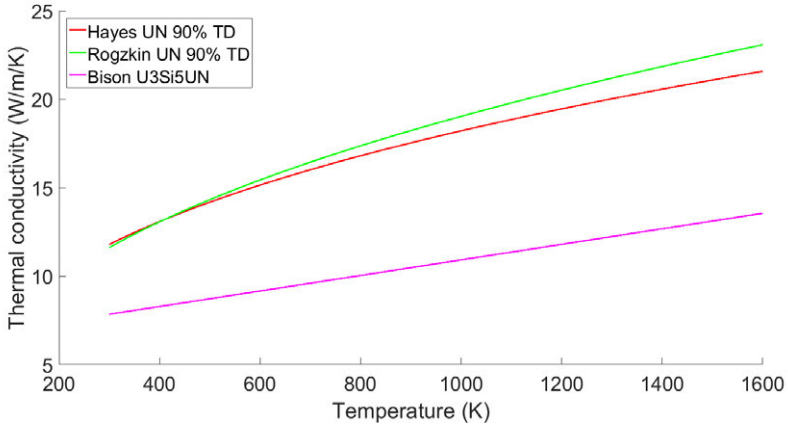

Figure 11.1: Thermal conductivity of uranium nitride

11.8 Uranium nitride with gadolinium nitride

In order to meet power peaking constraints we have added burnable poisons to the fuel. In addition to IFBA pins, we have chosen to mix gadolium nitride (GdN) with uranium nitride. Gadolinium 155-157 are strong neutron absorbers. Mixing GdN is directly inspired from the common nuclear industry practice of adding gadolinium oxide (Gd_2O_3) to oxide fuels. This has a non-negligible effect on reactivity, as up to 5

weight percent of GdN was mixed in the fuel. However, no measurement has ever been made of the thermal conductivity of this mix. Gadolinium nitride is being used in the semi-conductor industry, and its thermal conductivity has been measured, see figure 11.2.

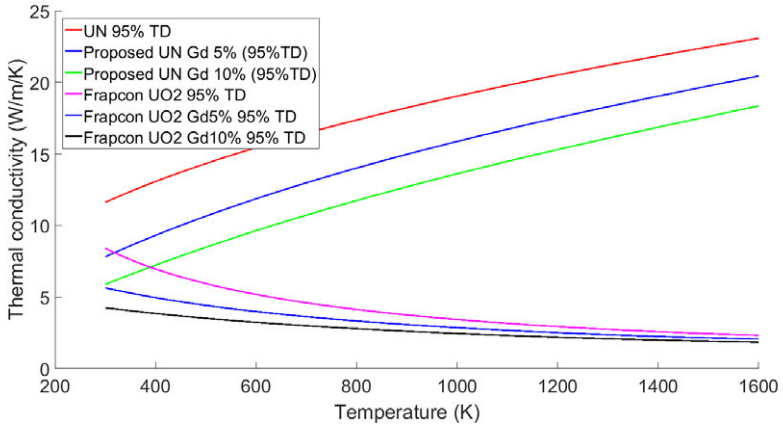

Figure 11.2: Thermal conductivity of uranium nitride mixed with gadolinium nitride, scaled with thermal conductivity of uranium oxide mixed with gadolinium oxide

However the thermal conductivity of a mix, and its temperature and burnup dependence cannot be easily obtained from the thermal conductivity of the two components. The only example we know of gadolinium reducing the fuel thermal conductivity is with oxide fuels. For this fuel, the following formula is used for thermal conductivity in FRAPCON [46]. It is based on the expression developed by the Nuclear Fuels Industries (NFI) model (Ohira and Itagaki, 1997) with modifications. This model applies to UO2 and UO2-Gd2O3 fuel pellets at 95% of theoretical density.

$$\lambda_{UO_2Gd_2O_3} = \frac{1}{A + a.gad + BT + f(Bu) + (1 - 0.9\exp(-0.04Bu))g(Bu)h(T)} + \frac{E}{T^2}\exp(-\frac{F}{T})$$

- T is the temperature in Kelvin
- Bu is the burnup in GWd/MTU
- f(Bu) is the effect of fission products on the crystal matrix, f(Bu) = 0.00187*Bu
- g(Bu) is the effect of irradiation defects, g(Bu) = 0.038*Bu^0.28
- h(T) is the temperature dependence of annealing on irradiation defects, $h(T) = \frac{1}{1 + 396e^{-Q/T}}$
- Q is a temperature dependence parameter (Q/R = 6380 K)
- A = 0.0452 (m-K/W)
- a = constant = 1.1599
- gad = weight fraction of gadolinia

- B = 2.46E-4 (m-K/W/K)
- E = 3.5E9 (W-K/m)
- F = 16361 (K)

Another expression adjusts for density, and another adjusts for Pu content. This model has the thermal conductivity of the oxide fuel decrease with temperature, and decrease with Gd content. We know that the nitride fuel thermal conductivity increases with temperature, but we don't know the variation when the Gd content increases. We make the choice to have the same scaling as the oxide fuel for Gd content. That is to say :

$$\frac{\lambda_{UO_2Gd_2O_3}(gad,T)}{\lambda_{UO_2Gd_2O_3}(gad=0,T)} = \frac{\lambda_{UNGdN}(gad,T)}{\lambda_{UNGdN}(gad=0,T)}$$

In SIMULATE, we need thermal feedback and burnup dependence of the cross-sections to accurately deplete cores. The burnup dependence appears in the thermal conductivity of the fuel. The thermal conductivity of uranium nitride diminishes with burnup, and as a result the fuel heats up. SIMULATE can then use the branch cases done in CASMO4E to interpolate the cross sections at a given burnup and at the required temperature. The burnup dependence of the thermal conductivity was obtained using FRAPCON [46] by Yanin Sukjai, and its effect on the fuel temperature can be seen in Figure 11.3. This is specified in SIMULATE3 using the TAB.TFU card.

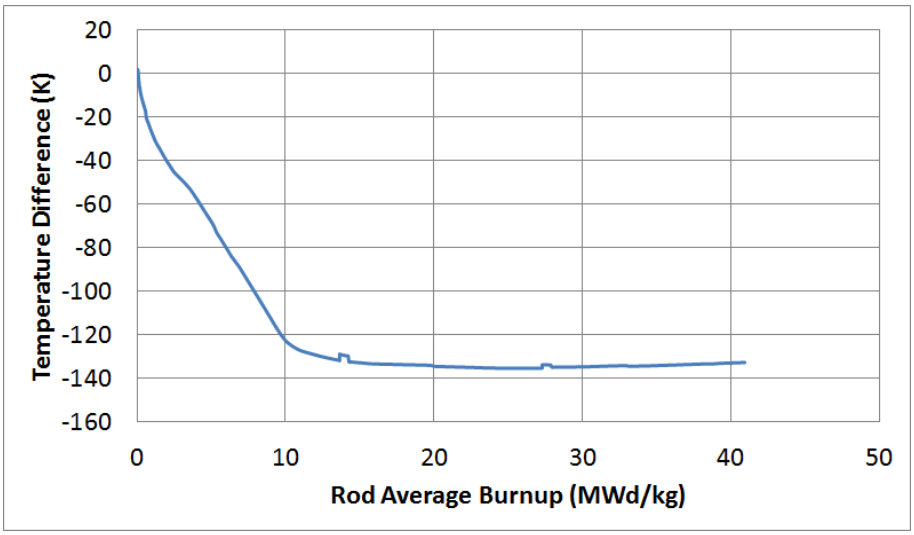

Figure 11.3: Change in fuel average temperature due to decrease in fuel thermal conductivity with burnup

The temperature of the fuel also depends on the relative power fraction, the ratio of local to average power, and this can also be obtained using FRAPCON. Figure 11.4 shows the variation of the fuel temperature with the relative power fraction. This can be specified in SIMULATE3 using the SEG.TFU card.

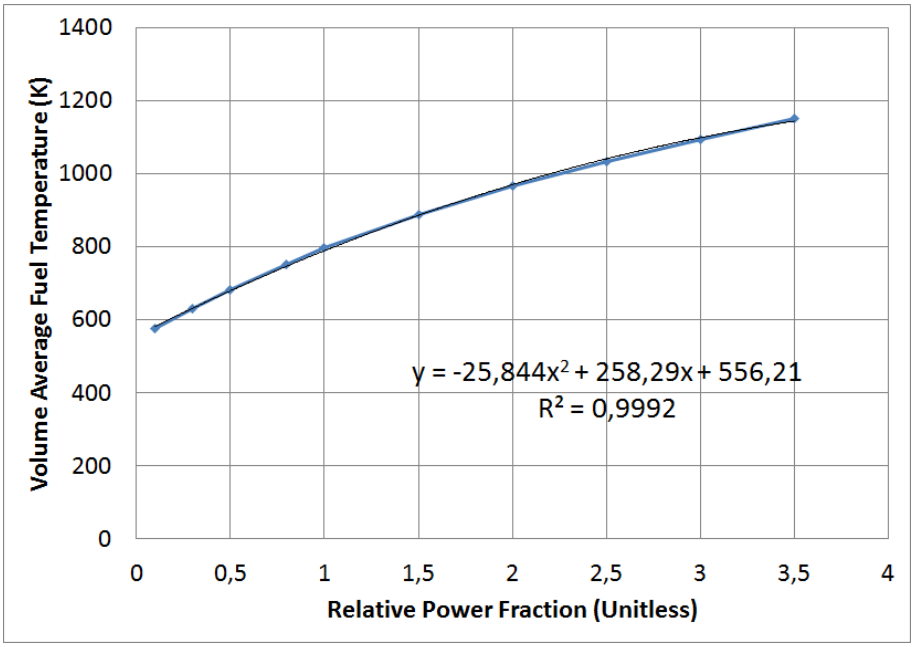

Figure 11.4: Average fuel temperature for a range of relative power fractions

Annex 2: Density of Uranium Nitride fuels

According to previous studies on uranium nitride fuels [20], uranium nitride with a higher porosity, up to 15%, would have lower fuel failure rates from cladding collapse and grid-to-rod fretting. For this reason, we chose to use a lower density, of 90% of the theoretical density rather than the usual 95.5% for oxide fuels. A 100% TD uranium nitride was achieved by Vandervoort [47] using isostatic hot pressing, so 90% is not unfeasible.

In order to account for gadolinium content in the density, four models were proposed. The theoretical density of gadolinium nitride is 9.1 g/cc [48], while the theoretical density of uranium nitride is 14.3 g/cc. The four models proposed are

- a correlation created from the density change in uranium oxide when adding gadolinium oxide, and adapted to UNGdN
- a model accounting for the atomic volumes of U, Gd and N, based on the cubic square root of their atomic mass
- a model accounting for the molecular volumes of UN and GdN based on the cubic square root of the sum of their atomic mass
- a model with a simple volumetric mixing of the two densities

The density change with Gad content in these models are shown in figure 11.5. We can see that the 3 last models agree pretty tightly. The most intuitive being the atomic one, we used this one to account for gadolinium content in UN-GdN.

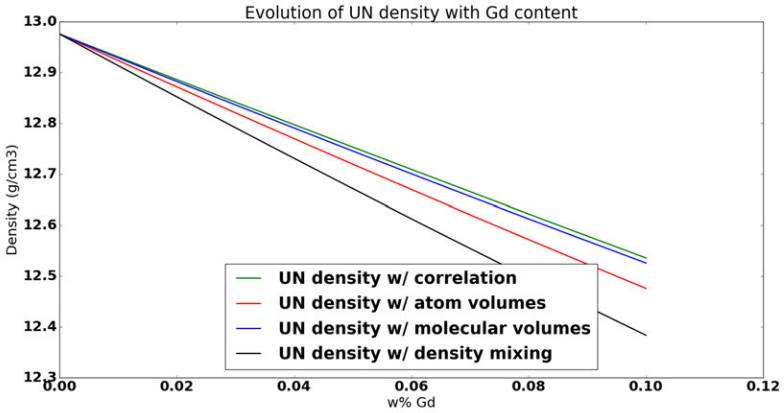

Figure 11.5: Proposed models for the density of a UN-GdN mix as a function of gadolinium nitride content

Annex 3: MATLAB Script for Power Uprates

```
%Script for determination of max power for alternative pitch and diameters
%Computes mdnbr, pressure drop, fuel temperature and clad wear rates to
%determine if an uprate is possible by changing core primary mass flow rate
%or inlet temperature
%Authors : Guillaume Giudicelli, Nathan Andrews

clear all % clear results
clc       % clear command prompt
tic       % initialization of time
format compact

% List of options to set
% core geometry, run_mode, fuel, core_shape, operating parameters
% Check that the cross-flow profile is good for your run_mode and your reactor
% Check that the wear rates reference are for the appropriate geometry

% Hard-coded (besides inputs)
% - spacer properties in w3l correlation for mdnbr, in pressure drop corr.
% - cladding and gap properties for fuel temperature
% - cladding mechanical properties for vibration analysis
% - design and positionning of mixing vanes

%%Geometry parameters
D_pin_min=0.65/100;  % min diameter
D_pin_max=1.25/100;  % max diameter
P_ov_D_min=1.1;      % minimum pitch
P_ov_D_max=1.55;     % max pitch
N_grids_min=10;      % min number of spacers
N_grids_max=15;      % max number of spacers (>15 span/De <20 in design range)

%%Run parameters
run_mode= 'trends'; % 'mdot' to raise mass flow to reach higher power, 'Tinlet' to lower inlet temperatu
%'trends' to see performances trends at constant power, 'selected_core' to see the perf of the core in TH
P_steps=20;                % steps between min and max pitch
D_steps=20;                % steps between min and max diameter
core_pow_step=100;         % core power iteration step size in MW
core_pow_max=4500;         % start of core power iteration, max core power solved for (in MW).
%Redefined for Tinlet mode below
core_pow_min=100;          % lower limit for core power iteration (in kW).
%Redefined for Tinlet mode lower
```

```
G_steps=1;                  % steps between min and max Ngrids, can be N_grids_max-N_grids_min+1
nominal=1;                  % set to 1 to calculate AP1000 nominal
speed_mode=[0,200];         % use a previous core_power_mat to do less power iterations,
%second argument is how much above we'll start in MW

%%Core Conditions
shape       ='-';  % 'AP1000' to have 157 assemblies,
%'-' to have same surface as A_nominal with no constraints on number of assemblies
tol         =0.06;      % tolerance on number of assemblies
fuel        ='nitride'; % 'nitride' or 'oxide'
P_op        =155.1;     % pressure in bar
z_assm      =4.2672;    % height of pin/assembly in m
z_assm_tot  =4.583;     % with top and bottom plenum, from DCD19
T_in_nominal=279.4;     % temperature of inlet for nominal case
T_co_in     =T_in_nominal;
T_co_out    =324.66;    % average coolant outlet temp in degrees C
n_nodes     =43;        % number of axial nodes
n_ass_nom   =157;       % nominal number of assemblies per core
n_row_nom   =17;        % nominal number of pin rows per assembly
n_heated_nom=264;       % nominal number of heated pins per assembly
diam_nom=0.94996;       % nominal pin diameter in cm
pd_nom=1.25984/0.94996; % nominal pitch on diameter ratio
A_nominal   =(n_ass_nom*n_row_nom^2)*(diam_nom*pd_nom*1e-2)^2; % core total area
%(amount of space inside reflectors) based on 157 initial AP1000 assemblies
T_c_new     =18;        % length of fuel cycle in months, to consider for total wear, from wear rates
core_power_nominal =3.4e6; % AP1000 nominal power
nominal_mass_flow = core_power_nominal /
(XSteam('h_pT',P_op,T_co_out) - XSteam('h_pT',P_op,T_in_nominal));
% core mass flow rate, for Tinlet mode only

%%Peaking
peak_assm=1.40;  % assembly peaking (full core value needed, 1.4 is approx)
peak_pin =1.; % pin peaking in an assembly, limited to this value to avoid boiling
% Cosine shape is assumed for axial power profile

count=0;            % to keep track of the status of calculation

%Thermo-mechanical and other limits
T_in_limit = 257;   % minimal inlet temperature in Tinlet mode
T_in_max = 300;     % maximal inlet temperature (above isn't interesting)
mdnbr_lim = 2.985;  % performance of the AP1000 in this script
P_drop_lim= 1.8486e+05; % performance of the AP1000 in this script
x_e_lim=0.0;        % limit on equilibrium quality of liquid (no saturated boiling)
if strcmp(fuel,'nitride')
    T_fuel_ave_lim=3000; % celsius, no limit on average
    T_fuel_CL_lim =1700; % thermal dissociation of UN
elseif strcmp(fuel,'oxide')
    T_fuel_ave_lim=1400; % limit on fission gas release
    T_fuel_CL_lim =2800; % limit on melting
end
VSM_lim=0.3;  % vortex shedding margin
FIM_lim=1.0;  % fluid instabilites
wear_lim=1.0; % not more wear than nominal design

%%nominal values of fretting and sliding wear for UO2 fuel, using the script
%cladding is Zr4
T_c_ref = 18 ;              % months, length of reference cycle
load('Wear_rates_nominal') % wear rates previously calculated for an AP1000
```

```
%%state points
h_out_avg_core=XSteam('h_pT',P_op,T_co_out); % outlet enthalpy max f(P_op,T_in)
if strcmp(run_mode,'mdot')
    h_in=XSteam('h_pT',P_op,T_co_in);        % inlet enthalpy f(P_op,T_in)
    del_h_max=h_out_avg_core-h_in;           % core delta h for constant delta T
end
h_f=XSteam('hL_p',P_op);      % saturated fluid enthalpy in kJ/kg
h_g=XSteam('hV_p',P_op);      % saturated vapor enthalpy in kJ/kg
h_fg=h_g-h_f;                 % vaporization enthalpy in kJ/kg
if strcmp(run_mode,'Tinlet')  % calculating core power bounds for Tinlet mode
    core_pow_max = nominal_mass_flow*(h_out_avg_core-XSteam('h_pT',P_op,T_in_limit))/1e3;
    core_pow_min = nominal_mass_flow*(h_out_avg_core-XSteam('h_pT',P_op,T_in_max));
end

%No need for big matrices/loops if just want reference geometry
if nominal == 1                       % care: P_op and T_co_out have already been assigned
    D_steps=1;                        % to run one core
    P_steps=1;
    G_steps=1;
    N_grids_min=10;
    core_pow_max=core_power_nominal + core_pow_step;  % no matter
    speed_mode = [0,100];             % disactivate speed mode
    run_mode = 'mdot';                % compatible with running one core
    shape = '-';                      % shape should be the same as AP1000
    h_in=XSteam('h_pT',P_op,T_co_in); % inlet enthalpy f(P_op,T_in)
    del_h_max=h_out_avg_core-h_in;    % core delta h for constant delta T
end

if strcmp(run_mode,'selected_core') && nominal == 0
% care: P_op and T_co_out have already been assigned
    strcat('Was selected core chosen with_',run_mode,' strategy?') % printing a safety check
%     load('TH_optimized')                                          % load the core characteristics
    load('chosen_core.mat')
    strcat('Do you want to test the selected core with a power of_',num2str(core_power/1e6),' GWth?')
    %  other safety check
    D_steps=1;
    P_steps=1;
    G_steps=1;
%     D_pin_min= D_opt;
    D_pin_min= D_pin_opt;
    D_pin_max=D_pin_min;
    P_ov_D_min = P_ov_D_opt;
    P_ov_D_max = P_ov_D_min;
%     N_grids_min = G_opt;
    N_grids_min = N_grids;
    N_grids_max = N_grids_min;
    core_pow_step = 0;
    core_pow_max= core_power / 1e3; % in MW
    m_dot_core = mdot_core;
    h_in = h_out_avg_core - core_pow_max*1000/mdot_core;
    T_in = XSteam('T_ph',P_op,h_in);
    T_co_in = T_in;
    speed_mode = [0, 100];          % disactivate speed mode
    run_mode = '-';
    shape = 'AP1000';
    del_h_max=h_out_avg_core-h_in; % core delta h for constant delta T
end
```

```
%Fuel properties, constant at all temperatures
if strcmp(fuel,'nitride')
    tc_fuel=18;    %thermal conductivity uo2 is 3.6, UN 18 to 20
    rho_hm = 12.9; %density of fuel g/cc, for uo2 10.43, UN 12.9, 10% porosity
    M_f = 253;     %g/mol molar mass of fuel, 270 UO2, 253 UN
elseif strcmp(fuel,'oxide')
    tc_fuel=3.6;
    rho_hm = 10.43;
    M_f = 270;
end

%Pre-allocating
core_power_mat = zeros(D_steps,P_steps,G_steps);
m_dot_mat = zeros(D_steps,P_steps,G_steps);
n_pin_mat = zeros(D_steps,P_steps,G_steps);
entrance_region_mat = zeros(D_steps,P_steps,G_steps);
q_p_avg = zeros(D_steps,P_steps,G_steps);
xe_mat = zeros(D_steps,P_steps,G_steps);
h_out_avg_mat = zeros(D_steps,P_steps,G_steps);
mdnbr_mat = zeros(D_steps,P_steps,G_steps);
failure = cell(D_steps,P_steps,G_steps);
P_drop_tot_mat = zeros(D_steps,P_steps,G_steps);
yod_mat = zeros(D_steps,P_steps,G_steps);
T_fuel_ave_mat = zeros(D_steps,P_steps,G_steps);
T_fuel_CL_mat = zeros(D_steps,P_steps,G_steps);
VSM_min_lift_mat = zeros(D_steps,P_steps,G_steps);
VSM_min_drag_mat = zeros(D_steps,P_steps,G_steps);
FIM_mat = zeros(D_steps,P_steps,G_steps);
W_dot_fret_mat = zeros(D_steps,P_steps,G_steps);
W_dot_slide_mat = zeros(D_steps,P_steps,G_steps);
G_mat = zeros(D_steps,P_steps,G_steps);
V_crit = zeros(n_nodes,1);
FIM = zeros(n_nodes,1);
G_vec = zeros(G_steps,1);
D_vec =  zeros(D_steps,1);
D_pellet_vec =  zeros(D_steps,1);
D_ci_vec =  zeros(D_steps,1);
P_ov_D_vec = zeros(P_steps,1);
A_core_mat = zeros(D_steps,P_steps,G_steps);
T_in_mat = zeros(D_steps,P_steps,G_steps);
n_rod_assem_mat = zeros(D_steps,P_steps,G_steps);
H_ratio_mat = zeros(D_steps,P_steps,G_steps);
T_co = zeros(1,n_nodes,1);
int_fun_1 = zeros(1,n_nodes);
mu = zeros(1,n_nodes);
rho = zeros(1,n_nodes);
rho_mean = zeros(1,n_nodes);
C_f_CT = zeros(1,n_nodes);
cp = zeros(1,n_nodes);
tc = zeros(1,n_nodes);
P_ov_D_mat =zeros (D_steps,P_steps,G_steps);
D_mat = zeros(D_steps,P_steps,G_steps);


for l =1:G_steps % loop on number of spacer grids
        G_step=(N_grids_max-N_grids_min)/G_steps; %incremental increase per step in pin diameter
        N_grid= floor(N_grids_min+G_step*(l-1));
```

```
if nominal ==1 || isnan(N_grid)
    N_grid = N_grids_min;
end
G_vec(l)=N_grid; % vector of pin diameters
G_mat(:,:,l)=N_grid;

for m=1:D_steps % loop on pin diameter

    D_step=(D_pin_max-D_pin_min)/D_steps; %incremental increase per step in pin diameter
    D_pin=D_pin_min+D_step*(m-1);
    if nominal == 1
        D_pin = 0.94996/100;
    end
    D_vec(m)=D_pin; %vector of pin diameters

    %pin diameter calculation
    if D_pin > 0.007747
        thick=1e-3*(0.508+0.0362*(D_pin*1e3-7.747));%clad thickness in m
        gap=1e-3*(0.0635+0.0108*(D_pin*1e3-7.747)); %clad gap - eqn from shuffler paper
    else
        thick=0.508*1e-3;
        gap=0.0635*1e-3;
    end
    D_ci=D_pin-2*thick;  % cladding inner diameter calculation, assuming .57 mm thickness
    D_ci_vec(m)=D_ci;
    D_pellet=D_ci-gap*2; % fuel pellet diameter
    D_pellet_vec(m)=D_pellet;

    for n=1:P_steps  %loop on pitch to diameter ratio
        count=count+1;
        disp(count)
        A_core = A_nominal;          % reset A_core
        if strcmp(run_mode,'Tinlet') % presetting to steam cycle failure
            failure{m,n,l} = 'Steam cycle limit'; % default failure mode for Tinlet
        end
        P_ov_D_step=(P_ov_D_max-P_ov_D_min)/P_steps;

        P_ov_D=P_ov_D_min+P_ov_D_step*(n-1);
        if nominal == 1
            P_ov_D = pd_nom; %nominal AP1000 value from Nathan CASMO input files
        end
        pitch=D_pin*P_ov_D;

        P_ov_D_vec(n)=P_ov_D;

        %Check if has a pitch that can fit in a 157 assembly core,
        %selects the core that is closest in number of assemblies
        %and meets tolerance value
        if strcmp(shape,'AP1000')
            n_rods_possibilities = [ 15^2, 16^2, 17^2, 18^2, 19^2,
            20^2, 21^2, 22^2, 23^2, 24^2]; % number of rod per assemblies
            good = 0;
            prev_error = 1;
            for nn_rod_per_assemb = n_rods_possibilities
                error = abs(A_nominal/(nn_rod_per_assemb*pitch^2) - n_ass_nom)/n_ass_nom;
                %error on number of assemblies
                if A_nominal/(nn_rod_per_assemb*pitch^2) > (1-tol)*n_ass_nom
                && A_nominal/(nn_rod_per_assemb*pitch^2) <(1+tol)*n_ass_nom && error < prev_erro
```

```
                %+/- tol on surface
                    good = 1;
                    A_core = n_ass_nom/(A_nominal/(nn_rod_per_assemb*pitch^2))*A_nominal;
                    %to set the number of pins so that we have 157 assemblies
                    A_core_mat(m,n,l) = A_core;
                    n_rod_assem_mat(m,n,l) = sqrt(nn_rod_per_assemb);
                    prev_error = error;
                end
            end
            if good == 0;
                failure{m,n,l} = 'N assembly';
                continue
            end
        end

        core_power=core_pow_max*1000; % initial core power in MW*1000 to get kW
        % kW are used so that thermal state points calcution is easier with
        % XSteam module, XSteam uses kJ/kg for enthalpy

        if speed_mode(1) == 1
        % getting an initial guess from an interpolation from a previous result
            core_power = speed_mode_function(P_ov_D,D_pin,N_grid,run_mode,shape)
            +speed_mode(2)*1000;
        end
        pow_count = 0;
        % counts the number of iterations in power loop, to check speed_mode ok or not
        valid = 0;            % placeholder

        while (valid<0.1 && core_power>core_pow_min*1000) && (strcmp(run_mode,'trends')==0
        || pow_count<0.5)
            %while all limits havent been met and power high
            %enough, or if run_mode is trends, 1 iteration is run
            valid=1.0;
            pow_count = pow_count + 1;

            core_power = core_power - core_pow_step * 1000; %lower core power

            if core_power < core_pow_min
                disp('power lower than minimum power of interest')
            end
            if nominal == 1 || strcmp(run_mode,'trends')
                core_power = core_power_nominal;
            end
            core_power_mat(m,n,l)=core_power;

            if strcmp(run_mode,'Tinlet')
                m_dot_core=nominal_mass_flow;
            elseif strcmp(run_mode,'mdot')
                m_dot_core=core_power/del_h_max;
            elseif strcmp(run_mode,'trends')
                m_dot_core=nominal_mass_flow;
            end
            m_dot_mat(m,n,l)=m_dot_core;


%% Power input and calcs
n_pin=floor(A_core/pitch^2);                    % number of pins in a core
n_pin_heated = n_pin * n_heated_nom/n_row_nom^2; % same proportion of heated pins
```

```
%as nominal design
n_pin_mat(m,n,l)=n_pin;                              % number of pin for this pitch and diameter
avg_pin_power=core_power/n_pin_heated;               % average pin power in kW
peak_pin_power=avg_pin_power*peak_assm*peak_pin;     % max pin power in a core
q_p_max=peak_pin_power*pi/(2*z_assm);                % max linear heat rate, assuming cosine shape

%some calcs
del_z=z_assm/n_nodes;                                % height of a single node
A_flow=pitch^2-D_pin^2*pi/4;                         % flow area in m2 of single channel
m_dot=m_dot_core/n_pin;                              % mass flow rate in subchannel kg/s
G=m_dot/A_flow;                                      % mass flux in kg/m2s (pin)

if strcmp(run_mode,'Tinlet')
    h_in = h_out_avg_core - core_power/m_dot_core;
    T_in = XSteam('T_ph',P_op,h_in);
    T_in_mat(m,n,l) = T_in;
else
    T_in_mat(m,n,l) = T_co_in;
    h_in = XSteam('h_pT',P_op,T_co_in);
end

h_out_avg=avg_pin_power/m_dot+h_in;      % outlet enthalpy average of core
h_out_peak=peak_pin_power/m_dot+h_in;    % exit enthalpy of peak pin

delta_h=h_out_peak-h_in;    % change in enthalpy in peak channel
delta_h_avg=h_out_avg-h_in; % core average enthalpy rise
P_w=pi*D_pin;               % wetted pin perimeter

D_e=4*A_flow/P_w;           % hydraulic diameter in m

%Spacer span check
h_grid = 0.05715; % height of spacers
h_IFM  = 0.01676; % height of IFMs
S_span = (z_assm_tot - N_grid*h_grid)/(N_grid+1);
if S_span/D_e < 20
    entrance_region_mat(m,n,l) = S_span/D_e;
end

%% Channel H/HM ratio
rho_w = XSteam('rho_pT',P_op,(T_co_in+T_co_out)/2)*1e-3;
M_w = 18.0; % g/mol water

mols_w = (rho_w/M_w)*(pitch^2-D_pin^2*pi/4); % mols coolant per subchannel
mols_f = (rho_hm/M_f)*D_pellet^2*pi/4;       % mols fuel per subchannel

H_ratio_mat(m,n,l) = mols_w.*2./(mols_f);    % H/HM ratio for the subchannel (not for the core)


%% axially dependent variable initialization
z = linspace(0.5*del_z,(n_nodes-0.5)*del_z,n_nodes);

q_p=q_p_max*cos(pi*(z-z_assm/2)/z_assm); % local linear heat rate kW/m, assumption of cosine shap
q_p_avg(m,n,l)=mean(q_p);                % average heat flux
q_pp=q_p/(D_pin*pi);                     % local heat flux kW/m^2


%axial state points and temperatures
h_fraction = cumsum(q_p)/sum(q_p);
```

```
h= h_in+h_fraction*delta_h;              % local enthalpy (vector)

x_e=(h-h_f)/h_fg;                        % equilibrium quality at each nodal location

for i=1:n_nodes
    T_co(i)=XSteam('T_ph',P_op,h(i));    % local coolant temp f(h, P_op)
end

%% mDNBR
% W3 correlation calculation, Nuclear Systems vol1 Todreas and Kazimi
q_pp_ucr=((2.022-0.06238*P_op/10)+(0.1722-0.01427*P_op/10)*exp((18.177-0.5987*P_op/10)*x_e)).*..
    ((0.1484-1.596*x_e+0.1729*x_e.*abs(x_e))*2.326*G+3271).*(1.157-0.869*x_e).*...
    (0.2664+0.8357*exp(-124.1*D_e)).*(0.8258+0.0003413*(h_f-h_in)); % uniform axial heat flux w3
dnbr1=q_pp_ucr./q_pp;

% Correction for non-uniform axial heat flux
C_w3=185.6*(1-x_e).^4.31/G.^0.478;

% C_w3 in integrand evaluated at l_DNB, see 22.313 MIT OCW
% Riemann integration was replaced by MATLAB integral and now
% analytic for speed
int_fun_1 = q_p_max/(D_pin*pi) ./ ((pi/z_assm)^2 + C_w3.^2) .* (-pi/z_assm*cos(pi*z/z_assm) +
C_w3.*sin(pi*z/z_assm) + pi/z_assm.*exp(-C_w3.*z));
F=(C_w3.*int_fun_1)./(q_pp.*(1-exp(-C_w3.*z)));

q_pp_ncr=q_pp_ucr./F;  % nonuniform w3

%Spacer grid correction for mDNBR
Fg  = 1;     % to be modified, grid type modifier. Unknown
TDC = 0.038; % to be modified turbulent cross flow mixing parameter, conservative estimate
%from Shuffler
Ks  = 0.066;
% grid spacing factor, depends on grid type, propretary, here Feng value from Shuffler
F_gridRL = Fg.*((1.445-0.0371.*(z*3.28084)).*((P_op*14.5038)/225.896)^0.5.*(exp((x_e+0.2).^2)
-0.73) +Ks*(G*737.3422919)./1E6*(TDC/0.019)^0.35);  % grid factor, using british units
q_pp_nscr = F_gridRL .* q_pp_ncr;

dnbr=q_pp_nscr./q_pp;

mdnbr=min(dnbr);

if max(x_e) > x_e_lim && strcmp(run_mode,'trends')==0 %is it boiling check
    valid=0;
    failure{m,n,l} = 'Boiling';
    continue
else
    xe_mat(m,n,l)=max(x_e);
end
h_out_avg_mat(m,n,l)=h_out_avg;

if mdnbr < mdnbr_lim - 1E-6 && strcmp(run_mode,'trends')==0
    valid=0;
    failure{m,n,l}='mDNBR';
    continue
else
    mdnbr_mat(m,n,l)=mdnbr;
end
```

```
%% Pressure Drop

g=9.81;          % gravitational constant

if P_ov_D>=1.1   % constants for use in Cheng and Todreas friction pressure drop
   a=0.1339;
   b1=0.09059;
   b2=-0.09926;
else
   a=0.09423;
   b1=0.5806;
   b2=-1.239;
end

for i=1:n_nodes
    %State points
    mu(i)=XSteam('my_ph',P_op,h(i));
    rho(i)=XSteam('rho_ph',P_op,h(i));
    %Factor in CT model
    C_f_CT(i)=a+b1*(P_ov_D-1)+b2*(P_ov_D-1)^2;
end
rho_mean(m,n,l) = mean(rho);
Re_t=D_e.*G./mu;
f_CT=C_f_CT./(Re_t).^0.18;
P_fric=f_CT./D_e.*(G.^2./(2*rho)).*(del_z-N_grid*h_grid/n_nodes);
%compensating for rod friction taken into account in In model for spacers

%Gravity del_p
P_g=rho*g*del_z;

%Pressure loss in plenum from gravity and friction
P_drop_plenum = (z_assm_tot-z_assm)*g*rho(end) + f_CT(end)/D_e*(G(end)^2/(2*rho(end)))...
*(z_assm_tot-z_assm);

%form del_p from spacers and entry/exit of assembly
K_c=0.5;
K_e=1.0;
C_v_grid=6.5;                              % Rehme grid coefficient from TK book
grid_thick=0.45e-3;                        % grid strap thickness
A_grid_front=pitch^2-(pitch-grid_thick)^2; % grid frontal area

P_form_in=(K_c)*(G^2/(2*rho(1)));          %contraction loss
P_form_out=(K_e)*(G^2/(2*rho(n_nodes)));   %expansion loss
%Grid pressure loss, Rehme model
P_grid_rehme=N_grid*C_v_grid*(A_grid_front/A_flow)^2*G^2/(2*mean(rho)); %grid loss
%C_v_grid also has a dependance on rho (TK p506)

%Grid pressure loss at spacers, In model (TK p507)
grid_loc_vec = linspace(0,z_assm_tot,N_grid);

%Defining areas at pin level instead of assembly (ok since ratio ?) (to check)
eps2 = A_grid_front / A_flow;
A_grid_wetted = h_grid*(pitch-grid_thick)*4;
A_rod_grid = h_grid*pi*D_pin;
A_flow_grid = A_flow - A_grid_front;

%Getting density, viscosity and Reynolds at grid location
```

```
rho_grid = interp1(z,rho,grid_loc_vec); % finding pressure at exact location
rho_grid(1) = rho(1);                   % using node 1 to avoid looking for T_in
rho_grid(N_grid) = rho_grid(N_grid-1);  % approx to avoid looking for T_out in hot channel
mu_grid = interp1(z,mu,grid_loc_vec);
mu_grid(1) = XSteam('my_ph',P_op,h_in);
mu_grid(N_grid)=mu_grid(N_grid-1);
D_e_grid = 4*(A_flow_grid)/(pi * D_pin + 4*(pitch - grid_thick));
G_grid = G*A_flow / A_flow_grid;
Re_t_grid = D_e_grid.*G_grid./mu_grid;

C_form_grid = 2.75-0.27*log(Re_t_grid)/log(10);
C_fric_grid_lam = 1.328.*(G.*(h_grid-3E4.*mu_grid./G)./mu_grid).^(-1/2.);
C_fric_grid_turb= 0.523*log(0.06*G.*(h_grid-3E4.*mu_grid./G)./mu_grid).^(-2.);
C_fric_grid = C_fric_grid_lam .* 3E4.*mu_grid./G./h_grid + C_fric_grid_turb...
*(h_grid-3E4.*mu_grid./G)./h_grid;
C_fric_rod = 0.184*Re_t_grid.^(-0.2);  %according to TK, found different in Chun and Oh article
%mixing vanes on spacers and Intermediary Flow Mixers
%for lack of information, only modeling a mixing vane between spacers for IFMs
Cdmv = 0.72;                          % recommended by In in TK
eps_mv = 0.25;                        % split mixing vane from CHUN and OH
pos_vanes = linspace(1,1,N_grid);     % there are vanes on each spacer
pos_vanes(1) = 0;                     % except bottom one
pos_vanes(N_grid-5:N_grid) = [1.5 2 2 2 1.5 0]; %adding the IFM in the middle of top spacers
Cmv = Cdmv*eps_mv/(1-eps_mv)^2*pos_vanes;

K_in_grid = C_form_grid*eps2/(1-eps2)^2 + C_fric_grid*A_grid_wetted/A_flow*1/(1-eps2)^2 + ...
  C_fric_rod*A_rod_grid/A_flow*1/(1-eps2)^2 + Cmv;

P_grid_In =  K_in_grid.*G.^2./(2.*rho_grid);
P_grid = sum(P_grid_In);

%To compare 2 models
P_grid_in_mat(m,n,l)= P_grid;
P_grid_rehme_mat(m,n,l)= P_grid_rehme;
P_form_grid_mat(m,n,l) =  sum(C_form_grid*eps2/(1-eps2)^2.*G.^2./(2.*rho_grid));
P_fric_grid_mat(m,n,l) =  sum(C_fric_grid*A_grid_wetted/A_flow*1/(1-eps2)^2.*G.^2./
(2.*rho_grid));
P_fric_rod_mat(m,n,l) =  sum(C_fric_rod*A_rod_grid/A_flow*1/(1-eps2)^2.*G.^2...
/(2.*rho_grid));
P_Cmv_mat(m,n,l)      =  sum(Cmv.*G.^2./(2.*rho_grid));

%total P Loss
P_fric_tot=sum(P_fric);
P_g_tot=sum(P_g);
P_form_tot=P_form_in+P_form_out+P_grid;

P_drop_tot=P_fric_tot+P_g_tot+P_form_tot+P_drop_plenum;

if P_drop_tot > P_drop_lim && strcmp(run_mode,'trends')==0;
    valid=0;
    failure{m,n,l} = 'P_drop';
    continue
else
    P_drop_tot_mat(m,n,l)=P_drop_tot;
end

%% BOL Fuel Temperature
```

```
tc_clad=21.5; % thermal conductivity clad W/mk
emis_u=.8;    % emissivity u
emis_z=0.18;  % emissivity zirc

%Presser correlation assuming infinite array - modifier on DB correlation
%for Nu number
psi=0.9217+0.1478*P_ov_D-0.1130*exp(-7*(P_ov_D-1));

for i=1:n_nodes
    cp(i)=XSteam('cp_ph',P_op,h(i))*1000; % specific heat converted to J/kgk
    tc(i)=XSteam('tc_ph',P_op,h(i));      % thermal conductivity
end
Pr=cp.*mu./tc;

Nu_ct=0.023*Re_t.^.8.*Pr.^.4;   % DB correlation for nusselt number - circular tube

Nu_inf=psi*Nu_ct;               % nusselt number for infinite array of rods,
%based on presser correlation

heat_trans=Nu_inf.*tc./D_e;     % heat transfer coefficient

T_clad_out=T_co+q_p*1000./(pi*D_pin.*heat_trans);

T_clad_in=T_clad_out+q_p*1000*log(D_pin/D_ci)/(2*pi*tc_clad);

%vectorial iteration to find h_gap
%k_helium from TK, equation (8.140)
k_hel=15.8e-6*(T_clad_in+273.2+100).^0.79*100; % W/m
h_gap=k_hel./gap;
T_fuel_out=T_clad_in+q_p.*1000./(pi*D_pellet*h_gap);
for i = 1:4
    k_hel=15.8e-6*((T_clad_in+273.2+T_fuel_out+273.2)/2).^0.79*100;
    h_gap=k_hel./gap;
    T_fuel_out=T_clad_in+q_p.*1000./(pi*D_pellet*h_gap);
end

T_fuel_CL=T_fuel_out+q_p*1000/(pi*4*tc_fuel);
T_fuel_ave=(T_fuel_CL+T_fuel_out)/2;

if max(T_fuel_ave) > T_fuel_ave_lim && strcmp(run_mode,'trends')==0
    valid=0;
    failure{m,n,l}='Tf_ave';
    continue
else
    T_fuel_ave_mat(m,n,l)=max(T_fuel_ave);
end

if max(T_fuel_CL) > T_fuel_CL_lim && strcmp(run_mode,'trends')==0
    valid=0;
    failure{m,n,l}='Tf_cl';
    continue
else
    T_fuel_CL_mat(m,n,l)=max(T_fuel_CL);
end


%% Vortex Shedding Margin
```

```
K_vibr=5;        % 5 for turbulent flow
E_mod_clad = (108800-54.75*(T_clad_in+T_clad_out+2*273.15)/2.-5200)*1e6 / 0.88; % Young modulus
%correlation from High Performance Fuel Design for Next Generation PWRs: Final Report
del_grid=z_assm_tot/(N_grid+1);  % Length of span between spacers and top and bottom nozzles
alpha=.4;                        % maximum alpha for vibration reasons
iner=pi/64*((D_pin)^2-(D_ci)^2); % inertia modulus (units~~, same in VIPRE-MATLAB interface)

rho_clad=6560;                                  % zircaloy 4 density kg/m3

V_cross=core_power*2.239e-8-1.669e-2;           % maximum cross flow velocity - Thesis Diller

mass_lin_clad=rho_clad*(pi/4)*(D_pin^2-D_ci^2); % cladding linear mass

D_star=(1+0.5*P_ov_D)*P_ov_D;                   % D_star coefficient
C_addmass=(D_star^2+1)/(D_star^2-1);            % added mass coefficeint

strouhal=1/(2*(P_ov_D-1));                      % Strouhal number
f_s=strouhal*V_cross/D_pin;                     % vortex shedding frequency

mass_lin_cool=C_addmass*(pi/4)*rho*D_pin^2;     % coolant linear mass
mass_lin_tot=mass_lin_clad+mass_lin_cool;       % total linear mass, excludes fuel bcs of gap

f_1=(pi./(2*del_grid^2)*sqrt((E_mod_clad*iner)./mass_lin_tot));
% fundamental rod frequency, a cosinus with that frequency is null at every spacer location

VSM_lift=abs(f_1-f_s)./f_s;                     % vortex shedding margin - lift
VSM_drag=abs(f_1-2*f_s)./(2*f_s);               % vortex shedding margin - drag

VSM_min_lift=min(VSM_lift);                     % minimum margin VSM lift
VSM_min_drag=min(VSM_drag);                     % minimum margin VSM drag


if VSM_min_lift < VSM_lim && strcmp(run_mode,'trends')==0 % vortex shedding limit
    valid=0;
    failure{m,n,l}='VSM_lift';
    continue
else
    VSM_min_lift_mat(m,n,l)=VSM_min_lift;
end

if VSM_min_drag < VSM_lim && strcmp(run_mode,'trends')==0 % vortex shedding limit
    valid=0;
    failure{m,n,l}='VSM_drag';
    continue
else
    VSM_min_drag_mat(m,n,l)=VSM_min_drag;
end

%% Fluid Elastic Instability Margin- Connor's analysis from ASME
% described page 42 of Diller's master thesis on 'Wire Wrapped Fuel
% Pin Hexagonal Arrays for PWR Service'

beta_FIM=4.76*(P_ov_D-1)+0.76;  % Connors' constant
zeta_damp=0.01;                 % damping ratio conservative value of 0.01 chosen

V_crit=beta_FIM.*f_1.*sqrt((2*pi*zeta_damp.*mass_lin_tot)./rho);
% f_1 is being used for conservatism
FIM=V_cross./V_crit;
```

```
% cross flow velocity needs to remain below critical velocity

FIM_max=max(FIM);

if FIM_max > FIM_lim && strcmp(run_mode,'trends')==0             % FIM limit
    valid=0;
    failure{m,n,l}='FIM';
    continue
else
    FIM_mat(m,n,l)=FIM_max;
end

%% Fretting Wear : see Flow induced vibrations in power plants Au-Yang
% Vibrations due to cross flow : Au-Yang + Pettigrew and Goreman
% Vibrations due to axial flow : Paidoussis

% J_11=0.64; %Joint acceptance    Other value possible in article
L = del_grid; %assuming cross flow only exists between grids
%looking at plots from VIPRE, reasonable assumption
lambda = 0.2*P_ov_D*D_pin*(1+P_ov_D/2); % correlation length for tube bundle p253 Au-Yang
J_11 = 2*lambda/L;                      % Au-Yang (9.9)
N_span=N_grid+1;                        % number of spans, top and bottom nozzles create spans
alpha=pi;                               % for simply supported rods
eta_fret=del_grid/D_pin;
A_pin=D_pin^2/4*pi;

F_dimensionless=f_1*D_pin/V_cross;      % dimensionless frequency
G_p_norm = (0.01 .* (F_dimensionless<0.1)) + (5.3E-4./F_dimensionless.^3.5 .* (F_dimensionless>0

G_p = G_p_norm./4.*(rho.^2.*V_cross^3.*D_pin);

C_R=sqrt(G_p)./(0.5*rho*V_cross^2);     % ramdom lift coefficient

G_F=(C_R.*D_pin.*(0.5.*rho.*V_cross.^2)).^2;
% random force PSD for single-phase turbulent cross-flow

y_rms_cross=sqrt((2.*J_11.*N_span.*G_F)./(64*pi^3.*mass_lin_tot.^2.*f_1.^3.*zeta_damp)); % upper

V_ax=G./rho;                            % axial flow velocity

u_fret=V_ax.*del_grid.*sqrt((rho*A_pin)./(E_mod_clad.*iner));

beta_fret=rho.*A_pin./mass_lin_tot;

%max rod response from axial flow turbulence
y_max_axial=5E-5*D_pin.*K_vibr.*alpha.^(-4.0).*((u_fret.^1.6.*eta_fret.^1.8.*Re_t.^0.25)...
/(1+u_fret.^2)).*(D_e./D_pin).^0.4.*(beta_fret.^(2/3.)./(1+4.*beta_fret));
y_rms_axial=y_max_axial/3;         % upper bound RMS rod response from axial cross flow

y_rms_tot=y_rms_cross+y_rms_axial; % total rod RMS response

Psi_loc = 1;                       % placeholder, value of vibrating mode at location

W_dot_fret=32*pi^3*zeta_damp.*(f_1).^3*del_grid.*mass_lin_tot.*(y_rms_tot/Psi_loc).^2;
W_dot_fret_check=W_dot_fret./ W_dot_fret_nom;

if max(W_dot_fret_check) > wear_lim*T_c_ref/T_c_new +1E-6 && strcmp(run_mode,'trends')==0
% fretting wear limit
```

```
            valid=0;
            failure{m,n,l}='W_fret';
            continue
        else
             W_dot_fret_mat(m,n,l)=max(W_dot_fret_check);
        end

        %% Sliding Wear from Au Yang BOOK : Flow induced vibration of power and process plant components
        gap_grid=1.0; % gapdiametral gap between tube and support 1.0 is used as a holder cancels
        mu_fric=1.0;  % coefficient of friction 1.0 is a holder cancels
        T_hold=1.0;
        % holding variable for residence time cancels    (doesnt cancel if residence time is changed)
        A_clad=A_pin-D_ci^2*pi/4;

        S_d=pi*f_1*gap_grid*T_hold; % sliding distane

        Force_n=(3*pi*D_pin.*y_rms_tot)./(mu_fric.*(del_grid^2./(A_clad.*E_mod_clad)+D_pin.^2.
        *del_grid.^2/4./E_mod_clad./iner)); % contact normal force

        W_dot_slide=Force_n.*S_d;
        W_dot_slide_check=W_dot_slide./ W_dot_slide_nom;

        if max(W_dot_slide_check) > wear_lim*T_c_ref/T_c_new +1E-6 && strcmp(run_mode,'trends')==0
        % sliding wear limit
            valid=0;
            failure{m,n,l}='W_slide';
            continue
        else
            W_dot_slide_mat(m,n,l)=max(W_dot_slide_check);
        end
                end
                if speed_mode(1)==1 && pow_count == 1 && valid == 0
                % checks if speed_mode failed to see possible power increase
                    speed_fail = 1;
                end
                D_mat(m,n,l) = D_pin;         % to simplify finding the geometry when plotting
                P_ov_D_mat(m,n,l) = P_ov_D;
            end
        end
end
if speed_mode(1) == 1
    if speed_fail == 1
        disp('Possible power increase, run with higher margin (speed_mode(2)) or without speed mode')
    end
end
toc

save 'save_temp'

% % To save characteristics of best core
% HM_AP1000 = 3.02;                                                %objective H/HM ratio
% list1 = find(core_power_mat == max(max(max(core_power_mat))));  %list of optimal cores
% [~,list2] = min( abs(H_ratio_mat(list1)-HM_AP1000));            %closest to objective H/HM
% % list2 = find(n_rod_assem_mat == 17);
% list = list1(list2);
% P_ov_D_opt = P_ov_D_mat(list);
% D_opt = D_mat(list);
% G_opt = G_mat(list);
```

```
% fret_opt = W_dot_fret_mat(list);
% slide_opt = W_dot_slide_mat(list);
% H_HM = H_ratio_mat(list);
% Pdrop_opt = P_drop_tot_mat(list);
% mdnbr_opt = mdnbr_mat(list);
% T_fuel_ave_mat = T_fuel_ave_mat(list);
% n_pin_mat = n_pin_mat(list);
% core_power_mat_opt= core_power_mat(list);
% mdot_core = m_dot_mat(list);
% T_in = T_in_mat(list);
% rho_mean = rho_mean(list);
% n_h_out_peak_per_ass = n_rod_assem_mat(list);
% %save('TH_optimized.mat','D_opt','P_ov_D_opt','G_opt','H_HM','Pdrop_opt','mdnbr_opt','n_row_per_ass'
%,'T_fuel_ave_mat','n_pin_mat','core_power_mat','mdot_core','T_in','rho_mean','T_co_out','z_assm',
%'-v6')


% To update nominal design fretting and sliding wear, use sequence of this
% W_dot_fret_nom = 1000*linspace(1,1,n_nodes);
% W_dot_slide_nom = 1000*linspace(1,1,n_nodes);
% save Wear_rates_nominal W_dot_fret_nom W_dot_slide_nom %run script
% W_dot_fret_nom = W_dot_fret;
% W_dot_slide_nom = W_dot_slide;
% save Wear_rates_nominal W_dot_fret_nom W_dot_slide_nom %updated
```

Annex 5: VIPRE inputs

The VIPRE-MATLAB interface code is too long to reproduce here, we will only reproduce the VIPRE input for the nominal AP1000 oxide core and for the optimized UN core.

AP1000 oxide core VIPRE input

1,0,0
oxide Core Square Subchannel
geom,42,0, 100,0,19,0
180.00, 0.0,0.00
3, 0.068, 0.587, 0.441
10,15,21
1, 0.068, 0.587, 0.441
1
1, 0.068, 0.587, 0.441
6
2, 0.068, 0.587, 0.587
28,36
1, 0.068, 0.587, 0.587
3
3, 0.136, 1.175, 0.881
19,20,25
3, 0.136, 1.175, 0.881
7,16,22
3, 0.136, 1.175, 0.881
9,18,24
1, 0.136, 1.175, 0.881
4
7, 0.136, 1.175, 1.175
14,26,27,32,33,34,35
7, 0.136, 1.175, 1.175
8,11,12,17,23,29,30
3, 0.136, 1.175, 1.175
2,13,31
1, 0.136, 1.175, 1.175
5
1, 0.562, 4.847, 4.847

37
1, 39.350,339.562,310.188
38
1, 78.699,679.124,620.377
39
1,118.049,1018.687,930.565
40
1,157.398,1358.249,1240.753
41
1,373.821,3225.841,2946.789
42
69,0,1,0,0,0
1,1,2, 0.1220, 0.4215
2,2,3, 0.1220, 0.4215
3,2,4, 0.1220, 0.4960
4,3,5, 0.1220, 0.4215
5,4,5, 0.1220, 0.4960
6,4,7, 0.1220, 0.4960
7,5,6, 0.1220, 0.4215
8,5,8, 0.1220, 0.4960
9,6,9, 0.1220, 0.4215
10,7,8, 0.1220, 0.4960
11,7,11, 0.1220, 0.4960
12,8,9, 0.1220, 0.4960
13,8,12, 0.1220, 0.4960
14,9,10, 0.1220, 0.4215
15,9,13, 0.1220, 0.4960
16,10,14, 0.1220, 0.4215
17,11,12, 0.1220, 0.4960
18,11,16, 0.1220, 0.4960
19,12,13, 0.1220, 0.4960
20,12,17, 0.1220, 0.4960
21,13,14, 0.1220, 0.4960
22,13,18, 0.1220, 0.4960
23,14,15, 0.1220, 0.4215
24,14,19, 0.1220, 0.4960
25,15,20, 0.1220, 0.4215
26,16,17, 0.1220, 0.4960
27,16,22, 0.1220, 0.4960
28,17,18, 0.1220, 0.4960
29,17,23, 0.1220, 0.4960
30,18,19, 0.1220, 0.4960
31,18,24, 0.1220, 0.4960
32,19,20, 0.1220, 0.4960
33,19,25, 0.1220, 0.4960
34,20,21, 0.1220, 0.4215
35,20,26, 0.1220, 0.4960

36,21,27, 0.1220, 0.4215
37,22,23, 0.1220, 0.4960
38,22,29, 0.1220, 0.4960
39,23,24, 0.1220, 0.4960
40,23,30, 0.1220, 0.4960
41,24,25, 0.1220, 0.4960
42,24,31, 0.1220, 0.4960
43,25,26, 0.1220, 0.4960
44,25,32, 0.1220, 0.4960
45,26,27, 0.1220, 0.4960
46,26,33, 0.1220, 0.4960
47,27,28, 0.1220, 0.4215
48,27,34, 0.1220, 0.4960
49,28,35, 0.1220, 0.4215
50,29,30, 0.1220, 0.4960
51,29,37, 0.1220, 1.1177
52,30,31, 0.1220, 0.4960
53,30,37, 0.1220, 0.7769
54,31,32, 0.1220, 0.4960
55,31,37, 0.1220, 0.4842
56,32,33, 0.1220, 0.4960
57,32,37, 0.1220, 0.3771
58,33,34, 0.1220, 0.4960
59,33,37, 0.1220, 0.5716
60,34,35, 0.1220, 0.4960
61,34,37, 0.1220, 0.8877
62,35,36, 0.1220, 0.4215
63,35,37, 0.1220, 1.2353
64,36,37, 0.1220, 1.5940
65,37,38, 4.2160, 4.8523
66,38,39,12.6480, 9.4273
67,39,40,21.0800, 9.4273
68,40,41,29.5120, 9.4273
69,41,42,37.9440,15.9192
prop,0,1,2,1
rods,1,44,1,2,0,0,0,0,0,0,0
168,5.635,0,0
-1
1.55
1,1,1.3949,1,1,0.25,2,0.25
2,1,1.3959,1,1,0.125,2,0.25,3,0.125
3,1,1.3971,1,2,0.25,4,0.25
4,1,1.3976,1,2,0.25,3,0.25,4,0.25,5,0.25
5,1,1.3986,1,3,0.125,5,0.25,6,0.125
6,1,1.3991,1,4,0.25,5,0.25,7,0.25,8,0.25
7,1,1.3998,1,5,0.25,6,0.25,8,0.25,9,0.25
8,1,1.4003,1,7,0.25,11,0.25

9,1,1.4004,1,7,0.25,8,0.25,11,0.25,12,0.25
10,1,1.4008,1,8,0.25,9,0.25,12,0.25,13,0.25
11,1,1.4013,1,9,0.25,10,0.25,13,0.25,14,0.25
12,1,1.4017,1,10,0.125,14,0.25,15,0.125
13,1,1.4013,1,11,0.25,16,0.25
14,1,1.4014,1,11,0.25,12,0.25,16,0.25,17,0.25
15,1,1.4016,1,12,0.25,13,0.25,17,0.25,18,0.25
16,1,1.4018,1,13,0.25,14,0.25,18,0.25,19,0.25
17,1,1.402,1,14,0.25,15,0.25,19,0.25,20,0.25
18,1,1.4019,1,16,0.25,17,0.25,22,0.25,23,0.25
19,1,1.402,1,17,0.25,18,0.25,23,0.25,24,0.25
20,1,1.4021,1,19,0.25,20,0.25,25,0.25,26,0.25
21,1,1.402,1,20,0.25,21,0.25,26,0.25,27,0.25
22,1,1.4017,1,21,0.125,27,0.25,28,0.125
23,1,1.4021,1,22,0.25,29,0.25
24,1,1.4021,1,22,0.25,23,0.25,29,0.25,30,0.25
25,1,1.4021,1,23,0.25,24,0.25,30,0.25,31,0.25
26,1,1.402,1,24,0.25,25,0.25,31,0.25,32,0.25
27,1,1.4019,1,25,0.25,26,0.25,32,0.25,33,0.25
28,1,1.4016,1,26,0.25,27,0.25,33,0.25,34,0.25
29,1,1.4012,1,27,0.25,28,0.25,34,0.25,35,0.25
30,1,1.4006,1,28,0.125,35,0.25,36,0.125
31,1,1.4019,1,29,0.25,37,0.25
32,1,1.4019,1,29,0.25,30,0.25,37,0.5
33,1,1.4018,1,30,0.25,31,0.25,37,0.5
34,1,1.4017,1,31,0.25,32,0.25,37,0.5
35,1,1.4014,1,32,0.25,33,0.25,37,0.5
36,1,1.401,1,33,0.25,34,0.25,37,0.5
37,1,1.4005,1,34,0.25,35,0.25,37,0.5
38,1,1.3997,1,35,0.25,36,0.25,37,0.5
39,1,1.3987,1,36,0.125,37,0.375
40,2,1.3627,1,38,264
41,2,1.2352,1,39,528
42,2,1.0516,1,40,792
43,2,0.86417,1,41,1056
44,2,0.94791,1,42,2508
0
1,nucl, 0.3740, 0.3225, 6, 0.0000, 0.0225
0, 0, 0, 0, 0,3662.0000, 0.9550, 0.0000
2,dumy, 0.3740, 0.0000,0
oper,1,2,0,0,0,0,0,0,0
0.0000, 0.0000, 2.6000, 0.0010,0
2250.0000,534.9200, 2.4912, 5.8593,0
0,0,0,0,0,0
corr,2,1,0
levy,homo,homo,none,
ditb,thsp,thsp,epri,cond,g5.7,

w-3l,bowr,
0.0420, 0.0660, 1.0000
0.7000
-1,2
0
mixx,1,0,1
0.0000, 0.0000, 0.0000
0.0448, 0.0000, 0.0448, 0.0000, 0.0381, 0.0000, 0.0448, 0.0000,
0.0381, 0.0000, 0.0381, 0.0000, 0.0448, 0.0000, 0.0381, 0.0000,
0.0448, 0.0000, 0.0381, 0.0000, 0.0381, 0.0000, 0.0381, 0.0000,
0.0381, 0.0000, 0.0448, 0.0000, 0.0381, 0.0000, 0.0448, 0.0000,
0.0381, 0.0000, 0.0381, 0.0000, 0.0381, 0.0000, 0.0381, 0.0000,
0.0381, 0.0000, 0.0381, 0.0000, 0.0448, 0.0000, 0.0381, 0.0000,
0.0448, 0.0000, 0.0381, 0.0000, 0.0381, 0.0000, 0.0381, 0.0000,
0.0381, 0.0000, 0.0381, 0.0000, 0.0381, 0.0000, 0.0381, 0.0000,
0.0381, 0.0000, 0.0448, 0.0000, 0.0381, 0.0000, 0.0448, 0.0000,
0.0381, 0.0000, 0.0381, 0.0000, 0.0381, 0.0000, 0.0381, 0.0000,
0.0381, 0.0000, 0.0381, 0.0000, 0.0381, 0.0000, 0.0381, 0.0000,
0.0381, 0.0000, 0.0381, 0.0000, 0.0448, 0.0000, 0.0381, 0.0000,
0.0448, 0.0000, 0.0381, 0.0000, 0.0169, 0.0000, 0.0381, 0.0000,
0.0243, 0.0000, 0.0381, 0.0000, 0.0390, 0.0000, 0.0381, 0.0000,
0.0501, 0.0000, 0.0381, 0.0000, 0.0330, 0.0000, 0.0381, 0.0000,
0.0213, 0.0000, 0.0448, 0.0000, 0.0153, 0.0000, 0.0119, 0.0000,
0.0039, 0.0000, 0.0020, 0.0000, 0.0020, 0.0000, 0.0020, 0.0000,
0.0012, 0.0000
drag,1,0,1
0.1529,-0.1800, 0.0000,101.3309,-1.0000, 0.0000
0.5000, 0.4960
grid,0,2
0.4502, 0.7702
-1,10
1.8000,1,21.6000,2,41.4000,2,61.2000,2,?
81.0000,2,99.0000,2,118.8000,2,138.6000,2
158.4000,2,178.2000,1,
0
endd
0

Optimized nitride core VIPRE input

1,0,0
nitride Core Square Subchannel
geom,42,0, 100,0,23,0
180.00, 0.0,0.00
1, 0.013, 0.124, 0.124
1

2, 0.052, 0.495, 0.371
15,36
1, 0.052, 0.495, 0.371
21
1, 0.052, 0.495, 0.371
3
1, 0.052, 0.495, 0.371
6
2, 0.052, 0.495, 0.495
10,28
5, 0.052, 0.495, 0.495
7,11,16,22,29
2, 0.052, 0.495, 0.495
2,4
1, 0.105, 0.989, 0.742
33
1, 0.105, 0.989, 0.742
20
1, 0.105, 0.989, 0.742
34
2, 0.105, 0.989, 0.742
12,30
1, 0.105, 0.989, 0.742
17
3, 0.105, 0.989, 0.742
13,18,31
1, 0.105, 0.989, 0.742
5
7, 0.105, 0.989, 0.989
14,19,25,26,27,32,35
4, 0.105, 0.989, 0.989
8,9,23,24
1, 2.292, 21.645, 20.284
37
1, 41.920,395.791,360.170
38
1, 83.839,791.582,720.340
39
1,125.759,1187.374,1080.510
40

1,167.678,1583.165,1440.680
41
1,398.236,3760.017,3421.615
42
69,0,1,0,0,0
1,1,2, 0.0562, 0.2872
2,2,3, 0.1125, 0.2593
3,2,4, 0.0562, 0.4274
4,3,5, 0.1125, 0.3633
5,4,5, 0.1125, 0.3206
6,4,7, 0.0562, 0.4274
7,5,6, 0.1125, 0.3633
8,5,8, 0.1125, 0.4274
9,6,9, 0.1125, 0.3633
10,7,8, 0.1125, 0.3206
11,7,11, 0.0562, 0.4274
12,8,9, 0.1125, 0.4274
13,8,12, 0.1125, 0.4274
14,9,10, 0.1125, 0.3633
15,9,13, 0.1125, 0.4274
16,10,14, 0.1125, 0.3633
17,11,12, 0.1125, 0.3206
18,11,16, 0.0562, 0.4274
19,12,13, 0.1125, 0.4274
20,12,17, 0.1125, 0.4274
21,13,14, 0.1125, 0.4274
22,13,18, 0.1125, 0.4274
23,14,15, 0.1125, 0.3633
24,14,19, 0.1125, 0.4274
25,15,20, 0.1125, 0.3633
26,16,17, 0.1125, 0.3206
27,16,22, 0.0562, 0.4274
28,17,18, 0.1125, 0.4274
29,17,23, 0.1125, 0.4274
30,18,19, 0.1125, 0.4274
31,18,24, 0.1125, 0.4274
32,19,20, 0.1125, 0.4274
33,19,25, 0.1125, 0.4274
34,20,21, 0.1125, 0.3633
35,20,26, 0.1125, 0.4274

36,21,27, 0.1125, 0.3633
37,22,23, 0.1125, 0.3206
38,22,29, 0.0562, 0.4274
39,23,24, 0.1125, 0.4274
40,23,30, 0.1125, 0.4274
41,24,25, 0.1125, 0.4274
42,24,31, 0.1125, 0.4274
43,25,26, 0.1125, 0.4274
44,25,32, 0.1125, 0.4274
45,26,27, 0.1125, 0.4274
46,26,33, 0.1125, 0.4274
47,27,28, 0.1125, 0.3633
48,27,34, 0.1125, 0.4274
49,28,35, 0.1125, 0.3633
50,29,30, 0.1125, 0.3206
51,29,37, 0.0562, 1.3485
52,30,31, 0.1125, 0.4274
53,30,37, 0.1125, 1.1767
54,31,32, 0.1125, 0.4274
55,31,37, 0.1125, 0.9513
56,32,33, 0.1125, 0.4274
57,32,37, 0.1125, 0.7943
58,33,34, 0.1125, 0.4274
59,33,37, 0.1125, 0.7499
60,34,35, 0.1125, 0.4274
61,34,37, 0.1125, 0.8363
62,35,36, 0.1125, 0.3633
63,35,37, 0.1125, 1.0208
64,36,37, 0.1125, 1.2610
65,37,38, 4.2745, 5.3764
66,38,39,12.8234, 9.5580
67,39,40,21.3723, 9.5580
68,40,41,29.9213, 9.5580
69,41,42,38.4702,16.1446
prop,0,0,2,1
rods,1,54,1,2,1,0,0,0,0,0,0
168,5.635,0,0
-1
1.571
1,1,1.3939,1,1,0.125,2,0.25,3,0.125

2,1,1.3957,1,2,0.25,3,0.25,4,0.25,5,0.25
3,1,1.3975,1,4,0.25,5,0.25,7,0.25,8,0.25
4,1,1.3981,1,5,0.25,6,0.25,8,0.25,9,0.25
5,1,1.399,1,6,0.125,9,0.25,10,0.125
6,1,1.399,1,7,0.25,8,0.25,11,0.25,12,0.25
7,1,1.3993,1,8,0.25,9,0.25,12,0.25,13,0.25
8,1,1.3999,1,9,0.25,10,0.25,13,0.25,14,0.25
9,1,1.4006,1,10,0.125,14,0.25,15,0.125
10,1,1.4002,1,11,0.25,12,0.25,16,0.25,17,0.25
11,1,1.4008,1,13,0.25,14,0.25,18,0.25,19,0.25
12,1,1.4012,1,14,0.25,15,0.25,19,0.25,20,0.25
13,1,1.4011,1,16,0.25,17,0.25,22,0.25,23,0.25
14,1,1.4012,1,17,0.25,18,0.25,23,0.25,24,0.25
15,1,1.4014,1,18,0.25,19,0.25,24,0.25,25,0.25
16,1,1.4017,1,19,0.25,20,0.25,25,0.25,26,0.25
17,1,1.4019,1,20,0.25,21,0.25,26,0.25,27,0.25
18,1,1.4021,1,21,0.125,27,0.25,28,0.125
19,1,1.4017,1,22,0.25,23,0.25,29,0.25,30,0.25
20,1,1.4018,1,23,0.25,24,0.25,30,0.25,31,0.25
21,1,1.4019,1,24,0.25,25,0.25,31,0.25,32,0.25
22,1,1.402,1,25,0.25,26,0.25,32,0.25,33,0.25
23,1,1.4021,1,26,0.25,27,0.25,33,0.25,34,0.25
24,1,1.4021,1,27,0.25,28,0.25,34,0.25,35,0.25
25,1,1.4019,1,28,0.125,35,0.25,36,0.125
26,1,1.402,1,29,0.25,30,0.25,37,0.5
27,1,1.4021,1,31,0.25,32,0.25,37,0.5
28,1,1.4021,1,32,0.25,33,0.25,37,0.5
29,1,1.4019,1,34,0.25,35,0.25,37,0.5
30,1,1.4017,1,35,0.25,36,0.25,37,0.5
31,1,1.4021,1,37,1
32,1,1.4021,1,37,1
33,1,1.402,1,37,1
34,1,1.4019,1,37,1
35,1,1.4018,1,37,1
36,1,1.4016,1,37,1
37,1,1.4012,1,37,1
38,1,1.4007,1,37,1
39,1,1.4001,1,37,0.5
40,1,1.4018,1,37,1
41,1,1.4018,1,37,1

42,1,1.4017,1,37,1
43,1,1.4016,1,37,1
44,1,1.4013,1,37,1
45,1,1.401,1,37,1
46,1,1.4006,1,37,1
47,1,1.4,1,37,1
48,1,1.3992,1,37,1
49,1,1.3983,1,37,0.5
50,2,1.361,1,38,364
51,2,1.23,1,39,728
52,2,1.0429,1,40,1092
53,2,0.85425,1,41,1456
54,2,0.95612,1,42,3458
0
1,nucl, 0.3150, 0.2690, 6, 0.0000, 0.0204
0, 1, 0, 0, 0,810.1239, 0.9550, 0.0000
2,dumy, 0.3150, 0.0000,0
1, 36,854.0000
77.0,0.00024,6.80515, 257.0,0.01032,7.55412
437.0,0.02797,8.19057, 617.0,0.04478,8.74974
797.0,0.06095,9.25193, 977.0,0.07679,9.71000
1157.0,0.09243,10.13272, 1337.0,0.10795,10.52632
1517.0,0.12340,10.89547, 1697.0,0.13879,11.24371
1877.0,0.15414,11.57383, 2057.0,0.16948,11.88808
2237.0,0.18483,12.18828, 2417.0,0.20023,12.47593
2597.0,0.21573,12.75229, 2777.0,0.23140,13.01844
2957.0,0.24733,13.27530, 3137.0,0.26361,13.52364
3317.0,0.28033,13.76417, 3497.0,0.29759,13.99747
3677.0,0.31545,14.22409, 3857.0,0.33400,14.44449
4037.0,0.35326,14.65910, 4217.0,0.37328,14.86828
4397.0,0.39406,15.07238, 4577.0,0.41559,15.27170
4757.0,0.43785,15.46652, 4937.0,0.46081,15.65709
5117.0,0.48442,15.84364, 5297.0,0.50863,16.02638
5477.0,0.53337,16.20550, 5657.0,0.55860,16.38119
5837.0,0.58423,16.55361, 6017.0,0.61021,16.72290
6197.0,0.63647,16.88921, 6242.0,0.64307,16.93034
oper,1,2,0,0,0,0,0,0,0
0.0000, 0.0000, 2.0000, 0.0010,0
2250.0000,535.0000, 2.3391, 4.8746,0
0,0,0,0,0,0

corr,2,1,0
levy,homo,homo,none,
ditb,thsp,thsp,epri,cond,g5.7,
w-3l,bowr,
0.0420, 0.0660, 1.0000
0.7000
-1,1
0
mixx,1,0,1
0.0000, 0.0000, 0.0000
0.0568, 0.0000, 0.0629, 0.0000, 0.0382, 0.0000, 0.0449, 0.0000,
0.0509, 0.0000, 0.0382, 0.0000, 0.0449, 0.0000, 0.0382, 0.0000,
0.0449, 0.0000, 0.0509, 0.0000, 0.0382, 0.0000, 0.0382, 0.0000,
0.0382, 0.0000, 0.0449, 0.0000, 0.0382, 0.0000, 0.0449, 0.0000,
0.0509, 0.0000, 0.0382, 0.0000, 0.0382, 0.0000, 0.0382, 0.0000,
0.0382, 0.0000, 0.0382, 0.0000, 0.0449, 0.0000, 0.0382, 0.0000,
0.0449, 0.0000, 0.0509, 0.0000, 0.0382, 0.0000, 0.0382, 0.0000,
0.0382, 0.0000, 0.0382, 0.0000, 0.0382, 0.0000, 0.0382, 0.0000,
0.0382, 0.0000, 0.0449, 0.0000, 0.0382, 0.0000, 0.0449, 0.0000,
0.0509, 0.0000, 0.0382, 0.0000, 0.0382, 0.0000, 0.0382, 0.0000,
0.0382, 0.0000, 0.0382, 0.0000, 0.0382, 0.0000, 0.0382, 0.0000,
0.0382, 0.0000, 0.0382, 0.0000, 0.0449, 0.0000, 0.0382, 0.0000,
0.0449, 0.0000, 0.0509, 0.0000, 0.0121, 0.0000, 0.0382, 0.0000,
0.0139, 0.0000, 0.0382, 0.0000, 0.0171, 0.0000, 0.0382, 0.0000,
0.0205, 0.0000, 0.0382, 0.0000, 0.0218, 0.0000, 0.0382, 0.0000,
0.0195, 0.0000, 0.0449, 0.0000, 0.0160, 0.0000, 0.0129, 0.0000,
0.0030, 0.0000, 0.0017, 0.0000, 0.0017, 0.0000, 0.0017, 0.0000,
0.0010, 0.0000
drag,1,0,1
0.1536,-0.1800, 0.0000,105.4684,-1.0000, 0.0000
0.5000, 0.4274
grid,0,2
0.5270, 0.8470
-1,10
1.8000,1,21.6000,2,41.4000,2,61.2000,2,?
81.0000,2,99.0000,2,118.8000,2,138.6000,2
158.4000,2,178.2000,1,
0
endd
0

Annex6: CASMO4E inputs

Nitride-fueled optimized assembly

TTL * K2F3R3777E1290B2P1 Python

* State Parameters
PDE 36.397
PRE 155.130
TFU 1091.0
TMO 544.382554348
BOR 600
VOI 000

* Assembly Geometry Parameters
PWR 20 1.08571428571 21.8212857143 „„,8

* Pin Geometry Parameters
PIN 1 0.3416609 0.34828414 0.4 /'1' 'AIR' 'CAN'
PIN 2 0.3416609 0.342250373684 0.34828414 0.4 /'1' 'BP3' 'AIR' 'CAN'
PIN 3 0.980589569161 1.05934693878/'MOD' 'BOX' //4
PIN 4 0.49029478458 0.529673469388/'MOD' 'BOX' //1
PIN 4 0.373192743764 0.376467120181 0.416965986395 0.49029478458 0.529673469388
/'B4C' 'AIR' 'CRS' 'MOD' 'BOX'
//1 'RCC' 'ROD'
PIN 5 0.3416609 0.342250373684 0.34828414 0.4 /'2' 'BP5' 'AIR' 'CAN'
PIN 6 0.3416609 0.34828414 0.4 /'2' 'AIR' 'CAN'
PIN 7 0.3416609 0.34828414 0.4 /'5' 'AIR' 'CAN'

* Fuel Composition Parameters 6.35
FUE 1 12.975738252/4.66682633945 92234=0.0373346107156
92238=88.8194129867 7000=0.058927347887 8000=6.41749871527
64152=0.0 64154=0.0 64155=0.0
64156=0.0 64157=0.0 64158=0.0
64160=0.0
FUE 2 12.975733658/4.20016124485 92234=0.0336012899588
92238=89.2902019463 7000=0.0589237944246 8000=6.41711172448
64152=0.0 64154=0.0 64155=0.0

64156=0.0 64157=0.0 64158=0.0
64160=0.0
FUE 3 12.7697867114/4.49124108817 92234=0.0359299287053
92238=85.4776604093 7000=0.405628460187 8000=5.92900411203
64152=0.00757821076697 64154=0.0785367338569 64155=0.53914255473
64156=0.749444260106 64157=0.573718069039 64158=0.910531659913
64160=0.801584513213
FUE 4 12.7697536842/4.04213319924 92234=0.0323370655939
92238=85.9307223258 7000=0.405625097769 8000=5.9286456113
64152=0.00757821221349 64154=0.0785367488479 64155=0.539142657641
64156=0.749444403159 64157=0.57371817855 64158=0.910531833715
64160=0.801584666219
FUE 5 12.5718903492/4.31389428186 92234=0.0345111542549
92238=82.1023817754 7000=0.753894323367 8000=5.45759715021
64152=0.0151908897081 64154=0.157430678394 64155=1.08073730564
64156=1.50229723714 64157=1.15004559497 64158=1.82520471479
64160=1.60681489423
FUE 6 12.5718304211/3.88251984501 92234=0.0310601587601
92238=82.5375410163 7000=0.753891049066 8000=5.45726632678
64152=0.0151908903068 64154=0.157430684599 64155=1.08073734823
64156=1.50229729635 64157=1.1500456403 64158=1.82520478672
64160=1.60681495756

* Material Composition Parameters
* Density, thermal exp coeff, temperature / nuclide id and weight %
CAN 6.55, 7E-6, 600/ 306=100.0 *ZIRLO cladding
*stainless steel 304 from serpent example
MI1 7.76,,/14000=2.02 24000=19.52 25000=1.52 26000=67.34 28000=9.52 *carbon, no XS,
part distributed among others
*ZIRLO
BOX 6.55, 7E-6, 600/ 306=100.0
BP3 6.10 7.0E-6 /302=80 0=20 / 5010=0.64
BP5 6.10 7.0E-6 /302=80 0=20 / 5010=0.64

LPI
3
5 7
2 1 2
1 1 2 4
1 1 2 2 2
1 2 2 2 1 2
1 2 4 2 1 2 4
1 2 2 2 1 2 2 2
1 1 1 1 7 1 1 1 1
2 1 2 1 1 1 2 1 1 7

SIM ,'big_ifba192_Gd8_4.99'
S3C
STA

END

Oxide-fueled AP1000 nominal assembly

TTL * K2F3R3777E1290B2P1 Python

* State Parameters
PDE 43.311
PRE 155.130
TFU 1541.0
TMO 552.55
BOR 600
VOI 000

* Assembly Geometry Parameters
PWR 17 1.25984 21.52428 „„,8

* Pin Geometry Parameters
PIN 1 0.40959278 0.417835588 0.47498 /'1' 'AIR' 'CAN'
PIN 2 0.40959278 0.410292750526 0.417835588 0.47498 /'1' 'BP3' 'AIR' 'CAN'
PIN 3 0.568927746032 0.614621942857/'MOD' 'BOX' //1
PIN 4 0.568927746032 0.614621942857/'MOD' 'BOX' //1
PIN 4 0.433045003175 0.436844520635 0.483838552381 0.568927746032 0.614621942857
/'AIC' 'AIR' 'CRS' 'MOD' 'BOX'
//1 'RCC' 'ROD'
PIN 5 0.40959278 0.410292750526 0.417835588 0.47498 /'2' 'BP5' 'AIR' 'CAN'
PIN 6 0.40959278 0.417835588 0.47498 /'2' 'AIR' 'CAN'
PIN 7 0.40959278 0.417835588 0.47498 /'5' 'AIR' 'CAN'

* Fuel Composition Parameters 6.35
FUE 1 10.4/4.99 64016=0
FUE 2 10.4/4.4910000000000005 64016=0
FUE 3 10.3188031381/4.99 64016=1.0
FUE 4 10.3187975046/4.4910000000000005 64016=1.0
FUE 5 10.2379559254/4.99 64016=2.0
FUE 6 10.2379447708/4.4910000000000005 64016=2.0

* Material Composition Parameters
* Density, thermal exp coeff, temperature / nuclide id and weight %
CAN 6.55, 7E-6, 600/ 306=100.0 *ZIRLO cladding
*stainless steel 304 from serpent example

MI1 7.76,,/14000=2.02 24000=19.52 25000=1.52 26000=67.34 28000=9.52 *carbon, no XS,
part distributed among others
*ZIRLO
BOX 6.55, 7E-6, 600/ 306=100.0
BP3 6.10 7.0E-6 /302=80 0=20 / 5010=0.84
BP5 6.10 7.0E-6 /302=80 0=20 / 5010=0.84

LPI
3
7 1
1 1 1
4 2 2 4
2 1 1 2 1
2 1 1 2 7 4
4 2 2 4 1 2 1
2 1 1 2 1 1 1 1
2 1 2 1 2 1 2 1 7

DEP -70
SIM ,'nom_ifba192_Gd2_4.99'
S3C
STA

END